

For Reference

NOT TO BE TAKEN FROM THIS ROOM

Ex LIBRIS
UNIVERSITATIS
ALBERTAEASIS



THE UNIVERSITY OF ALBERTA

RELEASE FORM

NAME OF AUTHOR: Philippe Golaz

TITLE OF THESIS: A STUDY OF THE CENTRIFUGE METHOD OF CAPILLARY
PRESSURE MEASUREMENT

DEGREE FOR WHICH THESIS WAS PRESENTED: MASTER OF SCIENCE

YEAR THIS DEGREE GRANTED: 1979

Permission is hereby granted to THE UNIVERSITY OF ALBERTA
LIBRARY to reproduce single copies of this thesis and to lend
or sell such copies for private, scholarly or scientific
research purposes only.

The author reserves other publication rights, and neither
the thesis nor extensive extracts from it may be printed or
otherwise reproduced without the author's written permission.

THE UNIVERSITY OF ALBERTA

A STUDY OF THE CENTRIFUGE METHOD OF CAPILLARY
PRESSURE MEASUREMENT

by



Philippe Golaz

A THESIS

SUBMITTED TO THE FACULTY OF GRADUATE STUDIES AND RESEARCH
IN PARTIAL FULFILMENT OF THE REQUIREMENTS FOR THE DEGREE
OF MASTER OF SCIENCE

IN

PETROLEUM ENGINEERING

DEPARTMENT OF MINERAL ENGINEERING

EDMONTON, ALBERTA

FALL, 1979

THE UNIVERSITY OF ALBERTA
FACULTY OF GRADUATE STUDIES AND RESEARCH

The undersigned certify that they have read, and recommend to the Faculty of Graduate Studies and Research, for acceptance, a thesis entitled "A Study of the Centrifuge Method of Capillary Pressure Measurement", submitted by Philippe Golaz in partial fulfilment of the requirements for the degree of Master of Science in Petroleum Engineering.

ABSTRACT

Capillary forces may have a major effect on the behaviour of immiscible displacement, because they affect the saturation profiles and, consequently, the ultimate oil recovery. A quick method for capillary pressure measurement was investigated. It makes use of a centrifuge, but differs from the conventional centrifuge method in that, instead of using small core samples, measurements are made on large samples cut into slices. It was, therefore, possible to obtain simultaneously several points on the capillary pressure - average saturation curves. These data do not, however, represent the true capillary properties of the system under study. That is, they are affected by several experimental parameters, such as size of the slices and whether one or several speeds of rotation are used for obtaining a curve. These effects were studied in an attempt to get a better understanding of what the experimental data thus obtained really represent. Finally, a new mathematical model defined by four parameters is proposed to fit the data. It was shown that a reasonable estimate of the area under the curves may thus be obtained. This term is strongly related to the parameter, σ , used in the definition of the capillary number which appears in the immiscible displacement and fractional flow equations.

Unsuccessful attempts were made to obtain imbibition capillary pressure data. These failures seem to be the consequence of limitations in the equipment used.

ACKNOWLEDGEMENTS

The author wishes to express his sincere appreciation to Dr. R. G. Bentsen for his guidance and advice throughout the course of this study.

Thanks are also due to Mr. G. T. Walsh for his helpful suggestions concerning the design of the equipment.

Special thanks are due to the Provincial Government of Alberta for granting the 1976 Premier's Scholarship.

TABLE OF CONTENTS

CHAPTER	PAGE
I. INTRODUCTION	1
II. LITERATURE REVIEW	4
II.1 Capillary Pressure	4
II.2 Wettability	12
II.3 Hysteresis	17
II.4 Measurement of Capillary Pressure in Small Core Samples	19
III. STATEMENT OF PROBLEM	29
IV. CAPILLARY PRESSURE MODEL	31
IV.1 Drainage	31
IV.1.1 Drainage Model	31
IV.1.2 Application of the Model to the Drainage Data Obtained with the Centrifuge and the Multi-Slice Core Technique	36
IV.2 Imbibition	40
IV.2.1 Imbibition Model	40
IV.2.2 Application of the Model to the Imbibition Data Obtained with the Centrifuge and the Multi-Slice Core Technique	40
V. EXPERIMENTAL EQUIPMENT AND PROCEDURE	43
V.1 The Centrifuge	44
V.2 Drainage	44
V.2.1 Drainage Capillary Pressure Cell . . .	44
V.2.2 Core and Cell Preparation	46

	PAGE
V.2.3 Drainage Capillary Pressure and Saturation Measurement	47
V.3 Imbibition	48
V.3.1 Imbibition Capillary Pressure Cell . .	48
V.3.2 Core and Cell Preparation	51
V.3.3 Imbibition Capillary Pressure and Saturation Measurement	51
VI. RESULTS AND DISCUSSION	53
VI.1 Drainage	53
VI.1.1 Experimental Results	53
VI.1.2 Error Analysis	55
VI.1.3 Numerical Results	64
VI.2 Imbibition	64
VI.3 Discussion	69
VI.3.1 Drainage	69
VI.3.1.1 Experimental Results	69
VI.3.1.2 Numerical Results	82
VI.3.1.3 Capillary Displacement Pressure - End Effect	86
VI.3.2 Imbibition	89
VII. CONCLUSIONS AND RECOMMENDATIONS	93

* * * * *

	PAGE
REFERENCES	97
APPENDIX A. JUSTIFICATION FOR THE MODIFICATION OF EQ.(5-1) INTO EQ.(5-4)	104
APPENDIX B. DERIVATION OF EQ.(4-12) AND EQ.(4-11)	109
APPENDIX C. DERIVATION OF EQ.(4-24), EQ.(4-25), EQ.(4-26) AND EQ.(4-27)	113
APPENDIX D. DERIVATION OF EQ.(5-2), EQ.(5-1) AND EQ.(4-23) . . .	116
APPENDIX E. PARAMETERS OF THE EXPERIMENTS	124
APPENDIX F. EXPERIMENTAL AND CALCULATED DATA	129

LIST OF TABLES

TABLE		PAGE
VI-1	Core Properties	54
VI-2	Fluid Properties at 20°C	54
VI-3	Numerical Results	68
E-1	Parameters of the Experiment - Run 1	125
E-2	Parameters of the Experiment - Run 2	125
E-3	Parameters of the Experiment - Run 3	126
E-4	Parameters of the Experiment - Run 4	126
E-5	Parameters of the Experiment - Run 5	127
E-6	Parameters of the Experiment - Run 6	127
E-7	Parameters of the Experiment - Run 7	128
E-8	Parameters of the Experiment - Run 8	128
F-1	Experimental and Calculated Data - Run 1	130
F-2	Experimental and Calculated Data - Run 2	131
F-3	Experimental and Calculated Data - Run 3	132
F-4	Experimental and Calculated Data - Run 4	133
F-5	Experimental and Calculated Data - Run 5	134
F-6	Experimental and Calculated Data - Run 6	135
F-7	Experimental and Calculated Data - Run 7	136
F-8	Experimental and Calculated Data - Run 8	137

LIST OF FIGURES

	PAGE
VI-16 Corrected Value of the Saturation in the Bottom Slice and Modelled Curve - Run 2	76
VI-17 Corrected Value of the Saturation in the Bottom Slice and Modelled Curve - Run 3	77
VI-18 Corrected Value of the Saturation in the Bottom Slice and Modelled Curve - Run 7	78
VI-19 Raw Centrifuge Data - Run 6	80
VI-20 Comparison Between the Model Obtained for Run 6 and the Data Obtained with Thin Slices in Runs 3 and 4 . .	81
VI-21 Meaning of $\frac{\sigma}{2-n}$	83

NOMENCLATURE

A	=	Unit conversion factor
a_{nw}, b_{nw} }	=	Parameters in relative permeability models
a_w, b_w }	=	
$c(s)$	=	Capillary function
c	=	Mean curvature of an interface
c_i	=	Coefficient of s^{i-1} in the expansion in series of $c(s)$
D	=	Distance from the rotary axis to the location at which P_c is calculated in the imbibition process
$G(s)$	=	Gravity function
g	=	Gravitational field
g_i	=	Coefficient of s^{i-1} in the expansion in series of $G(s)$
h_j	=	Length of the j^{th} slice of a multi-slice core
h_o	=	Height of the column of oil in the drainage capillary pressure cell
h	=	Location inside the core at which P_c is calculated
h_j	=	Distance from the outlet end of the multi-slice core to the inner end of the j^{th} slice
h_o	=	Distance from the free oil surface to the point where P_c is calculated in the imbibition process
h^0	=	Location inside the core at which $P_c = 0$
h_s	=	Total length of the multi-slice core
h_w	=	Distance from the free water surface to the point where P_c is calculated in the imbibition process
h^*	=	Location at which $P_c = P_d$

$J(S_w)$	=	Leverett J-function
K	=	Permeability
$K_{rnw}(S)$	=	Normalized permeability to the non-wetting phase
$K_{rw}(S)$	=	Normalized permeability to the wetting phase
L	=	Length of a core sample
M_L	=	Mass of oil and water in a slice at the end of a run
M_O	=	Mass of oil in a slice at the end of a run
M_r	=	Mobility ratio
M_W	=	Mass of water in a slice at the end of a run
M'_W	=	Mass of water in a 100%-water-saturated slice
n	=	Parameter in the capillary pressure model
P_a	=	Atmospheric pressure
P_c	=	Capillary pressure
P_{cc}	=	Capillary pressure at the center of a slice
P_{ci}	=	Capillary pressure at the inner end of the core
P_d	=	Displacement capillary pressure
P_j	=	Capillary pressure at the top of the j^{th} slice
P_k^l	=	Capillary pressure at the top of the k^{th} slice at the rotational speed ω_l
P_{nw}	=	Pressure in the non-wetting phase
P_o	=	Capillary pressure at the outer end of the core
P_{oe}	=	Pressure in the oil phase at the outer end of the core

P_{oi}	=	Pressure in the oil phase at the inner end of the core
P_w	=	Pressure in the wetting phase
P_{wi}	=	Pressure in the water phase at the inner end of the core
R	=	Mean radius of an interface
r_e	=	Distance from the rotary axis to the outer end of the core
r_i	=	Distance from the rotary axis to the inner end of the core
r_o	=	Distance from the rotary axis to the free oil surface
r_w	=	Distance from the rotary axis to the free water surface
S	=	Normalized saturation
\overline{S}_k^l	=	Average saturation in the k^{th} slice at the rotational speed ω_l
S_{or}	=	Residual oil saturation
S_w	=	Water saturation
S_{wi}	=	Interstitial water saturation
\overline{S}_{wj}^l	=	Average water saturation in the j^{th} slice
$\overline{\overline{S}}_{wj}^l$	=	Average water saturation in the first j slices
T	=	Time
V_i	=	Volume of water in the i^{th} slice
V_p	=	Pore volume
V_{Pi}	=	Pore volume of the i^{th} slice
$x(s, T)$	=	Distance along the core

x_i	=	Coefficient of S^{i-1} in the expansion in series of $X(S, T)$
α	=	Arbitrary exponent of S in the expansion in series of $X(S, T)$
β	=	Arbitrary exponent of S in the expansion in series of $G(S)$
γ	=	Interfacial tension
$\Delta\rho$	=	Density difference
$\overline{\Delta\rho}$	=	Average density difference
$\delta(S)$	=	Influence function in normalized wetting phase permeability curve
ϵ	=	Convergence criterion
ζ	=	Arbitrary exponent of S in the expansion in series of $C(S)$
$\eta(S)$	=	Influence function in normalized non-wetting phase permeability curve
θ	=	Contact angle
λ	=	Pore-size distribution index of a porous medium
ξ	=	Exponent of $1/P_c$ in the functional relationship between P_c and C_{S_w} in the residual desaturation zone
π_c	=	Normalized capillary pressure
ρ_o	=	Density of oil
ρ_w	=	Density of water
Σ	=	Summation
σ	=	Capillary pressure normalizing parameter
Φ	=	Porosity
Ψ	=	$\cos^{-1} r_i/r_e$
ω	=	Rotational speed

CHAPTER I

INTRODUCTION

Two or three immiscible fluids are generally present in petroleum reservoirs. As a consequence, forces are created because of differences in the thermodynamic properties, such as chemical potentials, associated with the various components present in the phases. These differences give rise to a physical interface, which has a finite thickness, and within which the thermodynamic properties are changing continuously. The forces created at the interfaces define the capillary properties of the system.

The initial distribution of the fluids present in a natural reservoir depends on the capillary properties of the rock and fluids system. Although the magnitude of the capillary forces is generally small, these forces may have, in some instances, a major effect on the behaviour of immiscible displacement; the saturation profiles, which determine the ultimate oil recovery, are dependent upon the capillary effects. It is, therefore, necessary to know the capillary pressure-saturation relationship for every system under study. This involves the acquisition of accurate experimental data, as well as a good understanding of what these data really represent.

Leverett (1) used the definition of capillary pressure, together with Darcy's law written for two phases and the continuity equation, to derive his fractional flow equation. In a subsequent paper, Buckley and Leverett (2) solved this equation, assuming

that the effects due to gravity and capillary pressure were negligible. The solution of this problem led to a saturation profile which was triple-valued over a portion of its length. Buckley and Leverett (3) recognized the physical impossibility of this solution, and introduced a discontinuity in the saturation-distance curve to resolve the problem. In 1959, Fayers and Sheldon (4) showed that the introduction of the capillary term eliminates the multiple-valued behaviour of the saturation, and in 1976, Bentsen (5) derived the conditions under which the non-capillary solution to the immiscible displacement equation is an acceptable approximation to the transient solution.

Mathematical models of relative permeability-saturation and capillary pressure-saturation curves are used in numerical simulators, and must, of course, comply with the experimental evidence, as well as, for the capillary pressure-saturation relationship at least, with some mathematical criteria.

Several methods of capillary pressure measurement have been discussed in the literature. The most commonly used are:

- i) the diaphragm method
- ii) the mercury injection method
- iii) the dynamic method
- iv) the centrifugal technique

It is the purpose of this study to investigate a quick method, first proposed by Szabo (6) in 1974, for determining the capillary properties of consolidated porous media. It makes use of a centrifuge, and was reported to be suitable for obtaining the

entire hysteresis loop in a matter of days. Drainage and imbibition cells, designed in principle after those developed by Szabo (6), were constructed and used in the experimental work. A new mathematical model is proposed to fit the data and is compared with another model previously studied by Bentsen and Anli (7).

CHAPTER II

LITERATURE REVIEW

II.1 CAPILLARY PRESSURE

The capillary pressure across the interface between two immiscible fluids contained in a capillary is, by definition, the pressure difference between the non-wetting and the wetting phases (8); it can be related to the difference in level between the interface in the capillary and the free fluid-fluid interface at which $P_c = 0$ (9), and to the curvature of the interface in the capillary (10, 11). The corresponding expressions are:

$$P_c = P_{nw} - P_w \quad (2-1)$$

$$P_c = \overline{\Delta\rho} gh \quad (2-2)$$

$$P_c = \gamma c \quad (2-3)$$

where

P_{nw} is the pressure in the non-wetting phase

P_w is the pressure in the wetting phase

h is the level of the interface above or below the free fluid-fluid interface

$\overline{\Delta\rho}$ is the average value of the density difference between both fluids over the height h

γ is the interfacial tension

c is the mean curvature of the interface

These equations are based on the assumptions that the fluids are isothermal and in capillary equilibrium (12), without any other assumptions regarding the fluids or system.

Because, in a given pore and for a given system, the mean curvature is a function of saturation, it may be stated that a functional relationship should exist between the capillary pressure and the saturation (13). This will be considered in a later section.

It is well known that rings of isolated bulk liquid are formed during drainage and that some of the non-wetting phase is bypassed during imbibition. Hassler et al. (14) recognized that these immobile rings and blobs are not in true equilibrium with the main body of fluid which surrounds them, but are in apparent equilibrium; that is, the changes within the system are very slow. Morrow and Harris (15) have shown that these isolated rings and blobs of liquid are formed at the capillary pressure which existed within the continuous bulk fluid at the time of their formation, and that they remain at this pressure for a long period of time, so that their pressure is considered to be constant. Second order mass transfers such as evaporation, pellicular fluid flow, diffusion, etc., although they occur, are very slow processes and are generally not taken into account in the study of immiscible displacement. Therefore, when bulk liquid flow is complete, the system is said to be in equilibrium. It is important to make the distinction between true and apparent equilibrium and to bear in mind the fact that the isolated rings are in apparent equilibrium; it is neither possible

for the desaturation to result from the diminution of pendular rings, nor for these rings to grow in the early stage of imbibition until they coalesce, as it is sometimes suggested in the literature (16). The fact that equilibrium is apparent also explains the existence of an infinite number of families of hysteresis loops for a given system (17), and, if sufficient time were allowed for true equilibrium to occur, imbibition would cease only at full saturation (18).

White et al. (19) made an interesting study on the physics of desaturation in porous materials, with the following assumptions:

- i) gravity effects may be neglected
- ii) the porous matrix is chemically and physically stable
- iii) the porous medium is homogeneous

Figure II-1 shows how they divided the drainage curve in four sections corresponding to different modes of desaturation, for which they propose some mathematical relationships between capillary pressure and saturation, based on the assumption of relatively simple models of porous media. These divisions are:

- i) the boundary effect zone, where the capillary pressure is still less than the displacement pressure, and for which they assumed a linear relationship between saturation and capillary pressure.
- ii) the primary transition zone, where desaturation occurs in a discrete manner, and for which a logarithmic relationship is proposed.

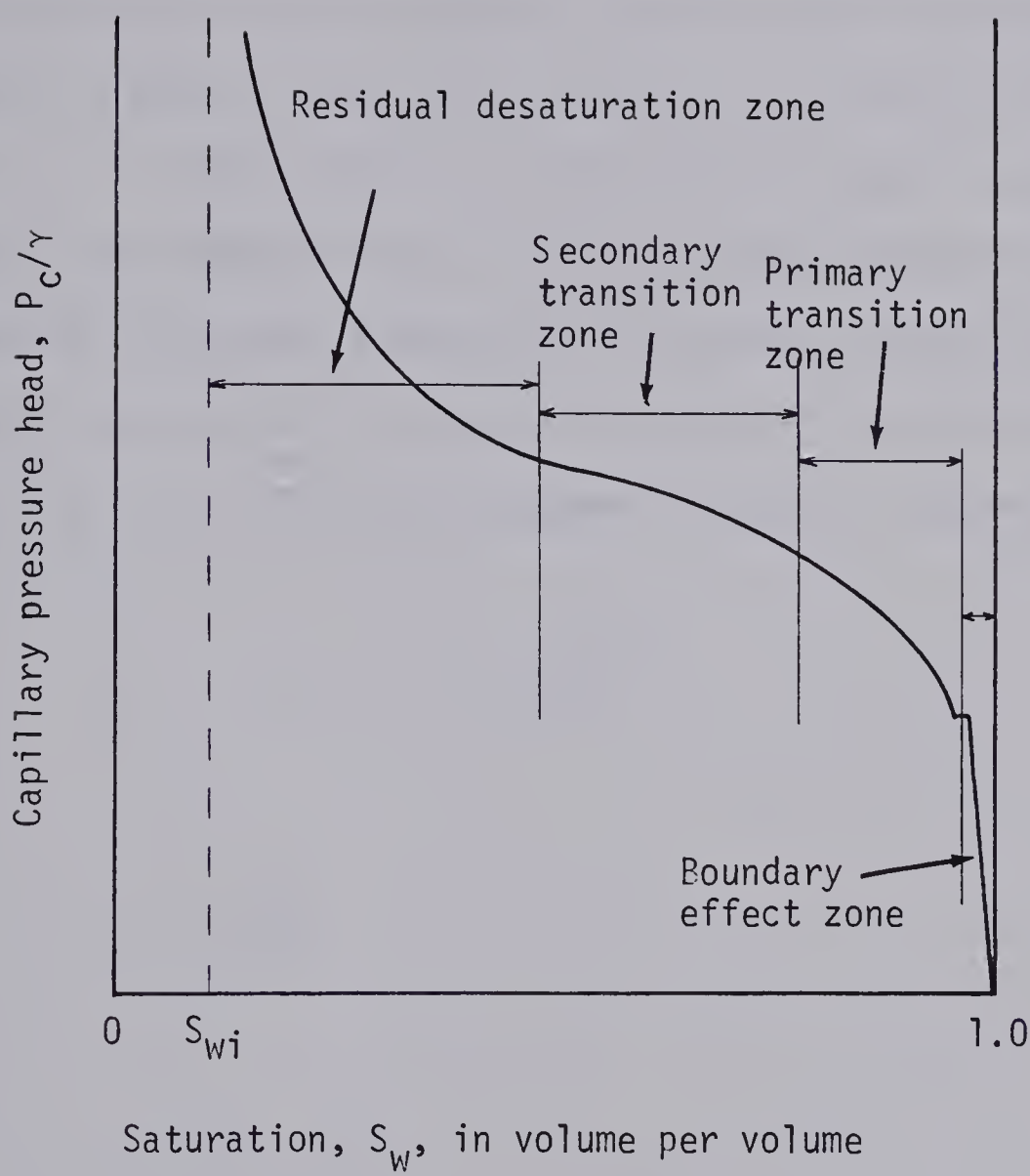


FIGURE II-1 PARTITION OF CAPILLARY PRESSURE-SATURATION CURVE
AFTER WHITE ET AL. (32)

iii) the secondary transition zone, where a relative permeability to the non-wetting phase is established and the effect of pore isolation can be neglected. Here the authors assumed, without giving any justification, that the frequency of pores that can desaturate for an incremental change in the length parameter R , measured in terms of constriction widths, is a normal distribution.

iv) the residual desaturation zone, where desaturation is due to the retreat of the non-wetting phase interface into the recesses of the pores, a mechanism difficult to accept, because pendular rings are not in true equilibrium with the main body of fluid. Here the relationship between S_w and P_c is given as

$$S_w = S_{wi} + (1 - S_{wi}) \left(\frac{P_d}{P_c} \right)^\xi \quad (2-4)$$

or

$$P_c = \frac{P_d}{S^{1/\xi}} \quad (2-5)$$

where

$$S = \frac{S_w - S_{wi}}{1 - S_{wi}}$$

P_d is the capillary displacement pressure

ξ is a constant

Although it is not stated in their paper, ξ should be greater than one in order for the area under the curve to be finite, a condition which is necessary, because this area represents the external work done on the system during the displacement (20).

White et al. (21) report some values of ξ which are less than unity, and Eq.(2-4) is, therefore, not generally applicable.

The discrete mechanism of displacement taking place in the primary transition zone was first observed by Haines (22) and is often referred to as a Haines jump or rheon (23-25). Such jumps are observed when an interface changes from an unstable to a more stable configuration. The term ison was adopted (24) to define the segments of pressure-volume displacement curve between rheons; the isons correspond to reversible displacements. It is, then, evident that such irreversible phenomena as the formation of pendular rings occur during rheons, as well as the reunion of entrapped fluid with the corresponding bulk fluid (26). It was already mentioned that the capillary pressure-saturation curve is time-independent (apparent equilibrium), and it becomes clear that this is so because rheons take place on time scale which is many orders of magnitude shorter than that of the macroscopic displacement experiment (27).

Melrose (28) pointed out that the mechanism of non-wetting phase entrapment during imbibition is different from the trapping of the wetting phase during drainage; during drainage the wetting phase is trapped in the small pores, whereas during imbibition the probability for the large pores to be bypassed is the largest. However, the imbibition curve is also made of a succession of rheons and isons, and may be considered as time-independent for practical purposes.

Such microscopic studies of the desaturation and imbibition processes (29-33), although of interest for a better understanding of the physics involved, are primarily concerned with ideal systems, and have yet to yield a sufficient degree of sophistication so as to provide a capillary pressure-saturation relationship universally applicable to any natural system. The literature is, therefore, rich in empirical or semi-empirical relationships, based on experimental observations, which are satisfactory for particular systems. In 1941, Leverett (34) proposed his widely used J-function for unconsolidated sands; it is the product of interfacial curvature and a property of the rock itself, referred to as "equivalent circular diameter of the voids in the sand" (35). It is expressed as

$$J(S) = \frac{\Delta \rho g h}{\gamma} \sqrt{\frac{K}{\Phi}} \quad (2-6)$$

where

K is the permeability of the sand

Φ is the porosity

This function was modified by Rose and Bruce (36), who introduced a contact angle as follows:

$$J(S) = \frac{\Delta \rho g h}{\gamma \cos \theta} \sqrt{\frac{K}{\Phi}} \quad (2-7)$$

Brown (37) used this form of the J-function to show that the correlation was improved by restricting its use to data obtained from a single formation, and could be further improved by dividing materials according to their lithologic types in the same formation.

In 1952, Burdine (38) used pore-size distribution data to calculate

relative permeabilities, and in 1954, Corey (39) used this work to show that, for a large number of consolidated porous rocks, the dimensionless saturation, S , is a linear function of $1/P_c^2$, i.e.

$$S = \left(\frac{P_d}{P_c}\right)^2 \quad \text{for } P_c \geq P_d \quad (2-8)$$

where P_d is the displacement capillary pressure. This relationship is, however, not generally applicable, because the approximations on which it is based are valid only for a particular pore-size distribution (40). In 1964, Brooks and Corey (41), on the observation that $\log S$ is a linear function of $\log P_c/\gamma$ for numerous isotropic unconsolidated media, suggested the following relationship:

$$S = \left(\frac{P_d}{P_c}\right)^\lambda \quad \text{for } P_c \geq P_d \quad (2-9)$$

where λ is called the pore-size distribution index of the medium and is the negative of the slope of the log-log plot mentioned above. Very recently, this model was used by Sigmund and McCaffery (42).

Any capillary pressure-saturation model should explicitly or implicitly allow for variations of wettability from one system to another. It is therefore expected that λ , in the latter model, not only reflects a characteristic of the porous medium itself, but also varies according to the pair of fluids used in each experiment conducted on a single porous medium.

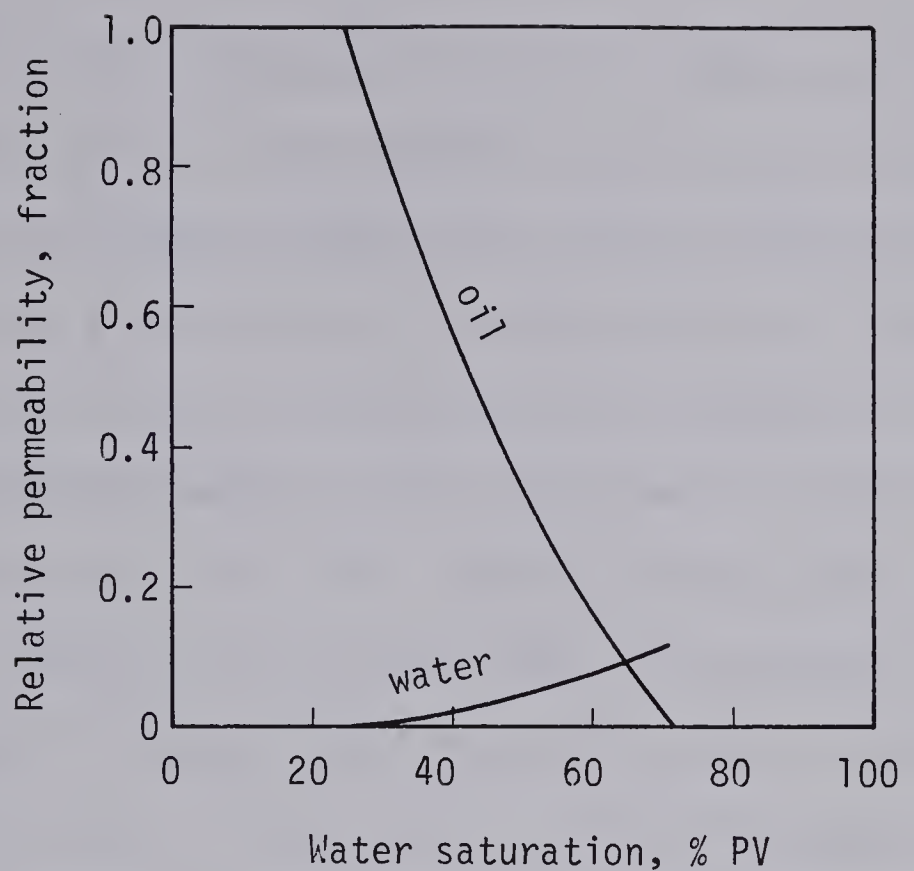
II.2 WETTABILITY

Craig (43) defines wettability as "the tendency of one fluid to spread on or adhere to a solid in the presence of other immiscible fluids". The behaviours exhibited by various systems can be totally different, and much controversy still exists in the literature regarding the wettability of reservoir rocks. Some authors (44) state that rocks are preferentially water-wet, other (45) that they are totally water-wet, some (46) have found certain cases of preferentially oil-wet rocks; Hassler et al. (47) showed the wettability to be a function of saturation, the rocks being water-wet at high saturation and more oil-wet at low saturation. They explain this fact by pointing out that the larger grains are generally quartz and calcite, which, because of their strong molecular force field, are water-wet, whereas the fine grains are generally clays and other kinds of soft minerals, which do not have a strong surface attraction and exert significant capillary action upon the fluid boundaries at low saturation only. It cannot be said, however, that soft minerals have always a tendency to be oil-wet; clays, in particular, are water-wet. The argument, therefore, does not seem to be very strong. Kinney and Nielsen (48) showed that the wettability of natural cores depends on which phase was first in place, whereas Kinney et al. (49) showed that the wettability characteristics were not always determined by the phase which initially saturated the rock. Finally, Alba (50) suggested that before oil migration occurred in the reservoirs, the rocks were probably water-wet, but that when oil migration ended, the pores filled with oil, that is, the biggest pores, became oil-wet. His conclusion is therefore contrary to that of

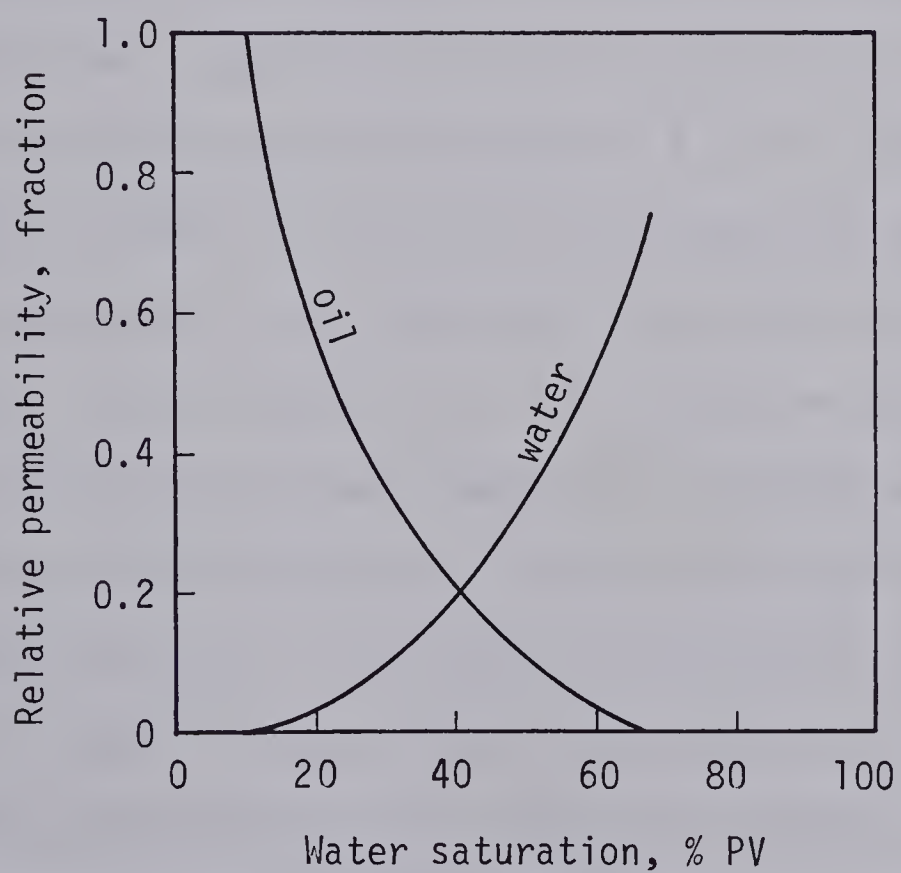
Hassler et al. (47).

Wettability is a very important factor in oil production and has a major effect on the characteristics, such as relative permeabilities, of multiphase flow in porous media, due to the very large surface area per unit volume of reservoir rocks (51). The relative mobility of oil and water is partially a function of wettability, and this accounts, among other factors, for the differences in relative permeability-saturation curves for typical water- and oil-wet rocks [Figure II-2]. For a given oil viscosity, the mobility ratio is more favourable in the case of a strongly water-wet rock than in the case of a strongly oil-wet rock, and the displacement efficiency of the former is higher than that of the latter.

Wettability is, however, not easy to measure. It is generally accepted that contact angles give the true specification of wettability (52, 53); and some very extensive studies on the relationship between contact angle and capillarity (54) and the effects of surface roughness on contact angle (55) have been reported in the literature. These studies have been made on porous samples of PTFE (polytetrafluoroethylene) with highly purified liquids, and are interesting as far as the fundamental knowledge and understanding of phenomena related to contact angles are concerned; but it would be difficult to extrapolate these results to natural systems, due to the heterogeneity of mineral composition and the highly complicated composition of crude oils. It has also been recognized (56-58) that contact angles vary with time, due to the adsorption on the solid



TYPICAL WATER-OIL RELATIVE PERMEABILITY CURVES,
STRONGLY WATER-WET ROCK (43)



TYPICAL WATER-OIL RELATIVE PERMEABILITY CURVES,
STRONGLY OIL-WET ROCK (43)

surface of polar components present in minute quantities in different crudes. Contact angles also vary due to deposits of asphalt or wax-like substances (59) and to other surface active agents which can also have an effect on interfacial tension. Hence, although still widely used, a single contact angle to characterize the wettability of a particular system may not always lead to satisfactory results. Thus, Brown and Fatt (60) used the nuclear magnetic relaxation method, instead of the contact angle, for measuring wettability. This method is based on the observation that the adjustment or relaxation rate of fluids put in a different magnetic environment is greatly affected by the surfaces of porous media. The same year, Coley et al. (61) suggested that the ratio S_{wi}/S_{or} be used as a scale for wettability, because it increases with wettability. Other tests have been suggested to evaluate wettability. Amott (62) used a method whereby he measured the amount A of oil displaced by imbibition of water in a fully oil-saturated core, and the amount B of oil displaced by water when centrifuging the core after free imbibition. Taking the ratio $A/(A + B)$ gives an index of wettability: if the ratio approaches one, the core is strongly water-wet. A similar test is done in which the core is fully water-saturated and oil is the displacing fluid. If C and D are the amounts of water extracted in the two steps of the experiment, the ratio $C/(C + D)$ is calculated, and a value of one indicates that the core is strongly oil-wet. If both ratios are equal to zero, there is neutral wettability. Another suggestion (63) is to evaluate the logarithm of the

ratio of the areas under the drainage and imbibition curves obtained with the use of a centrifuge. The method did not allow for the acquisition of the water imbibition curve for pressures greater than zero, nor the water drainage curve for pressures less than zero. For water-wet systems the logarithm of the area ratio is positive, while for oil-wet systems it is negative. This method was reported by the author to be reliable, simple and fast.

Wettability may have an effect on the shape of the capillary pressure-saturation curve. Fatt and Klikoff (64) suggested that increasing the fractional oil wettability of a uniform grain-size sand pack lowers the capillary pressure curve without affecting its shape; but if the grain-size distribution is large, the shape is also affected. It may therefore be misleading to interpret capillary pressure curves in terms of pore size distribution, if the wettability is non uniform. In 1971, Morrow and Mungan (65) reported some results, obtained on a PTFE core, showing that the capillary pressure function does not depend on contact angles up to approximately 49° , and that it systematically decreases as contact angles increase from 73° to 108° .

The actual knowledge with respect to wettability is still sparse and does not allow quantitative analysis of the phenomenon. In particular, there is no agreement regarding the method of measurement which should be used. Contact angle as a scale for wettability has been widely challenged for the reasons referred to above; another difficulty regarding contact angle, as well as capillary pressure, is the hysteresis phenomenon.

II.3 HYSTERESIS

When the state of a physical system is changed from A to B, three types of behaviour may be encountered (66):

i) equilibrium processes: if a system is slowly changed from state A to state B, and if the path from B to A is the same at any instant as the path from A to B, the process is reversible or in equilibrium.

ii) hysteresis: if AB differs from BA, but the paths are stable, the system exhibits hysteresis.

iii) metastability or supersaturation: if the paths are not completely reproducible, the process is metastable.

Hysteresis is encountered in different fields of science and has been extensively studied (31, 67-71). A very general approach has been taken by Everett, Whitton and Smith, who postulated that systems comprising a large number of independent domains, some of which might exhibit metastability, exhibit hysteresis. These domains are so small that it is not possible to detect the behaviour of any one of them, and groups of similar domains are assumed to be small.

This theory has been used successfully by Poulovassilis (70), who was able to predict the path of the primary drying scanning curves from a knowledge of experimental primary wetting scanning curves; these curves originate respectively from the imbibition and drainage boundary curves of the hysteresis loop and terminate at the extremes of the loop. He worked on constant structured discs and assumed that advancing and receding contact angles were both equal to zero; the discs were made of glass beads and were therefore strongly water-wet.

Two basic assumptions, however, limit the use of this theory:

- i) each domain can be in either of two states only.
- ii) the state of each domain is independent of the state of its neighbours; in other words, no provision is made for cooperative behaviour.

Because the areas under the capillary pressure curves correspond to the reversible work done on or by the system during displacement (20), it is clear that hysteresis is a consequence of the fact that less energy is expended by the system during the imbibition process than has been absorbed during drainage. This energy may be stored by the system in two distinct ways (72):

- i) creation of an interface between the continuous wetting phase and the trapped non-wetting phase.
- ii) change in wettability and/or contact angle.

It should be mentioned here that contact angle and capillary pressure hysteresis are distinct phenomena. The latter is due to the morphology of the interconnected pore space, within which a definite range of stable fluid-fluid configurations may exist. Both interaction between pores (73) and a continuous range of values for the contact angles (74) have been shown to exist. In fact, it is the physics of saturation and desaturation itself which is responsible, at least partially, for the capillary pressure hysteresis: the advancing non-wetting phase preferentially penetrates the large pores upon drainage and bypasses the small pores,

saturated with the wetting-phase; whereas the advancing wetting-phase preferentially penetrates the small pores upon imbibition and bypasses the larger ones. It is then expected that, at any given capillary pressure, the imbibition curve will be under the drainage curve, if the wetting-phase saturation is plotted along the abscissa.

Because interaction between pores as well as a finite range of stable fluid-fluid configurations may exist, neither of the two basic assumptions made in the independent domain theory of hysteresis is an acceptable one, as far as immiscible flow in porous media is concerned. Topp and Miller (75) showed that the theory is not generally applicable.

II.4 MEASUREMENT OF CAPILLARY PRESSURE IN SMALL CORE SAMPLES

Special techniques have been devised in order to measure capillary pressure in small core samples. These are necessary because, according to the equation

$$P_c = \overline{\Delta \rho} gh \quad (2-2)$$

high capillary pressures, by natural gravitation, are obtainable only with the use of large cores. Long unconsolidated sand packs are easy to make, but long natural homogeneous consolidated cores are generally not available.

In 1947, Bruce and Welge (76) used the restored state technique, which is also known as the displacement cell or diaphragm method (77). One of the faces of the core to be studied is carefully machined flat; the core is then cleaned, saturated with brine and placed in capillary contact with a brine-saturated membrane,

whose average pore radius is several orders of magnitude smaller than that of the sample, so that its displacement pressure is higher than any pressure used in the experiment. The core is placed on top of the disc and is surrounded by oil, whereas the other side of the diaphragm is immersed in brine. The oil pressure is increased by steps in such a way that time is allowed between each pressure increment, so that equilibrium can be reached. When equilibrium is obtained, the saturation is measured and further desaturation is carried on by increasing the oil pressure.

The same method can be used, with minor changes, to obtain the imbibition branch of the hysteresis loop.

Any combination of fluids can be used in this test, and it is generally considered to be the best and most reliable method to obtain capillary pressure-saturation curves. Its biggest disadvantage is the time requirement, which is generally several weeks for a single sample.

In 1949, Purcell (78) used the mercury injection method, in which mercury is the non-wetting phase and mercury vapour and air are the wetting-phase. A clean, dry core is placed in a chamber of known volume, and a vacuum is drawn on the cell. The chamber is then filled with mercury, and nitrogen is used to apply pressure at the top of the chamber; mercury penetrates the core, and the corresponding displaced volume is accurately measured by refilling the cell. The nitrogen pressure is further increased, and the incremental volume of mercury in the core is measured. It is, then possible to get a pressure-volume of mercury injected curve. Because of the use of

mercury, the data must be converted in order to make the comparison with other systems possible, by taking into account the differences of interfacial tensions and contact angles. The author compared the results obtained with mercury with those obtained on similar cores with the water-air system. Assuming a capillary pressure equation of the form

$$P_c = \frac{2\gamma \cos\theta}{R} \quad (2-10)$$

a comparison of capillary pressures at corresponding saturations leads to the ratio:

$$\frac{P_{c \text{ Hg}}}{P_{c \text{ air/water}}} = \frac{(\gamma \cos\theta)_{\text{Hg}}}{(\gamma \cos\theta)_{\text{air/water}}} \quad (2-11)$$

The following values were assumed to be acceptable:

$$\gamma_{\text{Hg}} = 480 \text{ mN/m}$$

$$\gamma_{\text{water}} = 70 \text{ mN/m}$$

$$\theta_{\text{Hg/solid}} = 140^\circ$$

$$\theta_{\text{water/solid}} = 0^\circ$$

and consequently,

$$\frac{P_{c \text{ Hg}}}{P_{c \text{ water/air}}} = 5.25 \simeq 5.$$

Fairly good agreement was obtained for both systems. There are some doubts, however, concerning the validity of the assumptions made,

and in 1951, Brown (37) found that by using a conversion factor in the range 5.4 to 8.3 for different cores, he could get almost perfect agreement with other data.

The main advantages of the mercury injection method are that it is very fast, it allows very high pressures to be obtained, and any kind of irregularly shaped sample may be used. However, the interpretation of data is uncertain, and the test results in the permanent loss of the samples.

In 1951, Brown (79) pointed out that, in spite of the fact that both the diaphragm and the mercury injection methods give the capillary pressure curves measured under static equilibrium, the results thus obtained were used to solve dynamic flow problems. He modified, therefore, a test previously devised by Hassler (80) for permeability measurements, and rendered it suitable for capillary pressure measurements under dynamic equilibrium. In this test, a simultaneous steady flow of oil and gas is allowed through one end of the core. The pressure drop in the oil phase is measured through specially designed semi-permeable membranes placed at the inlet and outlet ends of the core, and the flow of gas is monitored so that the pressure difference in both phases - that is, the capillary pressure - is the same on both sides. As a constant capillary pressure is established along the core, a constant saturation also exists. By varying the flow rates, a complete curve may be obtained. The agreement between dynamic and static methods was found to be very good; Brown (37) concluded, therefore, that it is justified to use data obtained under static equilibrium for dynamic flow problems. Such

a conclusion, however, is not totally justified; it is true that a dynamic method is closer to actual flow and displacement systems than a static method, and automatically corrects, at least partially, for such related factors as the difference between static and dynamic interfacial tensions or receding and advancing contact angles. However, it should be borne in mind that this method is also a method in which equilibrium is established before measurements can be made. An interesting feature of this test is that the measured saturations are true and not average saturations, provided the core is homogeneous. It is, however, slow and requires much care.

It was deemed necessary to devise a method whereby equilibrium would obtain quickly. The centrifuge method was probably used for the first time by McCullough et al.(81), but the first extensive consideration of its mathematical aspect is due to Hassler and Brunner (82), who also used an entirely different core-holding cell. Referring to Eq.(2-2), it is obvious that high capillary pressures can be obtained either with very long core samples in the earth field of gravity, or with an increased field of gravity on small core samples. The centrifuge method makes use of the latter option.

The capillary pressure may be determined provided the speed of rotation, the density difference between the fluids, and a few geometrical parameters, resulting from the design of the equipment used, are known; the average saturation within the core is derived from a material balance. It is thus possible to get a curve relating the capillary pressure at any point in the core to the average

saturation within the core at this capillary pressure. In the following derivation, two assumptions are made:

- i) the capillary pressure is zero at the outer end of the core.
- ii) the variation of acceleration along the core is negligible.

Let L be the length of the core
 $\Delta\rho$ the density difference between the fluids used
 g the acceleration
 h the distance above the outer end of the core at which the capillary pressure is calculated.

The saturation S_w along the core is a function of the capillary pressure, and the average saturation is given by

$$\overline{S_w} = \frac{1}{L} \int_0^L S_w(\Delta\rho gh) dh \quad (2-12)$$

By choosing $P_{ci} = \Delta\rho g L$ as the variable, Eq.(2-12) may be written as

$$P_{ci} \overline{S_w} = \int_0^{P_{ci}} S_w(P_c) dP_c \quad (2-13)$$

from which it follows that

$$S_w(P_{ci}) = \frac{d}{dP_{ci}} (\overline{S_w} P_{ci}) \quad (2-14)$$

Hassler and Brunner (83) used graphical differentiation to obtain the capillary pressure-saturation curve.

Let r_i and r_e be, respectively, the distances of the inner and outer ends of the core to the axis of rotation, and ω the angular velocity of the centrifuge. If the variation of the centrifugal field is taken into account, the following equations apply:

$$P_c = \Delta \rho \omega^2 (r_e - \frac{h}{2}) h \quad (2-15)$$

$$P_{ci} = \frac{1}{2} \Delta \rho \omega^2 (r_e^2 - r_i^2) = \Delta \rho \omega^2 (r_e - \frac{L}{2}) L \quad (2-16)$$

$$dh = \frac{dP_c}{\Delta \rho \omega^2 \sqrt{r_e^2 - \frac{P_c}{P_{ci}} (r_e^2 - r_i^2)}} \quad (2-17)$$

Therefore, Eq.(2-12) may be written as follows:

$$\overline{S_w} = \frac{1}{\Delta \rho L \omega^2} \int_0^{P_{ci}} \frac{S_w(P_c) dP_c}{\sqrt{r_e^2 - \frac{P_c}{P_{ci}} (r_e^2 - r_i^2)}} \quad (2-18)$$

or

$$\overline{S_w} = \frac{r_e - \frac{L}{2}}{r_e P_{ci}} \int_0^{P_{ci}} \frac{S_w(P_c) dP_c}{\sqrt{1 - \frac{P_c}{P_{ci}} (1 - \frac{r_i^2}{r_e^2})}} \quad (2-19)$$

Therefore,

$$P_{ci} \overline{S_w} = \frac{1}{2} (1 + \frac{r_i}{r_e}) \int_0^{P_{ci}} \frac{S_w(P_c) dP_c}{\sqrt{1 - \frac{P_c}{P_{ci}} (1 - \frac{r_i^2}{r_e^2})}} \quad (2-20)$$

and

$$P_{ci} \overline{S_w} = \cos^2 \frac{\Psi}{2} \int_0^{P_{ci}} \frac{S_w(P_c) dP_c}{\sqrt{1 - \frac{P_c}{P_{ci}} \sin^2 \Psi}} \quad (2-21)$$

where $\cos \Psi = r_i/r_e$.

Equation (2-21) cannot be solved simply for the function S_w , and a method of successive approximations was proposed by the authors. This method, however, is very tedious, and they reported that for values of the ratio r_i/r_e as small as 0.7, the approximation given by Eq.(2-14) is usually sufficient.

Few data were given by Hassler and Brunner (82). In 1951, Slobod et al. (84) reported results which showed the method to be rapid and reliable; high capillary pressures were obtained as well as values of connate water and residual oil saturations.

At this point in time, however, only one branch of the hysteresis loop, namely drainage, could be obtained by this method, and according to Donaldson et al. (63):

"the water imbibition curve for pressures greater than zero and the water drainage curve for pressures less than zero cannot be obtained by the centrifugal technique".

In 1974, Szabo (6) devised three different core-holding cells, whereby it is possible to measure imbibition capillary pressure using the centrifugal technique. All of them meet the following necessary requirements:

i) the direction of phase exchange occurs as a result of the natural fluid differences; that is, the water enters the sample moving off the rotary axis.

ii) the quantity of imbibed water is controllable.

To achieve this, a semi-permeable filter disc, which separates the water reservoir from the sample, is placed in capillary contact with the inner end of the sample. The water reservoir is above the filter

disc and is opened to the atmosphere. The disc is water saturated, and the sample is surrounded by the oil phase. When starting the imbibition, a speed is chosen that will allow the capillary pressure inside the core to be somewhat smaller than the capillary pressure created at the end of the drainage experiment. When equilibrium is obtained, the average saturation is determined by weighing or by material balance, and a lower speed is selected to allow further imbibition. A decrease in speed results in a decrease in capillary pressure, and therefore imbibition occurs. The time necessary to stop the centrifuge is so small as compared to the time necessary for the fluids inside the core to reach equilibrium, that Szabo (85) assumed it does not allow further imbibition within the core to occur.

The first technique consists of measuring the capillary pressure within a small core sample. Imbibition as well as drainage could be obtained, but the design of the cell is such that both oil and water columns are large and limit the maximum speed of rotation required. Moreover, the cell must be disassembled after each run, and the method is therefore slow and tedious.

A second method was designed to measure the imbibition capillary pressure in cores of intermediate length. Because of the length of the samples used in this method, the difference in the capillary pressures at both ends of the samples is significant, and the saturation varies along their length. An average saturation is thus obtained, and the author proposed the use of graphical differentiation in order to calculate the saturation at the inner end of the core. Provided an acceptable capillary pressure model is

found, a numerical solution to this problem would be preferable (86).

The third method suitable for drainage as well as imbibition capillary pressure measurements was referred to as the "quick method" by the author. It consists of using a long core sample cut into slices, which are held in capillary contact by discs of filter paper placed in between each slice. Upon reaching equilibrium the average saturation within each slice is measured by weighing, and Szabo (87) plotted the capillary pressure calculated at the center of each slice against the average saturation of the corresponding slice.

CHAPTER III

STATEMENT OF PROBLEM

Capillary pressure is a very important phenomenon, and it is deemed necessary to be able to obtain reliable capillary pressure-saturation data in short periods of time. The centrifuge method seems to be the only one which satisfies this time requirement. This method, however, is not direct, and it is necessary to convert the experimental data into a true capillary pressure curve. It is, therefore, important to get a good understanding of what the centrifuge data really represent.

The quick method proposed by Szabo (88) was selected to obtain capillary pressure-saturation curves. Reasons for the choice of this technique were:

- i) it seems suitable to obtain drainage and imbibition curves.
- ii) several points are obtained at once, and therefore the method is fast.
- iii) a saturation close to the irreducible saturation may be obtained more easily than if a core of intermediate length were used.
- iv) if the slices are small, there is a lesser effect of gravity as compared to conventional methods; therefore, the experimental curve should be closer to the true curve.

v) the end effect is expected to be of lesser importance, as compared to that obtained in the conventional centrifugal technique, because the range of rotational speeds for the quick method is smaller than that necessary to obtain the capillary pressure curve with one core of small or intermediate length.

Most capillary pressure studies are restrained to the drainage process, whereas waterflooding is mainly concerned with the imbibition mechanism. Attempts were therefore made to obtain imbibition data using the centrifugal method.

Finally, a new mathematical model relating capillary pressure and saturation was studied to convert the experimental data into a true capillary pressure curve; this was rendered necessary due to the fact that the average saturation in the core, and not the saturation corresponding to the calculated capillary pressure, was measured.

CHAPTER IV

CAPILLARY PRESSURE MODEL

IV.1 DRAINAGE

IV.1.1 Drainage Model

Because the capillary pressure at any point is directly related to the mean curvature of the interface at that point, and because, for a given system, the mean curvature is a function of the saturation (9), it should be possible to express the capillary pressure as a function of saturation.

Two kinds of drainage capillary pressure curves are found in the literature [Figure IV-1]. In his study of the role of gravity in capillary pressure measurements, Szabo (89) showed that the concavity of curve 2, near the maximum saturation, is due to the effect of gravity on cores of finite dimensions and is not a characteristic of the drainage capillary pressure-saturation relationship itself. Curve 1, on the contrary, represents the capillary pressure-saturation curve for a very thin porous disc; it approaches, therefore, the true capillary pressure curve, because it relates, in the limit, the capillary pressure and the saturation in the corresponding plane, excluding any gravity effect. Therefore, a mathematical model plotting as curve 1 is thought to be suitable.

Several empirical or semi-empirical mathematical models have been used in the literature (7, 19, 41, 90, 91); some of

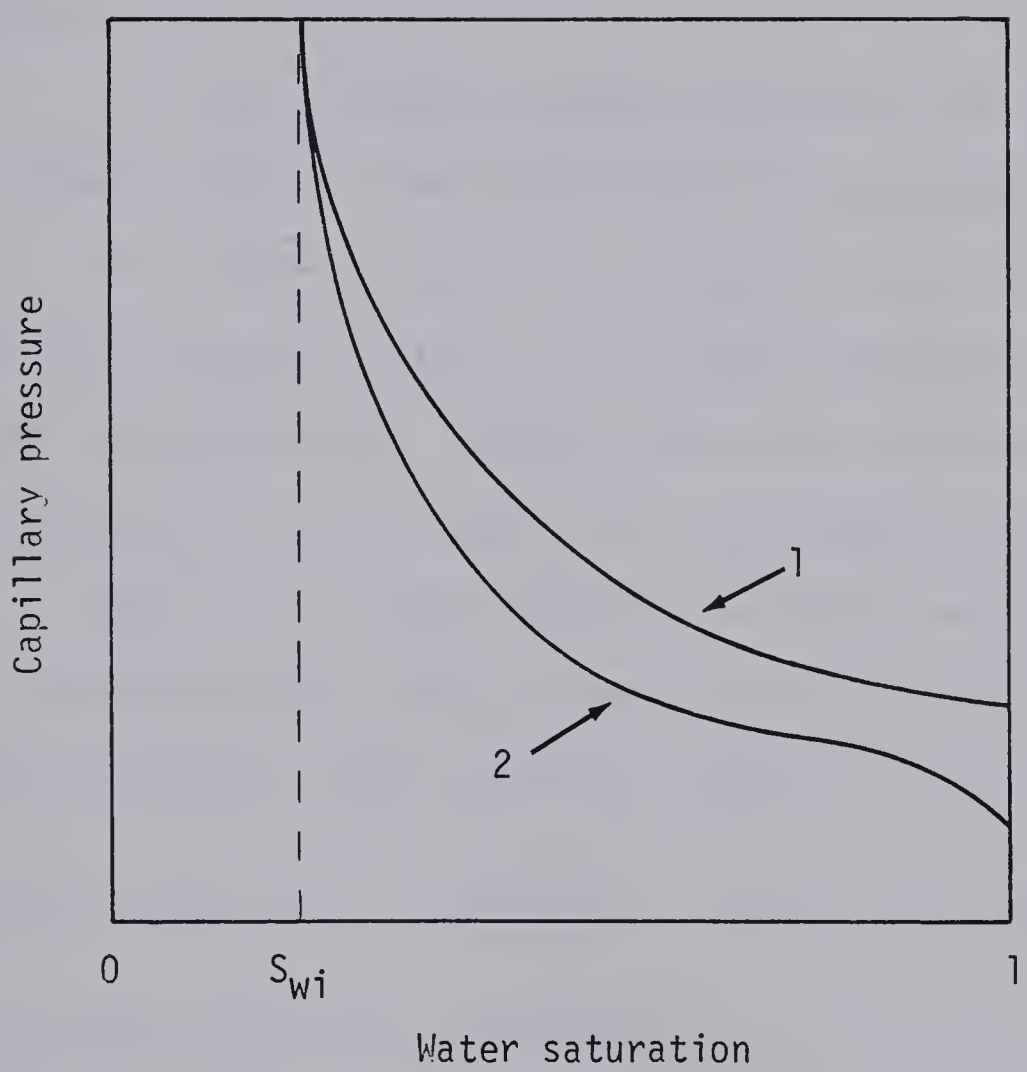


FIGURE IV-1 CAPILLARY PRESSURE CURVES ENCOUNTERED
IN THE LITERATURE (89)

them (90) are, a priori, not acceptable, because they fail to meet several basic requirements. These requirements are the consequence of the physics involved as well as of the necessary compatibility of the models with the displacement equation of one fluid by another, and may be summarized as follows (7):

i) the slope of the drainage capillary pressure curve must tend to minus infinity when the water saturation approaches the irreducible water saturation.

ii) the drainage capillary pressure curve must tend to a fixed, finite value, as the water saturation approaches one.

iii) the area under the drainage capillary pressure-saturation curve must finite, as this area corresponds to the reversible external work. Moreover, any functional relationship postulated must of course, agree with experimental evidence.

The first of these modelling conditions was proposed by Fayers and Sheldon (92), who assumed that dP_c/dS behaves like $-1/S$ near the irreducible water saturation, where S is the saturation

in dimensionless form, $S = \frac{S_w - S_{wi}}{1 - S_{wi}}$. On this basis, Anli (93)

derived a model defined in the domain

$$0 < S \leq 1$$

$$P_d \leq P < \infty$$

where P_d is the displacement pressure and has a finite value according to the second requirement. Assuming

$$\frac{dP_c}{dS} = -\frac{\sigma}{S} \quad (4-1)$$

and integrating with respect to S in the domain previously defined, yields

$$P_c = -\sigma \ln S + P_d \quad (4-2)$$

where

σ is a parameter which includes the effects of wettability, interfacial tension and pore-size distribution, and has the dimensions of pressure.

This model can be written in dimensionless form as follows:

$$\pi_c = -\ln S \quad (4-3)$$

where

$$\pi_c = \frac{P_c - P_d}{\sigma} \text{ is a dimensionless capillary pressure.}$$

Although it meets all of the criteria mentioned above, this model suffers from the fact that, as the water saturation approaches the irreducible saturation, the capillary pressure goes to plus infinity. To remedy this situation, Eq.(4-1) was modified to

$$\frac{dP_c}{dS} = -\frac{\sigma}{S^n} \quad n \neq 1 \quad (4-4)$$

which, upon integration, yields

$$P_c = \frac{\sigma}{1-n} (1 - S^{1-n}) + P_d \quad (4-5)$$

Equation (4-5) may be written in dimensionless form as

$$\pi_c = \frac{1 - S^{1-n}}{1-n} \quad (4-6)$$

where

$$\pi_c = \frac{p_c - p_d}{\sigma} \text{ is a dimensionless capillary pressure.}$$

This modification does not, as it seems to, violate the condition imposed by Fayers and Sheldon (92), and is therefore valid; this is shown in Appendix A.

It is immediately evident that this model meets the first and second requirements. The area under the curve is given by

$$\text{area} = \frac{\sigma}{1-n} \left[S - \frac{S^{2-n}}{2-n} \right]_0^1 + p_d \quad (4-7)$$

and, therefore, n must be strictly less than 2 in order for the third requirement to be met. However, for $1 < n < 2$, the capillary pressure goes to plus infinity as the water saturation approaches the irreducible saturation; therefore, the condition that $0 < n < 1$, was imposed on the model. The agreement with the experimental evidence is one of the objects of the experimental study and will be considered later on.

Equation (4-5) may also be written as

$$S_w = S_{wi} + (1 - S_{wi}) \left(\frac{1-n}{\sigma} \right)^{\frac{1}{1-n}} (p_d - p_c + \frac{\sigma}{1-n})^{\frac{1}{1-n}} \quad (4-8)$$

The experimentally measured water saturation is, in fact, an average saturation, because a core has a definite thickness, whereas a relationship such as expressed by Eq.(4-8) relates the capillary pressure in a certain plane in the core to the saturation in the same plane; this equation must, therefore, be adapted to the kind of experimental data obtained.

IV.1.2 Application of the Model to the Drainage Data Obtained with the Centrifuge and the Multi-Slice Core Technique

The two directly available data, with this technique, are the average saturation in each slice and the capillary pressure at any point along the core. Assuming that the capillary pressure is zero at the outer end of the sample (83), the capillary pressure is given by

$$P_c = A\Delta\rho\omega^2 \left(r_e - \frac{h}{2}\right) h \quad (4-9)$$

Let us consider the core to be made of a superposition of q slices in capillary contact, and let us number the contact planes as shown in Figure IV-2. The average saturation in the j^{th} slice is

$$\overline{S_{wj}} = \frac{1}{H_j} \int_{h_{j-1}}^{h_j} S_w dh \quad (4-10)$$

where H_j and h_j are defined in Figure IV-2.

Combining Eq.(4-8), Eq.(4-9) and Eq.(4-10) yields

$$\overline{S_{wj}} = S_{wi} + \frac{1 - S_{wi}}{A\Delta\rho\omega^2 H_j} \left(\frac{1}{\sigma}\right)^{\frac{1}{1-n}} \int_{P_{j-1}}^{P_j} \frac{\left(P_d - P_c + \frac{\sigma}{1-n}\right)^{\frac{1}{1-n}}}{\sqrt{r_e^2 - \frac{2P_c}{A\Delta\rho\omega^2}}} dP_c \quad (4-11)$$

where A is the unit conversion factor.

Equation (4-11) is valid only for the slices for which $h_{j-1} \geq h^*$, where h^* is the location of the plane at which $P_c = P_d$. If h^* is located in the g^{th} slice, the average saturation, $\overline{S_{wg}}$, of this slice is given by

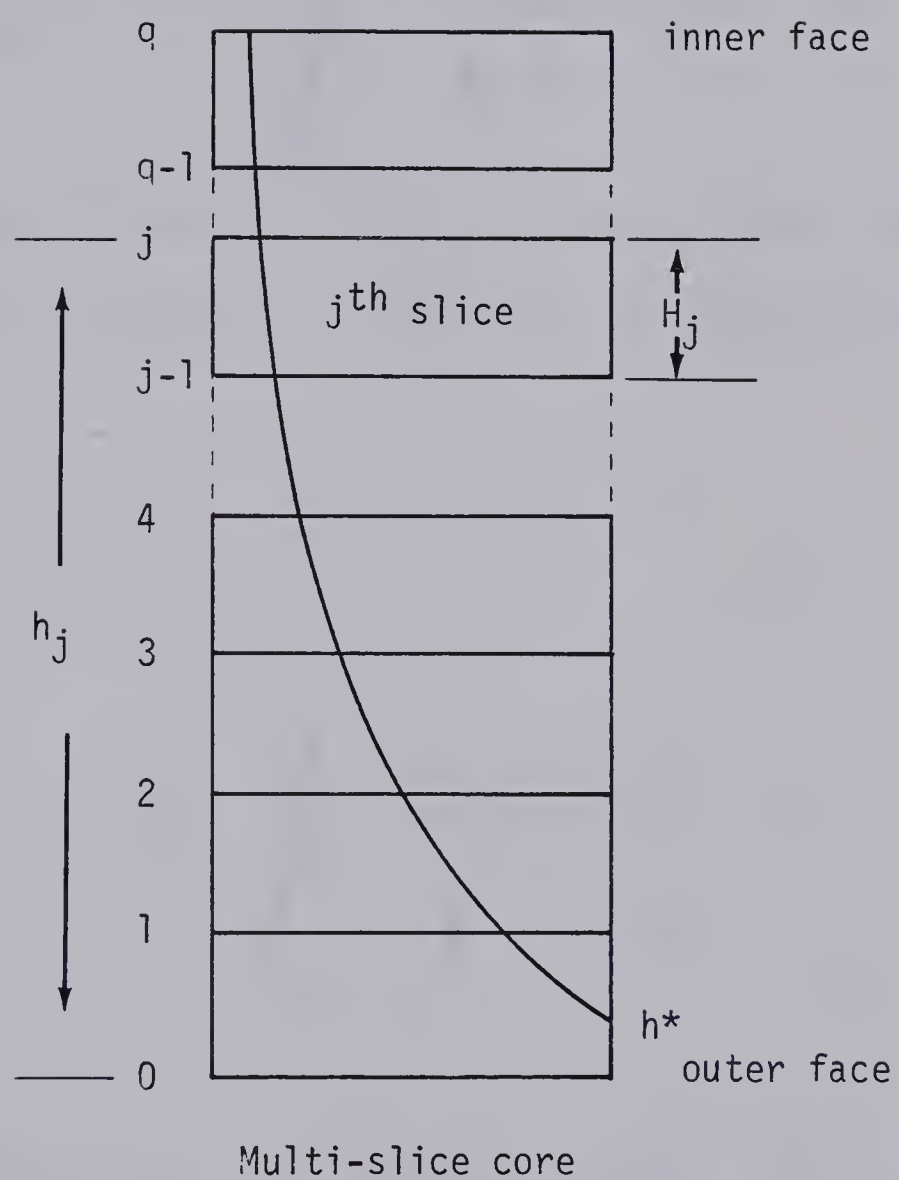


FIGURE IV-2

$$\overline{S_{wg}} = \frac{S_{wi} h_g - h_{g-1}}{H_g} + \frac{1 - S_{wi}}{H_g} \left(r_e - \sqrt{r_e^2 - \frac{2P_d}{A\Delta\rho\omega^2}} \right) + \frac{1 - S_{wi}}{AH_g \Delta\rho\omega^2} \left(\frac{1}{\sigma} \right)^{\frac{1}{1-n}} \int_{P_d}^{P_g} \frac{\frac{(P_d - P_c + \frac{\sigma}{1-n})}{1-n}}{\sqrt{r_e^2 - \frac{2P_c}{A\Delta\rho\omega^2}}} dP_c \quad (4-12)$$

The model proposed by Bentsen and Anli (7) was also used for comparison purposes. In this case, Eq.(4-2) must be rewritten as

$$S_w = S_{wi} + (1 - S_{wi}) \exp \left(- \frac{P_c - P_d}{\sigma} \right) \quad (4-13)$$

Then,

$$\overline{S_{wj}} = S_{wi} + \frac{1 - S_{wi}}{A\Delta\rho\omega^2 H_j} \int_{P_{j-1}}^{P_j} \frac{\exp \left(- \frac{P_c - P_d}{\sigma} \right)}{\sqrt{r_e^2 - \frac{2P_c}{A\Delta\rho\omega^2}}} dP_c \quad (4-14)$$

and

$$\overline{S_{wg}} = \frac{S_{wi} h_g - h_{g-1}}{H_g} + \frac{1 - S_{wi}}{H_g} \left(r_e - \sqrt{r_e^2 - \frac{2P_d}{A\Delta\rho\omega^2}} \right) + \frac{1 - S_{wi}}{A\Delta\rho\omega^2 H_g} \int_{P_d}^{P_g} \frac{\exp \left(- \frac{P_c - P_d}{\sigma} \right)}{\sqrt{r_e^2 - \frac{2P_c}{A\Delta\rho\omega^2}}} dP_c \quad (4-15)$$

Equations (4-11) and (4-12) are derived in Appendix B. These equations cannot be solved analytically and were solved numerically.

It is evident that two kinds of experimental curves may be obtained. On the one hand, one may plot P_j against $\overline{S_{wj}}$; on the other hand, one may plot P_j against $\overline{\overline{S_{wj}}}$, where

$$\overline{\overline{S_{wj}}} = \frac{1}{h_j} \int_0^{h_j} S_w dh \quad (4-16)$$

$$\begin{aligned} &= S_{wi} + \frac{1 - S_{wi}}{h_j} \left(r_e - \sqrt{r_e^2 - \frac{2P_d}{A\Delta\rho\omega^2}} \right) \\ &+ \frac{1 - S_{wi}}{h_j A\Delta\rho\omega^2} \left(\frac{1-n}{\sigma} \right)^{\frac{1}{1-n}} \int_{P_d}^{P_j} \frac{1}{\sqrt{r_e^2 - \frac{2P_c}{A\Delta\rho\omega^2}}} dP_c \quad (4-17) \end{aligned}$$

If the logarithmic model is used, then

$$\begin{aligned} \overline{\overline{S_{wj}}} &= S_{wi} + \frac{1 - S_{wi}}{h_j} \left(r_e - \sqrt{r_e^2 - \frac{2P_d}{A\Delta\rho\omega^2}} \right) \\ &+ \frac{1 - S_{wi}}{h_j A\Delta\rho\omega^2} \int_{P_d}^{P_j} \frac{\exp \left(-\frac{P_c - P_d}{\sigma} \right)}{\sqrt{r_e^2 - \frac{2P_c}{A\Delta\rho\omega^2}}} dP_c \quad (4-18) \end{aligned}$$

$\overline{\overline{S_{wj}}}$ can be obtained from the experimental results by Eq.(4-19):

$$\overline{\overline{S_{wj}}} = \frac{\sum_{i=1}^j v_i}{\sum_{i=1}^j v_{p_i}} \quad (4-19)$$

where

v_i is the volume of water in the i^{th} slice at the end of the experiment.

v_{p_i} is the pore volume of the i^{th} slice.

IV.2 IMBIBITION

IV.2.1 Imbibition Model

Assuming the imbibition curve to have the shape represented in Figure IV-3, the two previously defined models were supposed to be suitable to represent the imbibition capillary pressure-saturation relationship with, however, the following modifications:

$$S = \frac{S_w - S_{wi}}{1 - S_{wi} - S_{or}} \quad (4-20)$$

and

$$P_d = 0$$

Hence, Eq.(4-2) and Eq.(4-5) become, respectively,

$$P_c = -\sigma \ln S \quad (4-21)$$

and

$$P_c = \frac{\sigma}{1-n} (1 - S^{1-n}) \quad (4-22)$$

IV.2.2 Application of the Model to the Imbibition Data Obtained with the Centrifuge and the Multi-Slice Core Technique

The experimental capillary pressure is calculated by the following expression (87), derived in Appendix D:

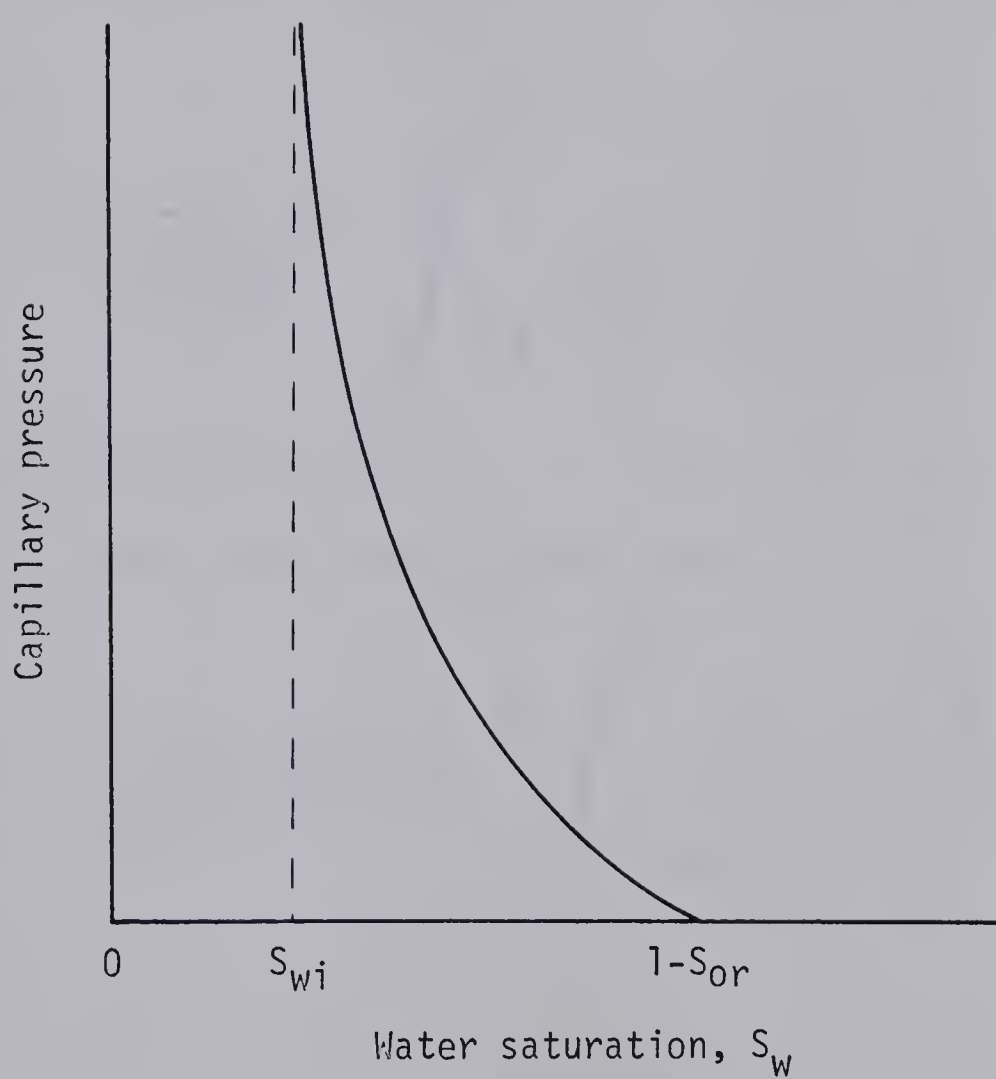


FIGURE IV-3 IMBIBITION CAPILLARY PRESSURE CURVE

$$P_c = \frac{A\omega^2}{2} [(r_e - h)^2(\rho_o - \rho_w) + r_w^2 \rho_w - r_o^2 \rho_o] \quad (4-23)$$

Combining Eq.(4-10), Eq.(4-20), Eq.(4-21) and Eq.(4-23) yields

$$\overline{S_{wj}} = S_{wi} + \frac{1 - S_{wi} - S_{or}}{h_j A\omega^2 \sqrt{\Delta\rho}} \int_{P_{j-1}}^{P_j} \frac{\exp(-\frac{P_c}{\sigma})}{\sqrt{-\frac{2P_c}{A\omega^2} + r_w^2 \rho_w - r_o^2 \rho_o}} dP_c \quad (4-24)$$

or,

$$\overline{\overline{S_{wj}}} = S_{wi} + \frac{1 - S_{wi} - S_{or}}{h_j A\omega^2 \sqrt{\Delta\rho}} \int_{P_0}^{P_j} \frac{\exp(-\frac{P_c}{\sigma})}{\sqrt{-\frac{2P_c}{A\omega^2} + r_w^2 \rho_w - r_o^2 \rho_o}} dP_c \quad (4-25)$$

where P_0 is the capillary pressure at the outer end of the core.

If Eq.(4-22) is used instead of Eq.(4-21), then

$$\overline{S_{wj}} = S_{wi} + \frac{1 - S_{wi} - S_{or}}{h_j A\omega^2 \sqrt{\Delta\rho}} \left(\frac{1-n}{\sigma}\right)^{\frac{1}{1-n}} \int_{P_{j-1}}^{P_j} \frac{\frac{1}{1-n} \left(\frac{\sigma}{1-n} - P_c\right)^{\frac{1}{1-n}}}{\sqrt{-\frac{2P_c}{A\omega^2} + r_w^2 \rho_w - r_o^2 \rho_o}} dP_c \quad (4-26)$$

or,

$$\overline{\overline{S_{wj}}} = S_{wi} + \frac{1 - S_{wi} - S_{or}}{h_j A\omega^2 \sqrt{\Delta\rho}} \left(\frac{1-n}{\sigma}\right)^{\frac{1}{1-n}} \int_{P_0}^{P_j} \frac{\frac{1}{1-n} \left(\frac{\sigma}{1-n} - P_c\right)^{\frac{1}{1-n}}}{\sqrt{-\frac{2P_c}{A\omega^2} + r_w^2 \rho_w - r_o^2 \rho_o}} dP_c \quad (4-27)$$

Equation (4-24), Eq.(4-25), Eq.(4-26) and Eq.(4-27) are derived in Appendix C.

CHAPTER V

EXPERIMENTAL EQUIPMENT AND PROCEDURE

The experimental procedure used in this study is similar to that used by Szabo (88); he referred to this method as the "quick method for capillary pressure measurement". A long core sample, cut into slices, is rotated in a centrifuge. The slices, which are supposed to be homogeneous and to have the same permeabilities, are maintained in capillary contact with the aid of Kleenex paper placed in between each slice; moreover, a coil spring acts on top of the core holder which forces the slices against each other. Several authors (88, 94, 95) have used this procedure to maintain samples in capillary contact; it does not appear to affect the capillary pressure distribution, and consequently, does not appear to affect the saturation distribution within the core.

The advantage of the quick method for capillary pressure measurement, as compared to the conventional use of the centrifuge in the study of capillary pressure, lies in the reduction of time which is required to obtain the whole drainage capillary pressure curve. Moreover, Szabo (85) presents some imbibition curves obtained with the same method, and according to his work, it seems possible to obtain the whole hysteresis loop in a matter of days.

V.1 THE CENTRIFUGE

An IEC PR-6000 centrifuge was used in this study, together with a model 276 four-place rotor for which the maximum authorized rotational speed is 3000 rpm. This centrifuge is provided with a feedback speed control, whereby the selected speed is kept constant within $\pm 1.5\%$, and a temperature control device, for temperatures ranging from -10°C to $+30^{\circ}\text{C}$. It also features a flexible drive shaft which eliminates the need for critical balancing of the cells. A window was cut in the cover of the centrifuge to allow accurate measurement of the speed of rotation with a stroboscope, because the scale of the electric tachometer provided on the centrifuge was graduated in 100 rpm increments, and was too coarse for the purpose of this study.

V.2 DRAINAGE

V.2.1 Drainage Capillary Pressure Cell

The drainage capillary pressure cell was designed to receive large cylindrical cores, about 7.2 cm long and 2.5 cm in diameter. A cross-section of the cell in actual dimensions is given in Figure V-1. The cell body and the core holder were made of lucite to allow for visual examination; this, however, has the disadvantage of limiting seriously the choice of fluids which can be used in the experiments. The core holder was grooved vertically and bored with a series of holes at its top to prevent the presence of air bubbles around the core. The top and bottom caps, as well as the core support disc, were made of aluminum; the core support disc was

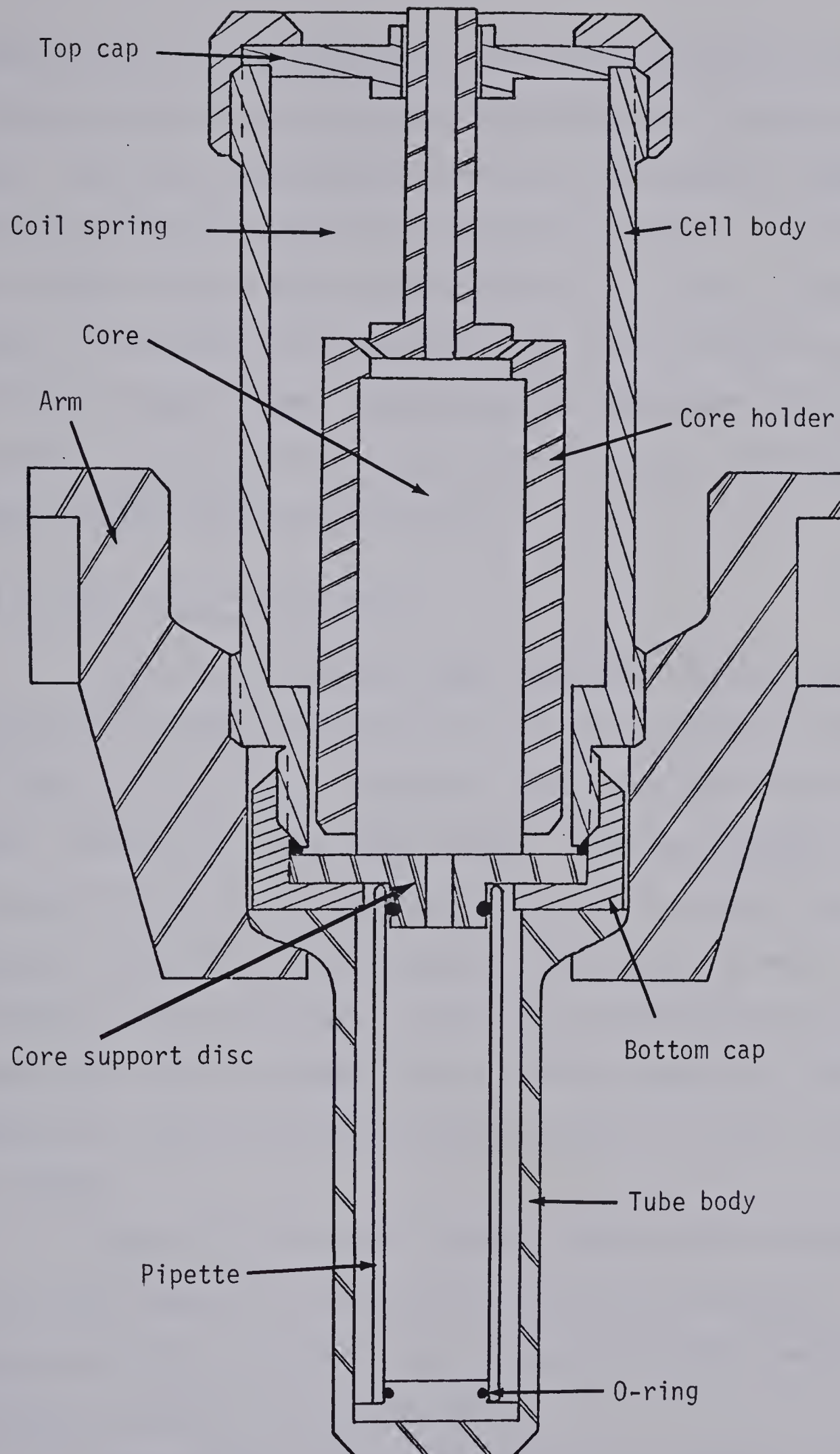


FIGURE V-1

DRAINAGE CAPILLARY PRESSURE CELL

radially and circularly grooved to allow free circulation of fluids from the core into the pipette, and from the pipette into the cell body. The pipette, provided to receive the water expelled from the core, was attached to the core support disc by means of a seal o-ring and was made of glass able to withstand an inside excess pressure of 16 MPa. The bottom plug of the pipette was made of teflon and sealed by means of a seal o-ring. The arm and tube bodies were made of mild steel for a proper location of the center of gravity. Two such equally weighed cells were constructed.

V.2.2 Core and Cell Preparation

The slices of the core under study were first cleaned with toluene in a soxhlet extractor, dried at 150°C, and heated at 500°C for about 10 to 12 hours to remove any organic residuals from the pore space. The dry slices were then weighed, placed under vacuum, and saturated with de-aerated distilled water. The saturated slices were weighed in water to prevent evaporation, and the mass of water present in each slice was calculated. It should be pointed out that this method might lead to erroneous values of water saturation in the case where cores containing large quantities of water of crystallization are studied.

Because each slice was slightly different from the others, it was very important to characterize them and to distinguish between the inlet and outlet faces. They were therefore numbered, so that no confusion could be possible.

After assembling the drainage capillary pressure cells, the pipettes were filled with oil. Excess water was blotted from the

surface of each slice, and the cores were made by alternating the slices, according to their numbers, and small discs of Kleenex paper having the diameter of the samples. The cores were then inserted in the core holders and placed in the cells; these were then filled with oil, so that the cores were totally immersed.

A speed of rotation was selected, and the drainage experiment was started. When apparent equilibrium was reached, that is, when no more water was expelled from the core over a sufficient period of time (10 to 12 hours), the centrifuge was stopped and the slices were weighed in oil to prevent evaporation.

V.2.3 Drainage Capillary Pressure and Saturation Measurement

The speed of rotation was accurately measured with a stroboscope, and the densities of the fluids were determined with an AP Paar DMA60-Digital Density Meter. The capillary pressure is given by

$$P_c = 1.097 \times 10^{-6} \Delta \rho \omega^2 (r_e - \frac{h}{2}) h \quad (5-1)$$

where

P_c , kPa

$\Delta \rho$, g/cc

ω , rpm

r_e is the distance from the axis of rotation to the bottom of the core, cm

h is the distance from the bottom of the core to the point where P_c is calculated, cm.

This equation is based on the assumption that the capillary pressure vanishes at the outlet end of the core.

The average saturation in each slice is

$$\overline{S_w} = 1 - \frac{M_w' - M_L}{V_p \Delta \rho} \quad (5-2)$$

where

M_w' is the mass of water in the 100%-water-saturated slice, g

M_L is the mass of water and oil contained in the slice at the end of the run, g

V_p is the pore volume of the slice, cm^3

Equations (5-1) and (5-2) are derived in Appendix D.

V.3 IMBIBITION

V.3.1 Imbibition Capillary Pressure Cell

The drainage capillary pressure cell was designed so that it could be used to study imbibition, provided the core holder were changed. As already mentioned, it is necessary for the water to move off the rotary axis in order to take advantage of the increased gravitational field; thus, the outlet end of the core should not be in contact with the water reservoir. Nor can a situation in which the core is immersed in water be considered, because, in this case, the amount of imbibition could not be regulated. Therefore, the water reservoir must be placed at the top of the core. Because it is desired to study the capillary pressure curve in the positive capillary pressure domain, the system must be such that, at all points, the pressure in the oil phase is higher than or equal to the pressure

in the water phase. This is true, in particular, at the top of the core, and therefore a semi-permeable membrane must be used to isolate the water reservoir from the oil reservoir; this membrane must be water-wet and such that its displacement pressure is higher than any capillary pressure reached in the course of the experiment. The imbibition capillary pressure cell is shown in actual dimensions in Figure V-2. The water reservoir was made of lucite to allow for visual examination of the water level, and the core holder was made of aluminum.

Many problems were encountered in preventing leakage of oil into the water reservoir. Because it was necessary for the membrane to be permeable to water only, it was, indeed, deemed important to be able to clean it and to heat it at high temperature, in order to eliminate any organic material from the pore space and render it strongly water-wet. Different solutions have been envisaged, among which a tight fit seemed to be the best. Lucite and titanium rings were precision-machined to shrink-fit the membrane, but, although much care was taken to machine the rings as well as the membranes, no fit was able to withstand an excess pressure of more than 28 kPa. A second possible solution was to cast a low melting-point metal around the membrane; many attempts were made with aluminum, but the presence of air in the pore space of the disc always resulted in the formation of a small air bubble at some point between the membrane and the aluminum mold. A third solution, considered as a compromise, was to place the disc in an epoxy resin; both faces of the membrane were protected by a piece of paper tape, prior to immersing it in the

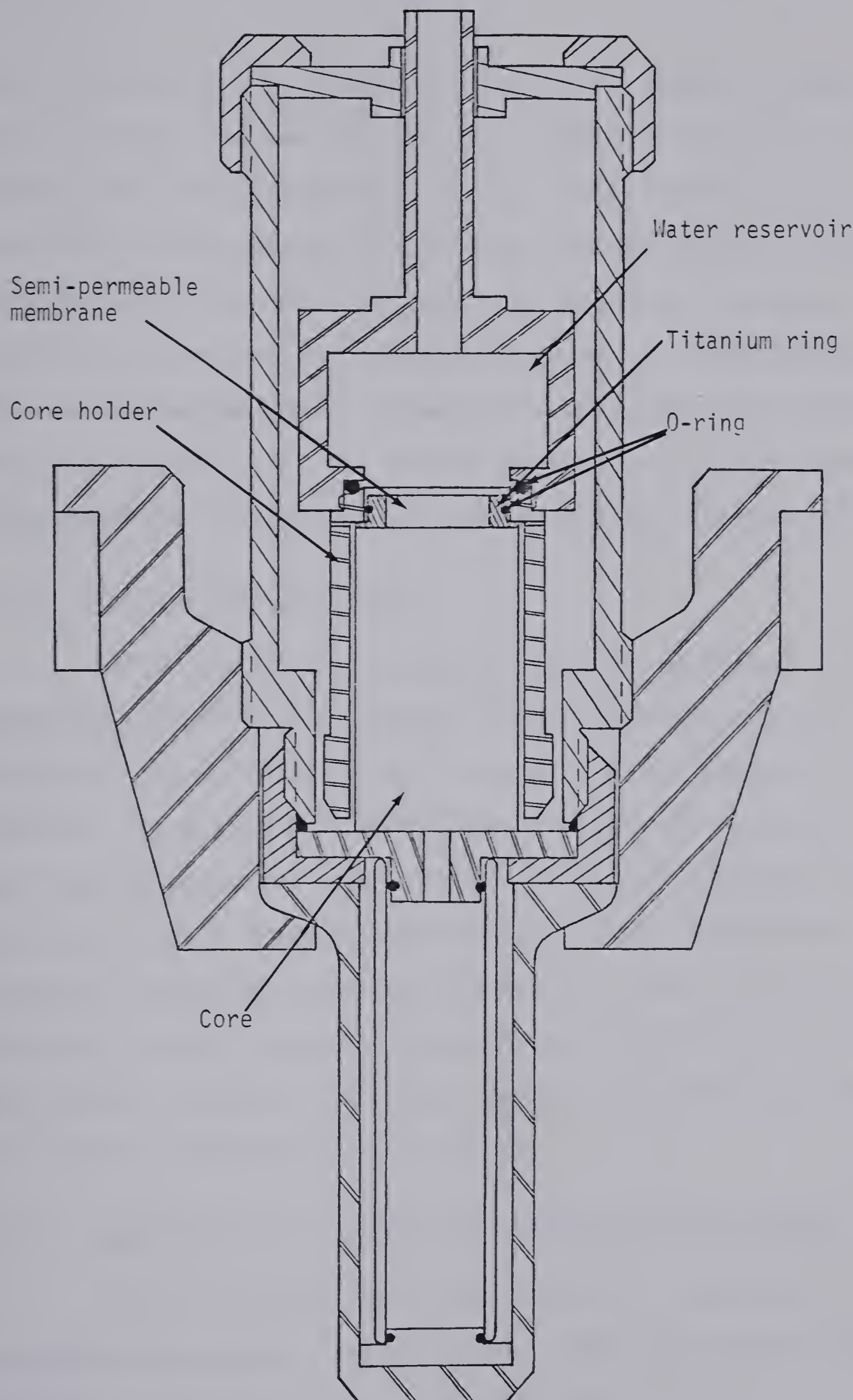


FIGURE V-2 IMBIBITION CAPILLARY PRESSURE CELL

resin, so that only its circumference would be in contact with the resin. The resin imbibed into the disc, so that the area open to flow was significantly decreased. It was finally decided to glue a previously cleaned membrane in a titanium ring with Devcon F, an 80% Aluminum - 20% Improved Epoxy Plastic. Because Devcon F cannot be heated to high temperatures, the glued membrane was constantly kept water-wet by letting a small stream of distilled water flow through it. Thus, the wettability was not allowed to change significantly between the experiments. This method was found to be fully satisfactory.

V.3.2 Core and Cell Preparation

After drainage was completed, the slices to be used in the imbibition experiment were rotated at maximum speed, in order to establish a saturation as close to irreducible water saturation as possible. The slices, kept in oil, were then weighed. The cores were reassembled and put in the cells. The free oil and water levels were very carefully measured and calculated so that the capillary pressure at the outlet end of the core would be close to zero, but positive in order to prevent the water from flowing out of the core. Equilibrium is assumed to be reached when the free water level does not vary for a sufficient period of time.

V.3.3 Imbibition Capillary Pressure and Saturation Measurement

The cell was designed so that both the oil and water reservoirs were opened to the atmosphere. Under this condition, the imbibition capillary pressure was expressed as

$$P_c = \frac{1.097 \times 10^{-6} \omega^2}{2} [D^2(\rho_o - \rho_w) + r_w^2 \rho_w - r_o^2 \rho_o] \quad (4-23)$$

where

r_w and r_o are the distances from the rotary axis to the free water and oil levels respectively, cm.

D is the distance from the rotary axis to the point where

P_c is calculated, cm.

P_c , kPa.

The average saturation in each slice was estimated using Eq.(5-2):

$$\overline{S_w} = 1 - \frac{M_w' - M_L}{V_p \Delta \rho} \quad (5-2)$$

Equations (4-23) and (5-2) are derived in Appendix D.

CHAPTER VI

RESULTS AND DISCUSSION

VI.1 DRAINAGE

VI.1.1 Experimental Results

The samples used in this study were taken from three different porous rods which were supposed to be homogeneous. Their physical properties are given in Table VI-1.

The fluids used were always water and kerosene; this combination was chosen because lucite is quite resistant to attack by kerosene, and the density difference between both fluids is relatively large, which is favourable to attaining high capillary pressures. The properties of the fluids are given in Table VI-2. All the experiments were done at a constant temperature of about 20°C, and the fluid properties were therefore considered to be identical for all the runs.

The experiments were conducted in various ways, some with slices about 2.4 cm long, some with slices about 1.2 cm long. Some runs were carried out at one single speed of rotation; in other experiments, the speed of rotation was increased by steps, and the saturation measured after each step. This was done in order to gain a better understanding of the experimental data obtained, because, as it has already been pointed out, different experimental curves can be obtained for a single run and for a single system of fluids and porous medium. It is, therefore, necessary to grasp the significance

TABLE VI-1

CORE PROPERTIES

	Sandstone	P-6-C Alundum	P-12-C Alundum
Porosity, %	18.5	36.9	41.7
Liquid permeability, μm^2	0.131	0.034	0.155

TABLE VI-2

FLUID PROPERTIES AT 20°C

	Density kg/m^3	Viscosity $\text{mPa}\cdot\text{sec}$
Water	998.2	1.00
Kerosene	788.3	1.23

Density difference, $\Delta\rho = 209.9 \text{ kg/m}^3$ Interfacial tension, $\gamma = 27.68 \text{ mN/m}$

of the experimental data, and to be able to distinguish between the capillary properties of the system, and the effects due to the parameters of the experiment, such as length of the slices and speed of rotation. These parameters are tabulated in Table E-1 through E-8 in Appendix E.

No problem was encountered with the centrifuge, whose flexible drive shaft and feedback speed control allowed the rotation to be smooth and steady.

Experimental curves are shown in Figure VI-1 to Figure VI-8, and data are given in Table F-1 through F-8 in Appendix F.

VI.1.2 Error Analysis

The drainage capillary pressure is given by Eq.(4-9). Therefore, the relative error on capillary pressure is given by

$$\frac{\delta P_c}{P_c} = \frac{\delta(\Delta\rho)}{\Delta\rho} + 2 \frac{\delta\omega}{\omega} + \frac{\delta r_e + \frac{\delta h}{2}}{r_e - \frac{h}{2}} + \frac{\delta h}{h}$$

where

$$\delta(\Delta\rho) \simeq 5 \times 10^{-4} \text{ g/cm}^3$$

$$\delta\omega \simeq 10 \text{ rpm at 1000 rpm}$$

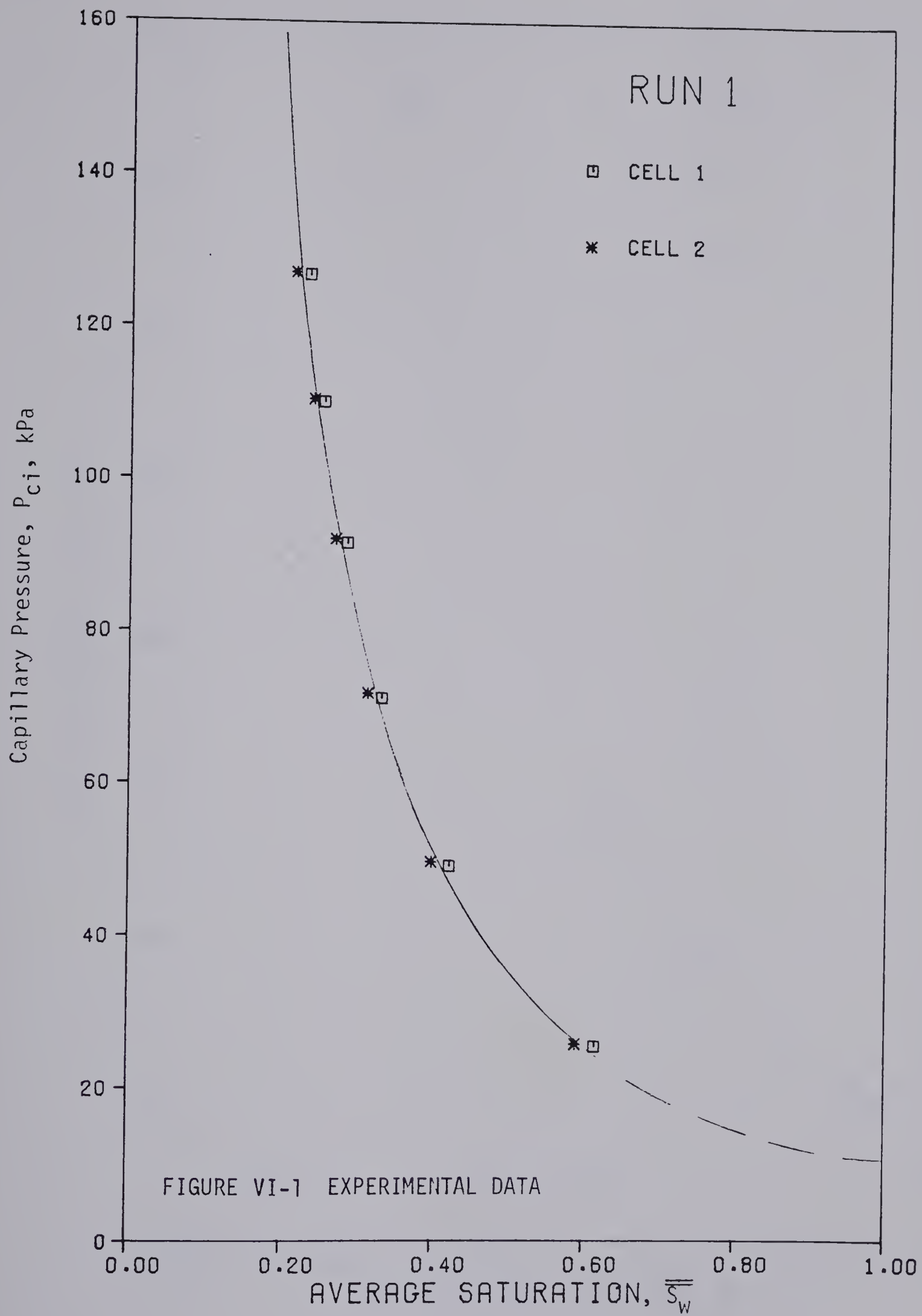
$$\delta r_e \simeq 10^{-2} \text{ cm}$$

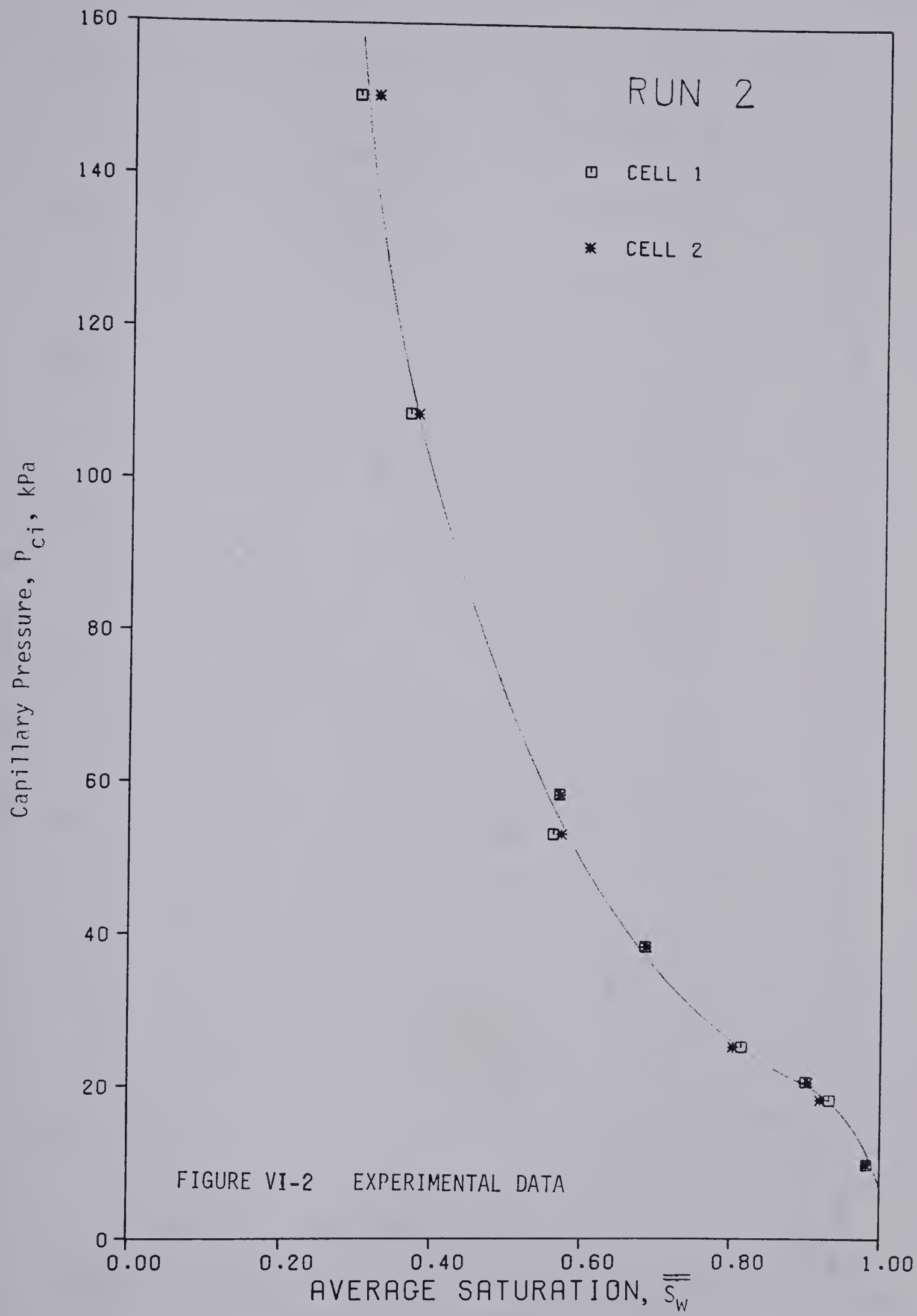
$$\delta h \simeq 10^{-3} \text{ cm}$$

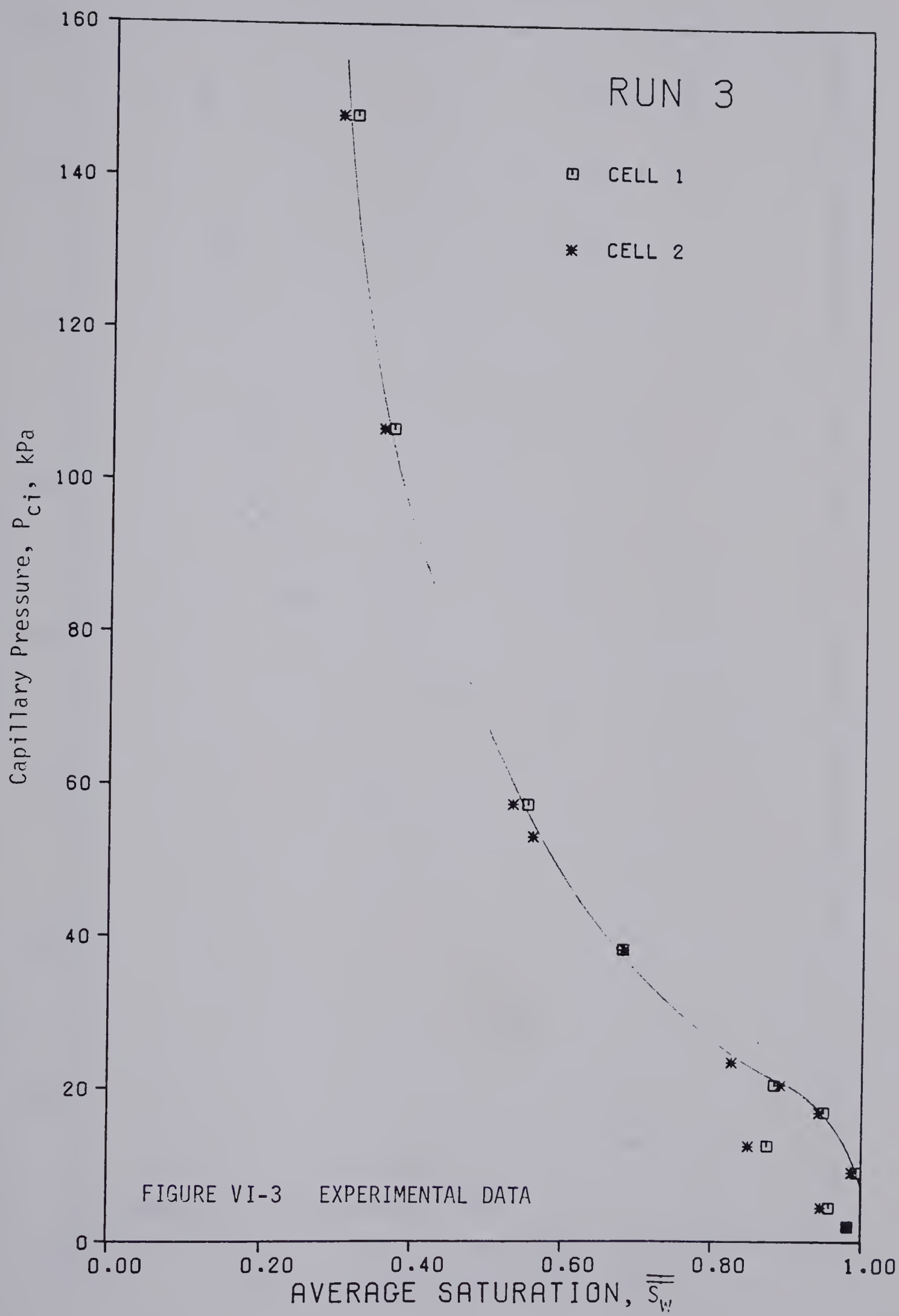
Thus, the relative error for capillary pressure should not exceed 3%.

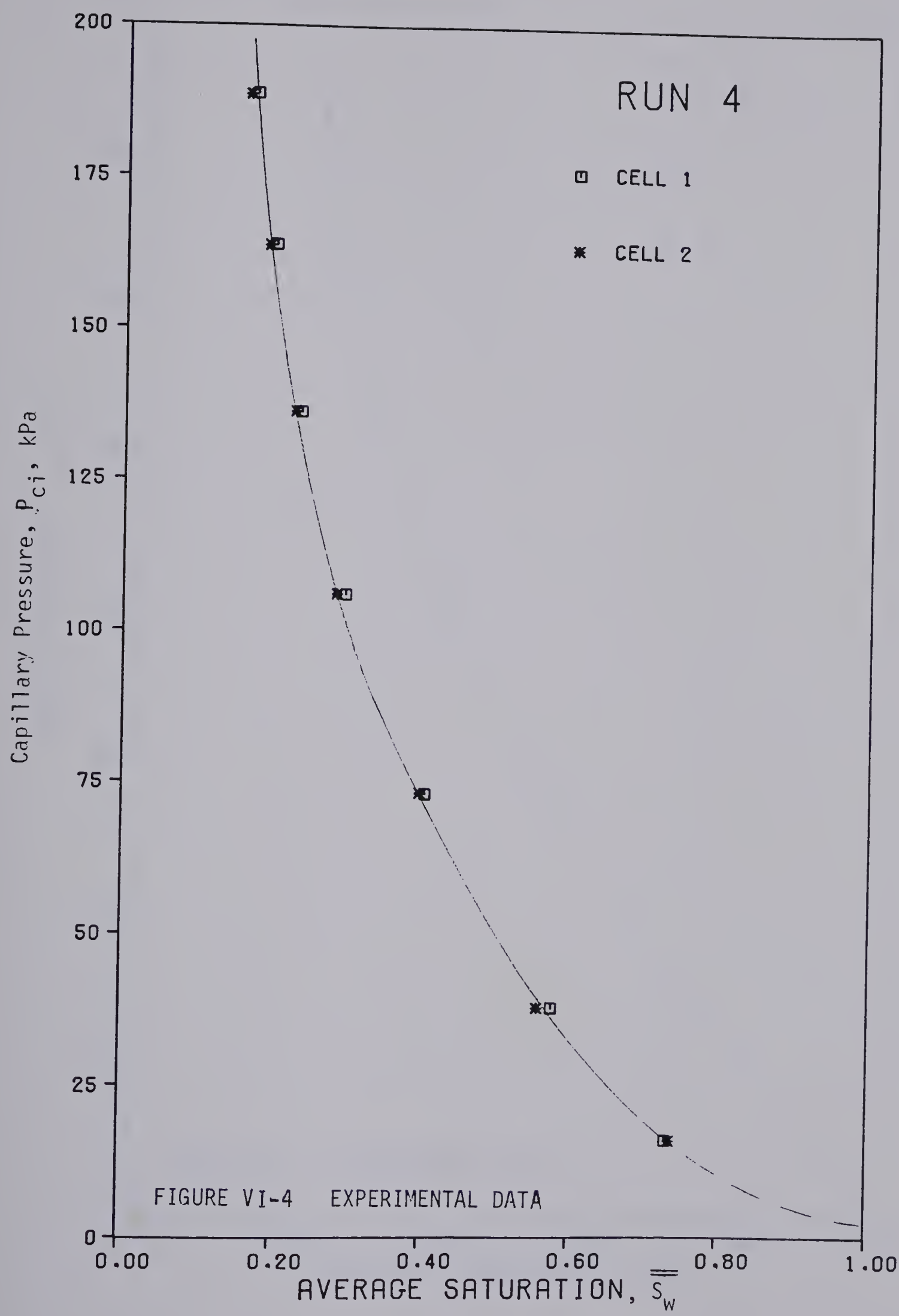
The average saturation was measured by Eq.(5-2). The relative error is, therefore,

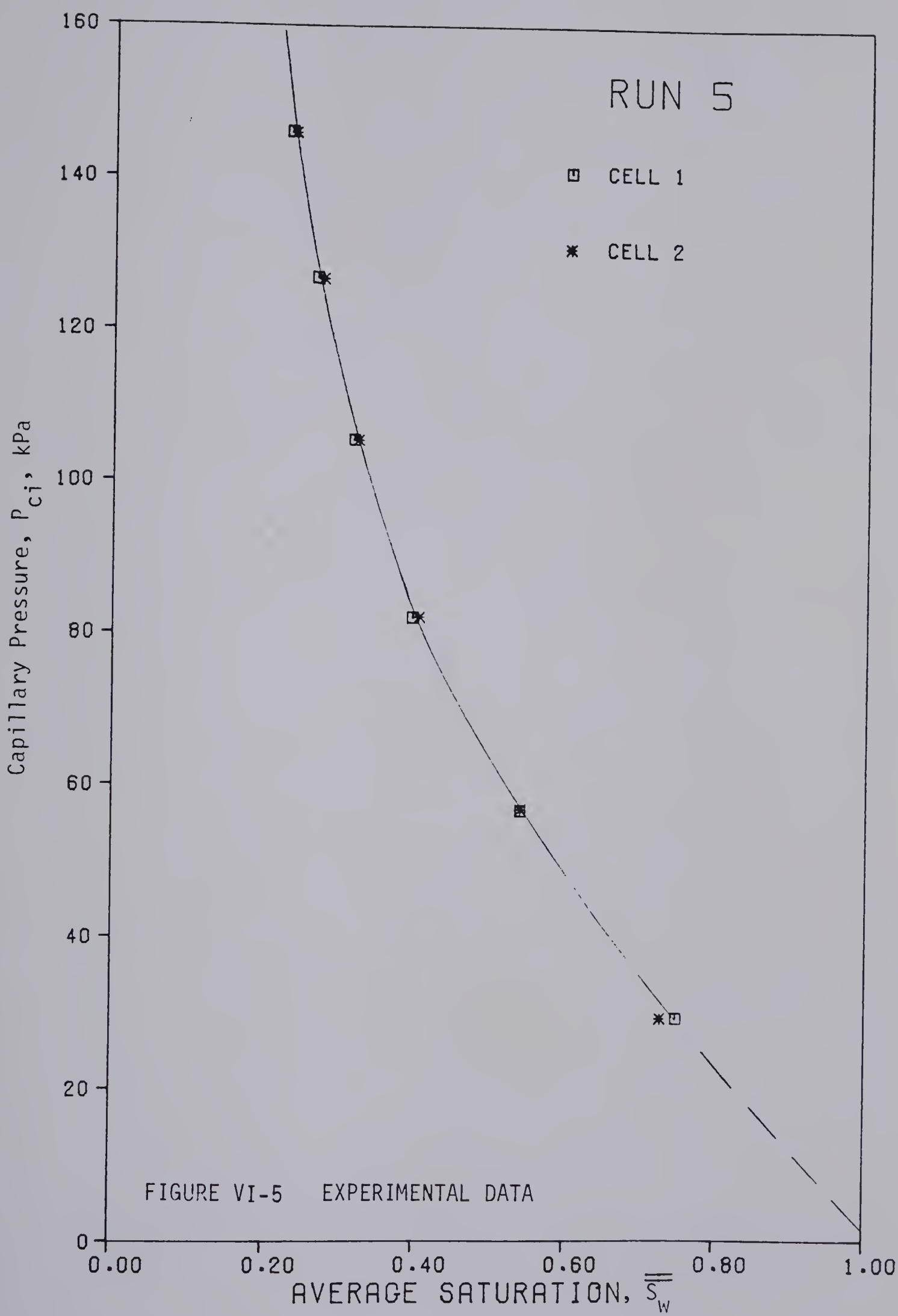
$$\frac{\delta \bar{S}_w}{\bar{S}_w} = \frac{\delta M'_w + \delta M'_L}{M'_w - M'_L} + \frac{\delta V_p}{V_p} + \frac{\delta(\Delta\rho)}{\Delta\rho}$$

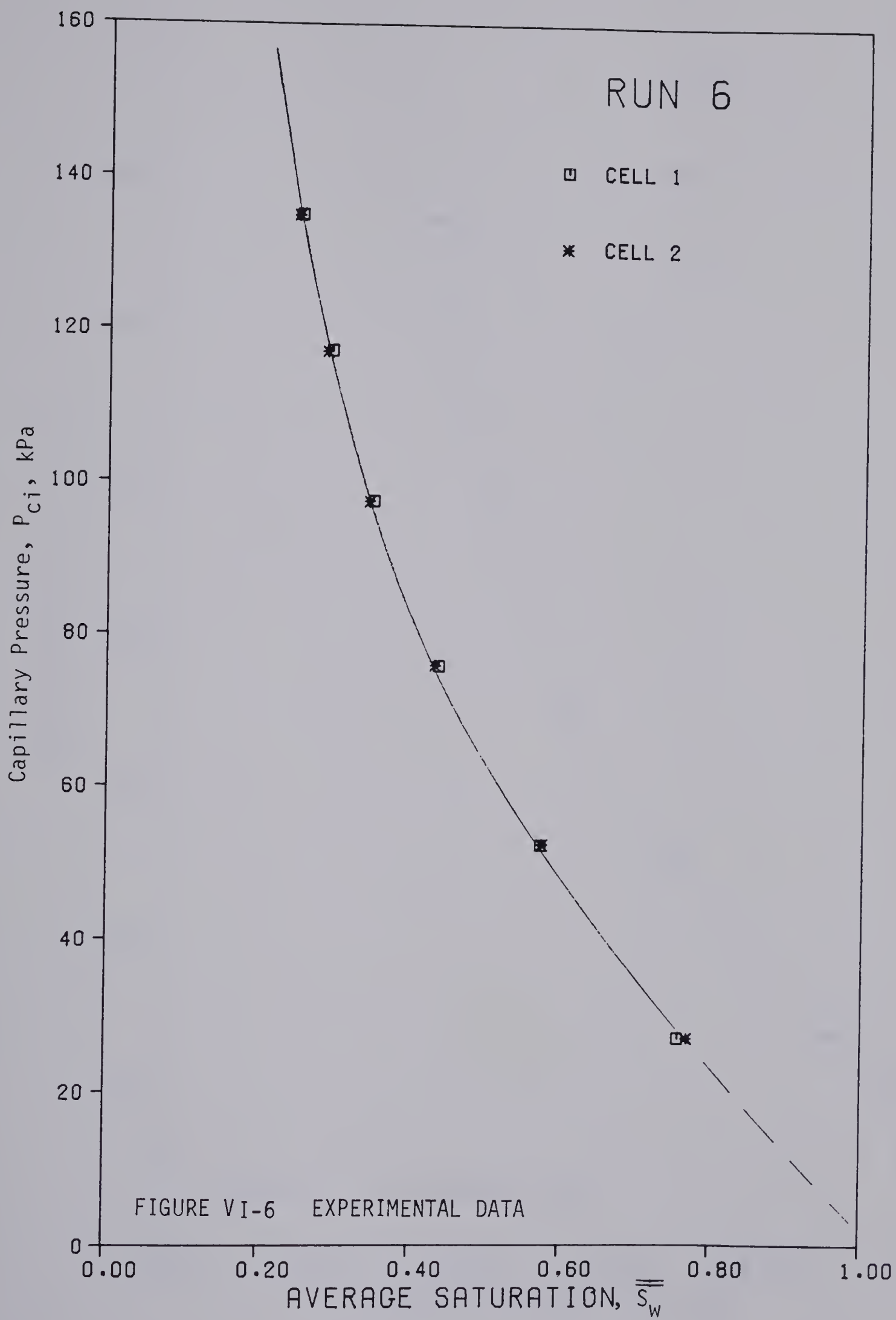


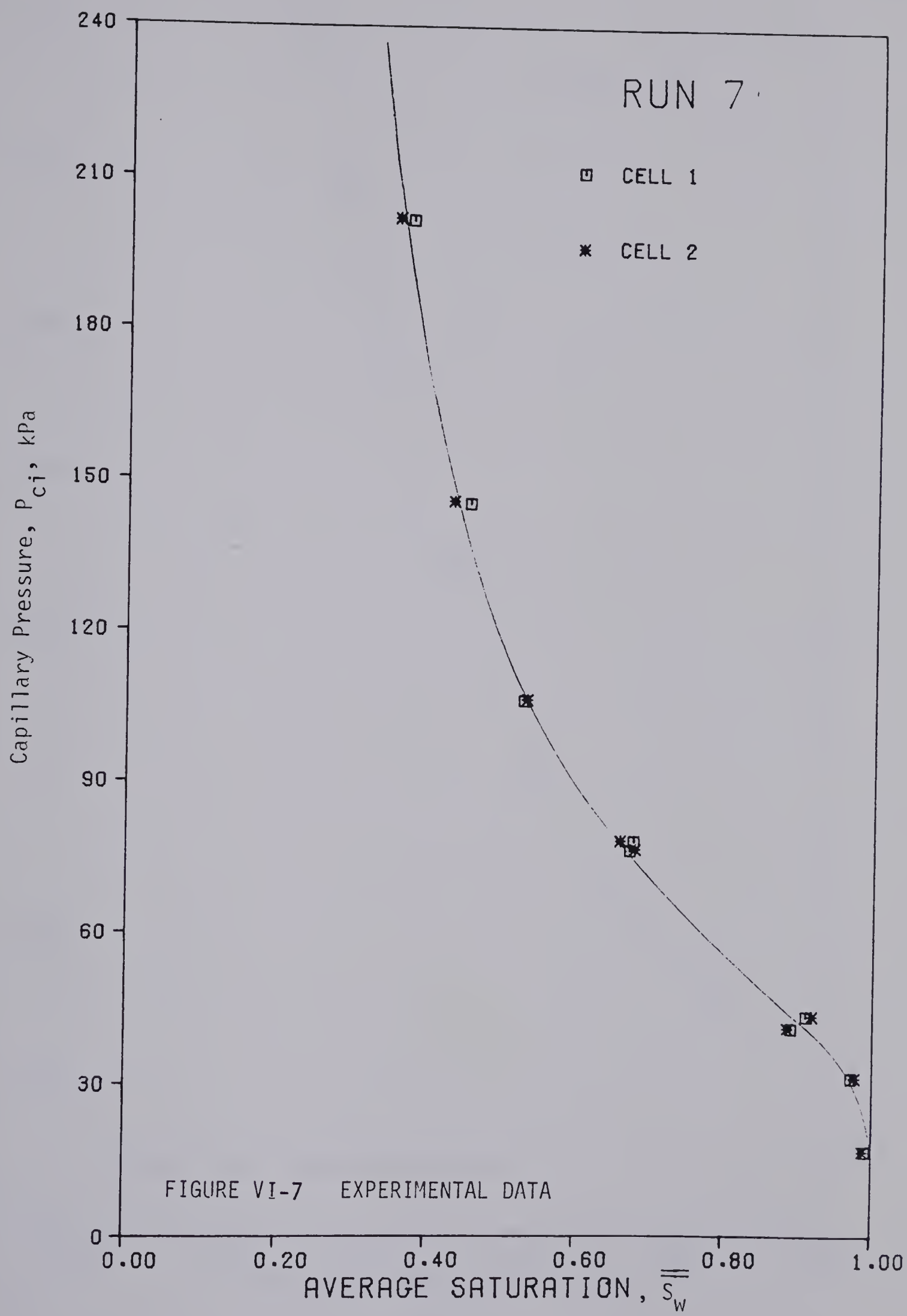


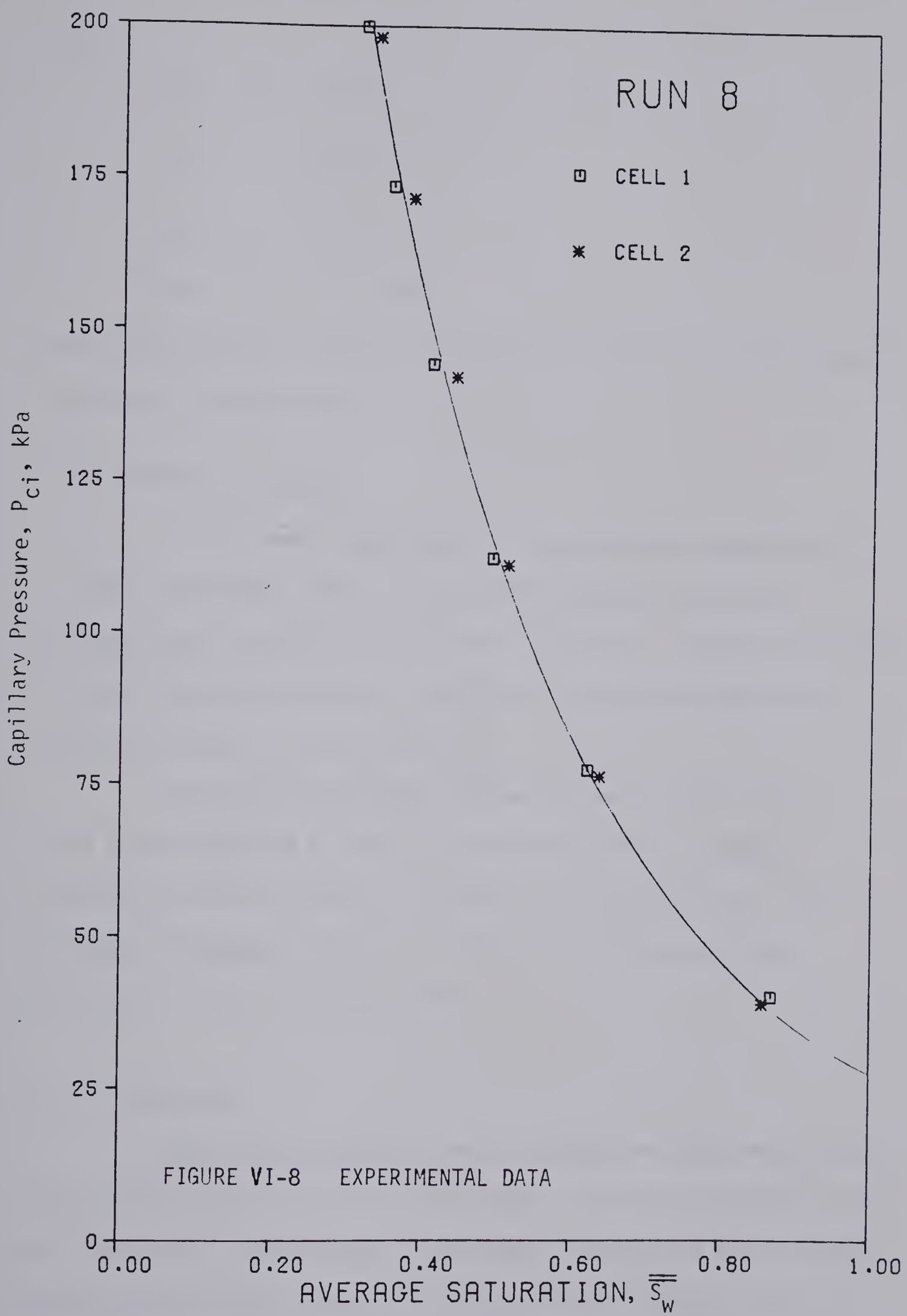












where

$$\begin{aligned}\delta M'_w &\simeq 5 \times 10^{-4} \text{ g} \\ \delta M_L &\simeq 5 \times 10^{-4} \text{ g} \\ \delta V_p &\simeq 10^{-3} \text{ cm}^3 \\ \delta(\Delta p) &\simeq 5 \times 10^{-4} \text{ g/cm}^3\end{aligned}$$

Hence, the relative error for the measured average saturation should not be more than about 3%.

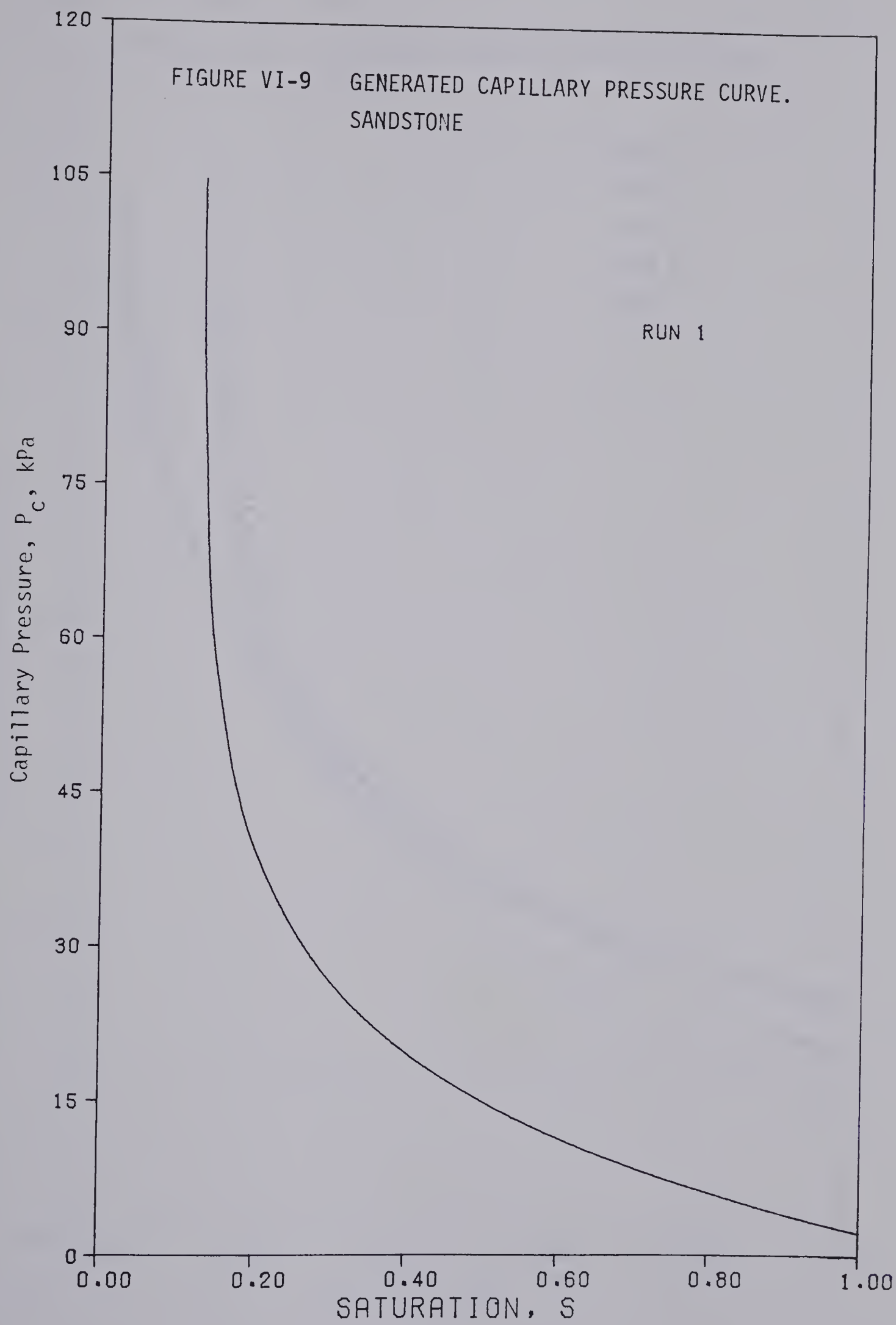
VI.1.3 Numerical Results

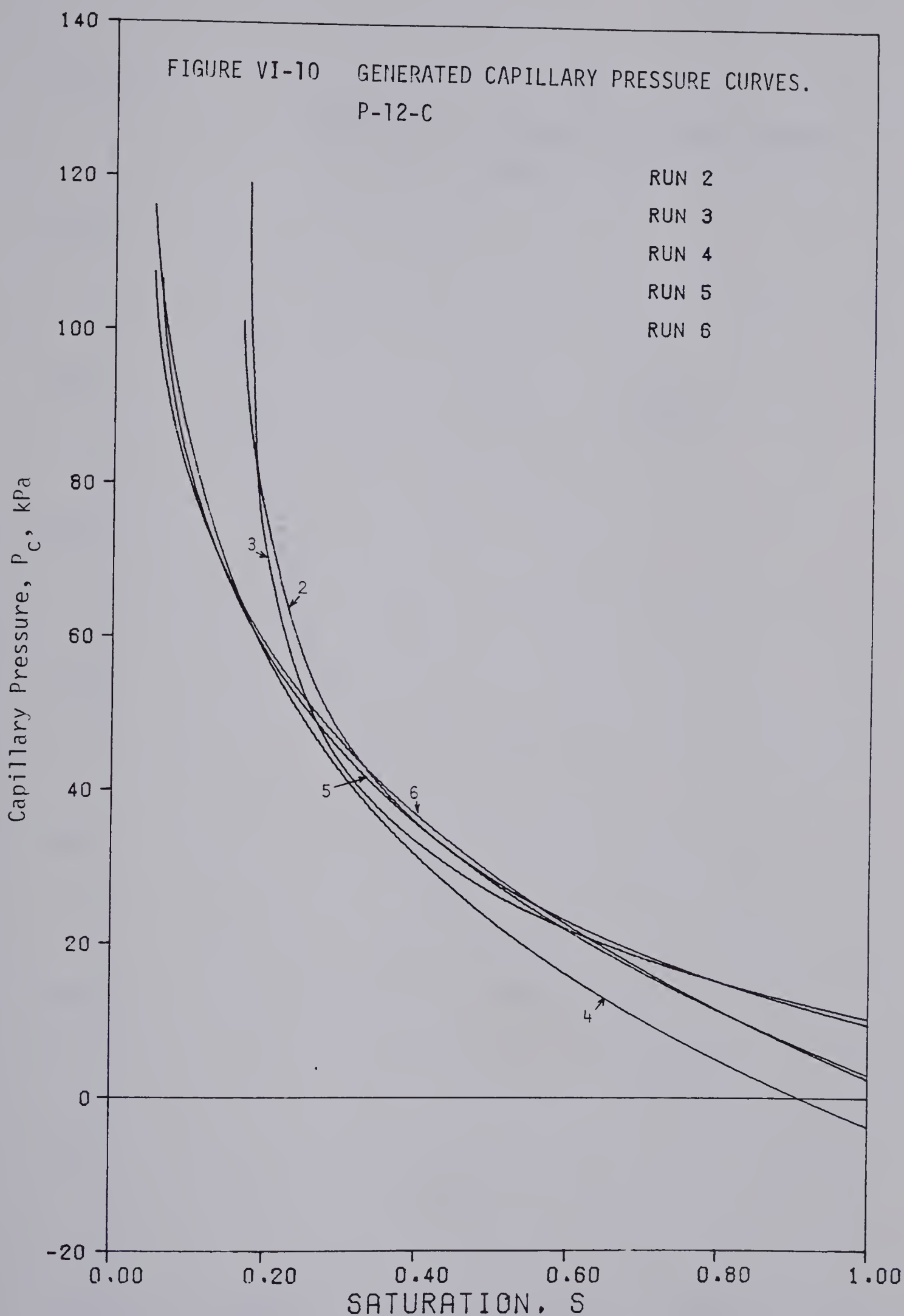
The Marquardt algorithm for least-squares estimation of nonlinear parameters (96) was used to fit the data points by estimating the parameters which define the model. Capillary pressure was the independent variable, and $\overline{\overline{S}_w}$ was the dependent variable, according to Eq.(4-17) and Eq.(4-18).

The calculated values of $\overline{\overline{S}_w}$ are given in Table F-1 to Table F-8 of Appendix F, and the generated capillary pressure-saturation curves are shown in Figure VI-9 to Figure VI-11. The estimated parameters are given in Table VI-3, along with the associated linear confidence limits.

VI.2 IMBIBITION

Imbibition experiments were conducted on cores made of four slices; each slice was about 1.2 cm long. It was not possible to use six slices, as in the drainage experiments, because it was necessary to keep the capillary pressure at the bottom of the cores positive. Prior to starting the experiments, the irreducible water saturation





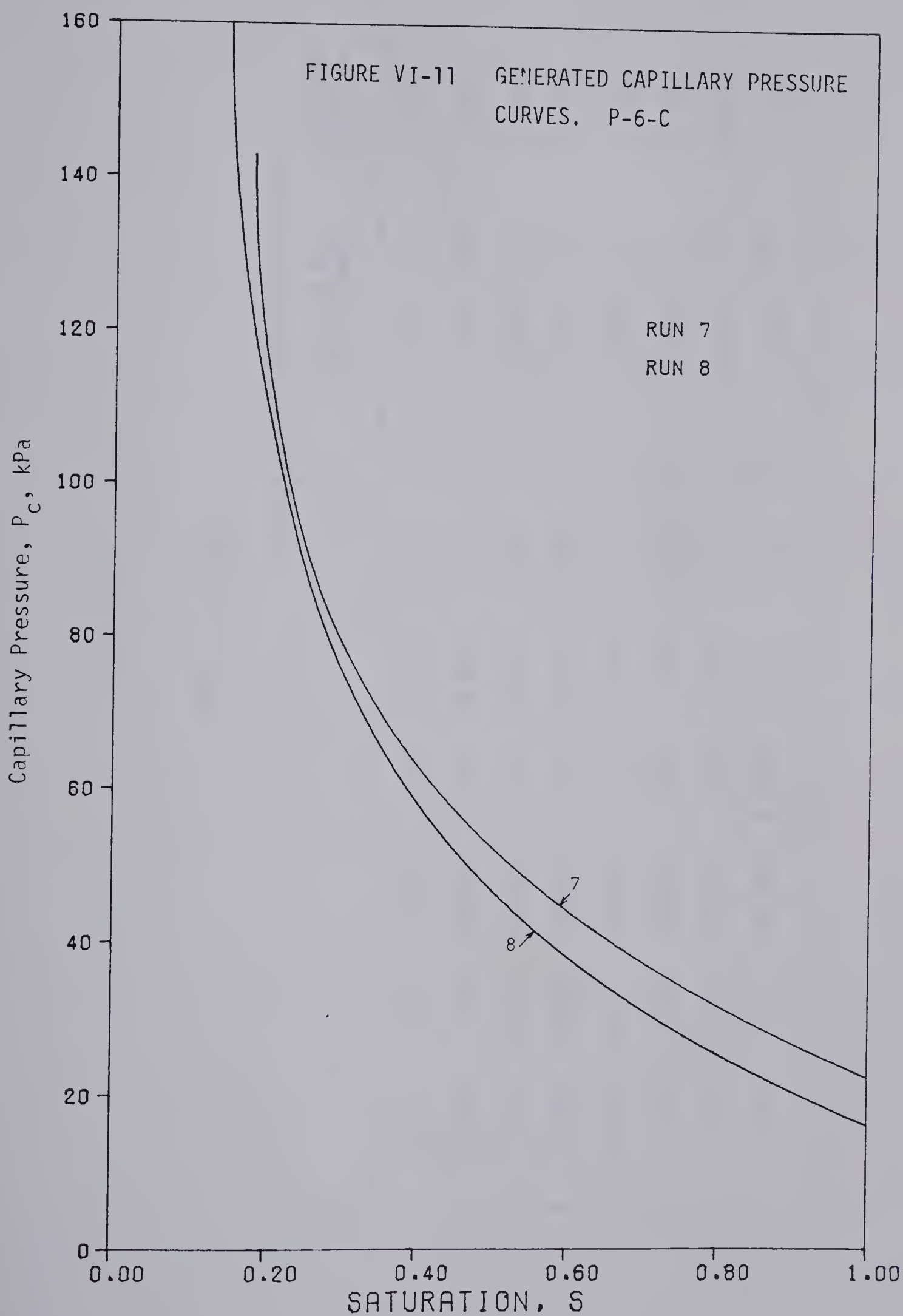


TABLE VI-3

NUMERICAL RESULTS

Run	S_{wi}	σ	P_d	n	Standard Error of Estimate	Area Under the Curve
1	0.125 \pm 0.012	15.066 \pm 2.321	2.297 \pm 1.341	1.00	1.040 \times 10 ⁻²	17.363
2	0.164 \pm 0.014	20.724 \pm 1.523	9.621 \pm 0.515	1.00	1.163 \times 10 ⁻²	30.345
3	0.173 \pm 0.011	17.650 \pm 1.160	10.353 \pm 0.416	1.00	1.045 \times 10 ⁻²	28.003
4	0.023 \pm 0.009	38.361 \pm 1.415	-3.707 \pm 0.393	0.92	0.699 \times 10 ⁻²	31.812
5	0.051 \pm 0.012	36.827 \pm 2.013	2.994 \pm 0.710	0.76	0.722 \times 10 ⁻²	32.693
6	0.043 \pm 0.009	40.140 \pm 1.414	2.494 \pm 0.438	0.71	0.484 \times 10 ⁻²	33.610
7	0.174 \pm 0.023	34.573 \pm 3.227	22.521 \pm 0.944	0.85	1.835 \times 10 ⁻²	52.584
8	0.139 \pm 0.023	35.208 \pm 4.479	16.322 \pm 1.654	1.00	1.232 \times 10 ⁻²	51.530

was established in each slice. When the saturation of the inner slice was S_{wi} , this slice was removed, and the core was raised. The second slice of the original core was then the top slice, and the bottom slice was replaced by an end butt made of the same material, and 100% water saturated. The centrifuge was restarted, and S_{wi} was established in the top slice; this procedure was repeated until S_{wi} was obtained in eight slices, that is in two complete cores.

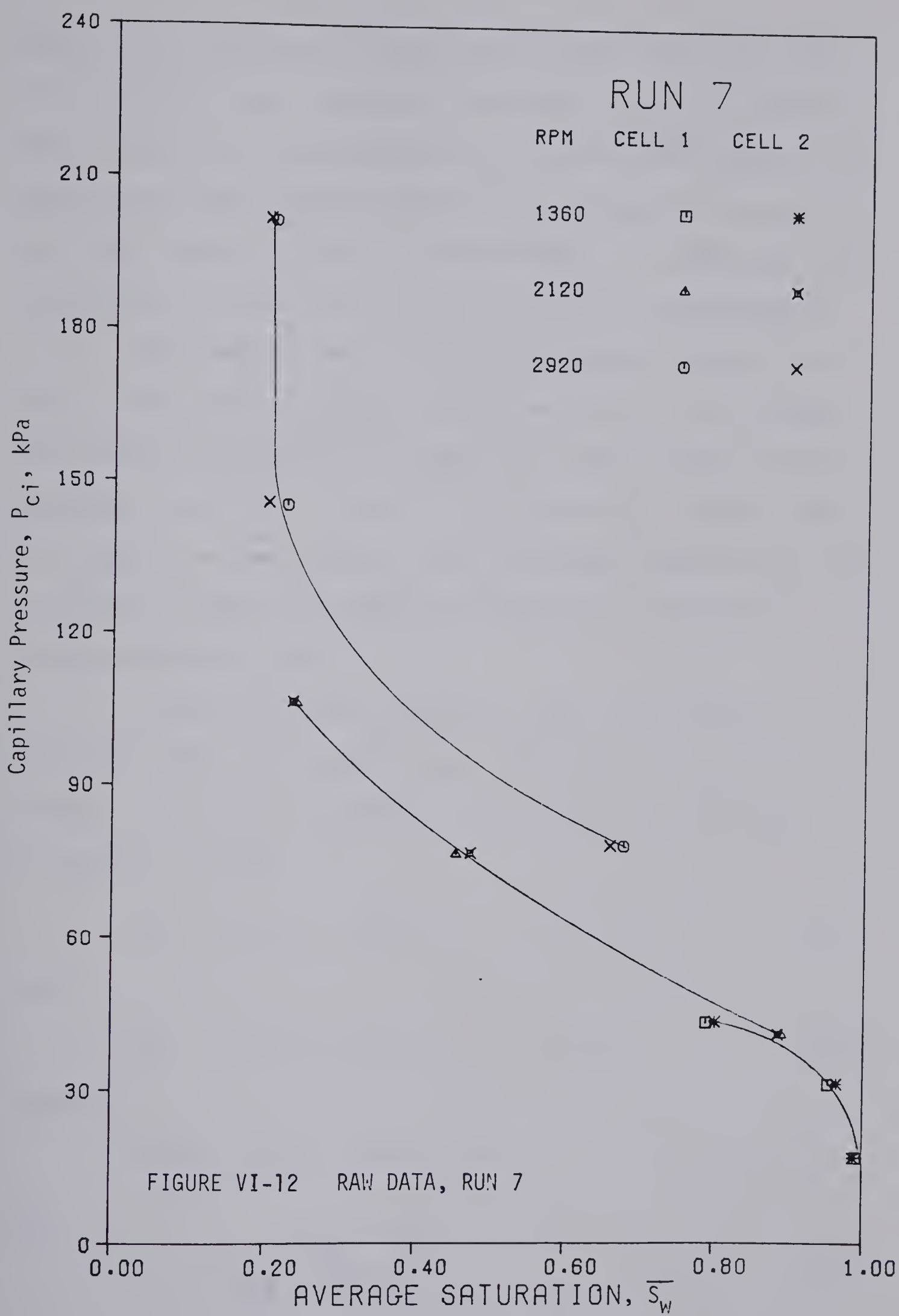
Extreme care was taken in the measurement of the water and oil levels, in their respective reservoirs. The duration of each experiment was about one week; the last experiment, conducted on P-12-C, was carried on during 24 days, but in spite of the fact that the capillary pressure at the inner end of the core was kept as low as 6.79 kPa, no imbibition whatsoever was obtained.

VI.3 DISCUSSION

VI.3.1 Drainage

VI.3.1.1 Experimental Results

Run 2 and Run 7 were conducted on cores made of three slices about 2.4 cm long; three speeds of rotation, in the range 1000 to 3000 rpm, were chosen in both runs, in order to obtain the complete capillary pressure curves. The saturation, \bar{S}_w , in each slice, was calculated after equilibrium was obtained at a particular speed, as well as the capillary pressure, P_{ci} , at the top of each slice, for that particular speed. The raw data thus obtained for Run 7 are plotted in Figure VI-12. Data obtained for Run 2 would lead to a similar kind of plot. Another interpretation of the data must



therefore be resorted to, in order to get a more conventional type of experimental curve. Szabo (87) obtained his curves by plotting the calculated capillary pressure, P_{cc} , at the center of each slice, against the related average saturation, \bar{S}_w . Figure VI-13 shows the curve thus obtained for Run 7. The improvement is evident, but the saturation in the lower part of the curve is still double-valued.

Such behaviour may be easily understood. Figure VI-14 shows a slice and the saturation profile within it. It is evident that a plot of P_{cc} versus \bar{S}_w is nearer to a true capillary pressure-saturation curve, than is a plot of P_{ci} against \bar{S}_w . However, there is, a priori, no reason why P_{cc} should correspond exactly to \bar{S}_w , and a plot of P_{cc} against \bar{S}_w cannot be accepted as a true capillary pressure-saturation curve.

Figure VI-15 shows two similar cores, one spinning at ω_1 rpm and the other spinning at ω_2 rpm. The values of P_{ci} at the top of each slice are also indicated. Let ω_2 be such that $P_2^2 = P_3^1$. By virtue of Eq.(4-9),

$$P_3^1 = A\Delta\rho\omega_1^2 (r_e - \frac{k}{2}) k, \quad k = 3h \quad (6-1)$$

and

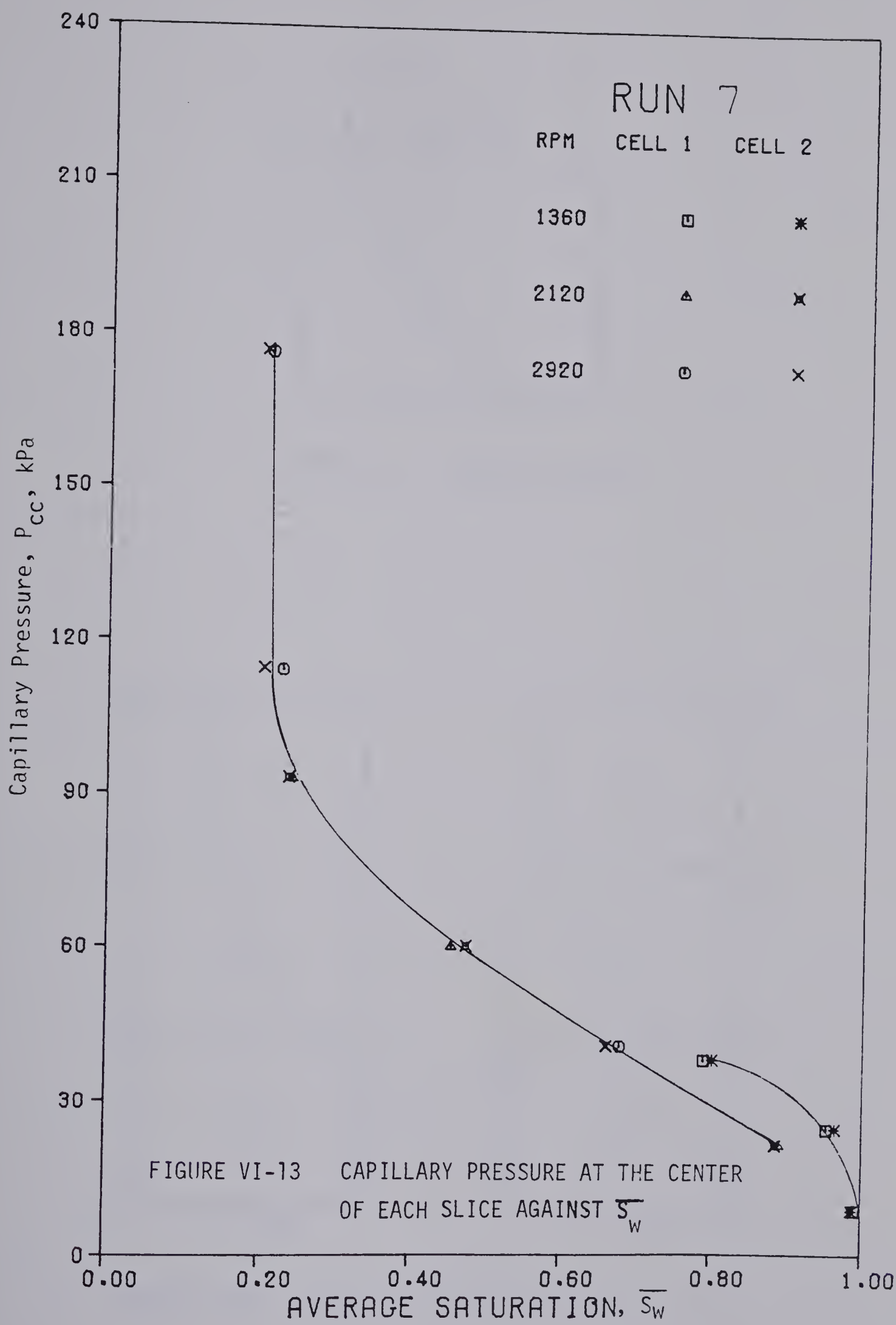
$$P_2^2 = A\Delta\rho\omega_2^2 (r_e - \frac{\ell}{2}) \ell, \quad \ell = 2h \quad (6-2)$$

Therefore

$$3\omega_1^2 (r_e - \frac{3h}{2}) = 2\omega_2^2 (r_e - h)$$

and

$$\omega_2 = \frac{\omega_1}{2} \sqrt{\frac{3(2r_e - 3h)}{r_e - h}} \quad (6-3)$$



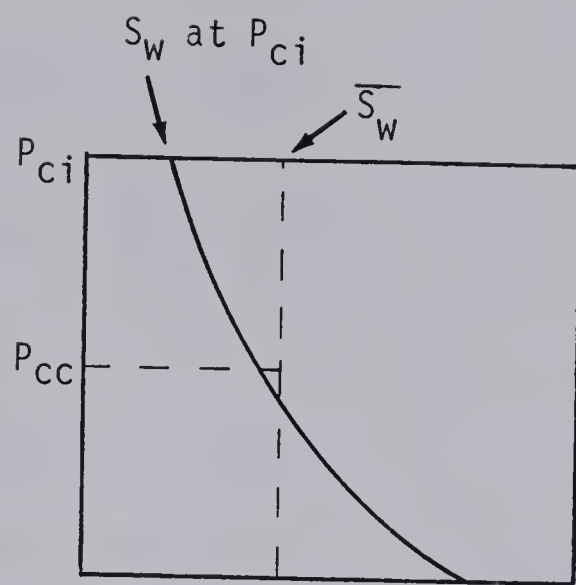
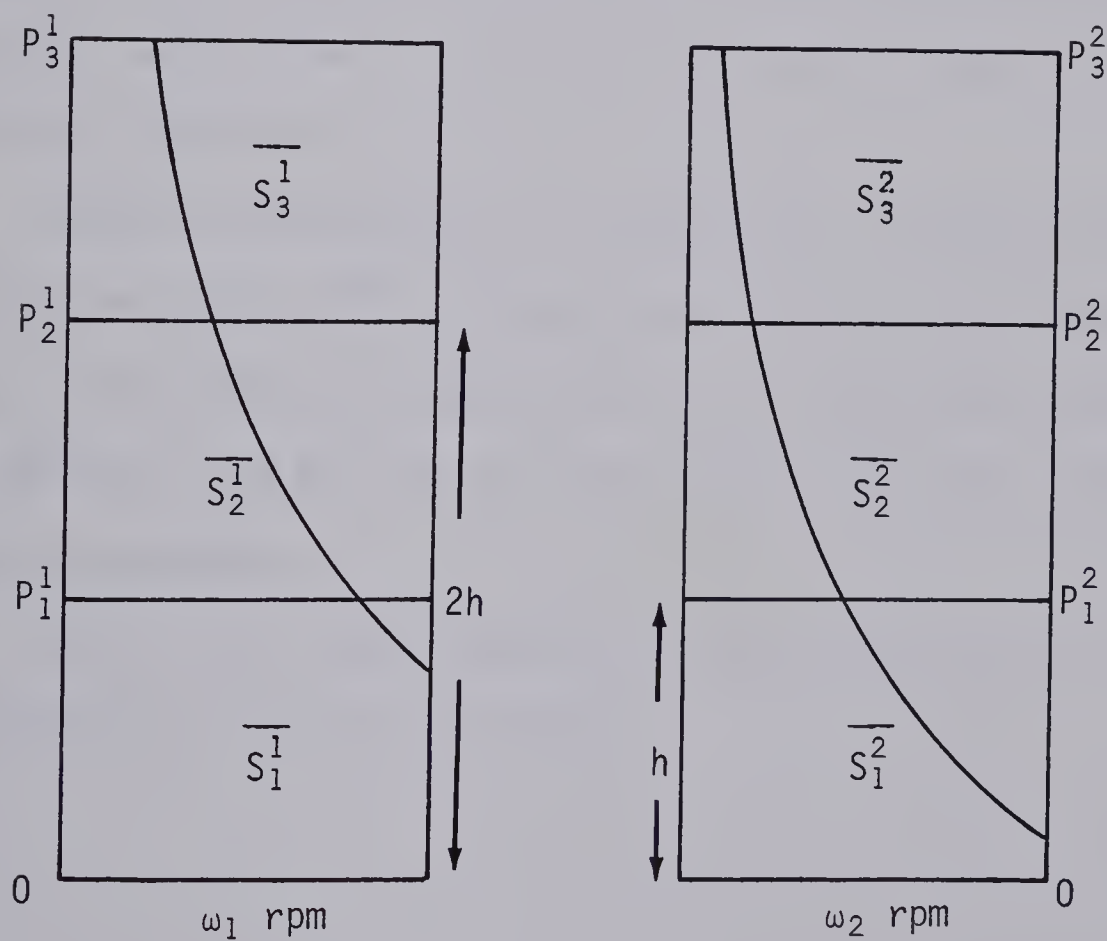


FIGURE VI-14 GRAVITY EFFECT

FIGURE VI-15 EFFECT OF SPEED VARIATION, $\omega_1 < \omega_2$

It follows that

$$\begin{aligned}
 P_1^2 &= A\Delta\rho\omega_2^2 (r_e - \frac{h}{2}) h \\
 &= A\Delta\rho\omega_1^2 \frac{3(2r_e - 3h)}{4(r_e - h)} (r_e - \frac{h}{2}) h
 \end{aligned} \tag{6-4}$$

Also,

$$P_2^1 = A\Delta\rho\omega_1^2 (r_e - h) 2h \tag{6-5}$$

By comparing Eq.(6-4) and Eq.(6-5), it is easy to see that

$$P_2^1 > P_1^2 \tag{6-6}$$

Consequently

$$\overline{S_3^1} < \overline{S_2^2} \tag{6-7}$$

Therefore, it is not possible to obtain a single curve by plotting the raw data, when different speeds of rotation are used in the course of one experiment.

Another interpretation of the data was necessary; that is, the average saturation, $\overline{\overline{S}_w}$, was calculated from the outlet end of the core, to the plane corresponding to P_{ci} . Such curves were plotted for Run 2 and Run 7 [Figure VI-2 and Figure VI-7]. They are much more satisfactory.

Let $P_1^2 = P_2^1$; then, according to Eq.(4-12) and Eq.(4-17), and combining Eq.(4-12) with Eq.(6-3),

$$\begin{aligned}
 \overline{\overline{S_1^2}} &= S_{wi} + \frac{1 - S_{wi}}{h} \left[r_e - \sqrt{r_e^2 - \frac{2P_d}{A\Delta\rho\omega_1^2} \frac{2r_e - h}{4(r_e - h)}} \right] \\
 &+ \frac{1 - S_{wi}}{A\Delta\rho\omega_1^2 2h} \frac{2r_e - h}{2(r_e - h)} \left(\frac{1-n}{\sigma} \right)^{\frac{1}{1-n}} \int_{P_d}^{P_1^2} \frac{\frac{1}{1-n} dP_c}{\sqrt{r_e^2 - \frac{2P_c}{A\Delta\rho\omega_1^2} \frac{2r_e - h}{4(r_e - h)}}}
 \end{aligned} \tag{6-8}$$

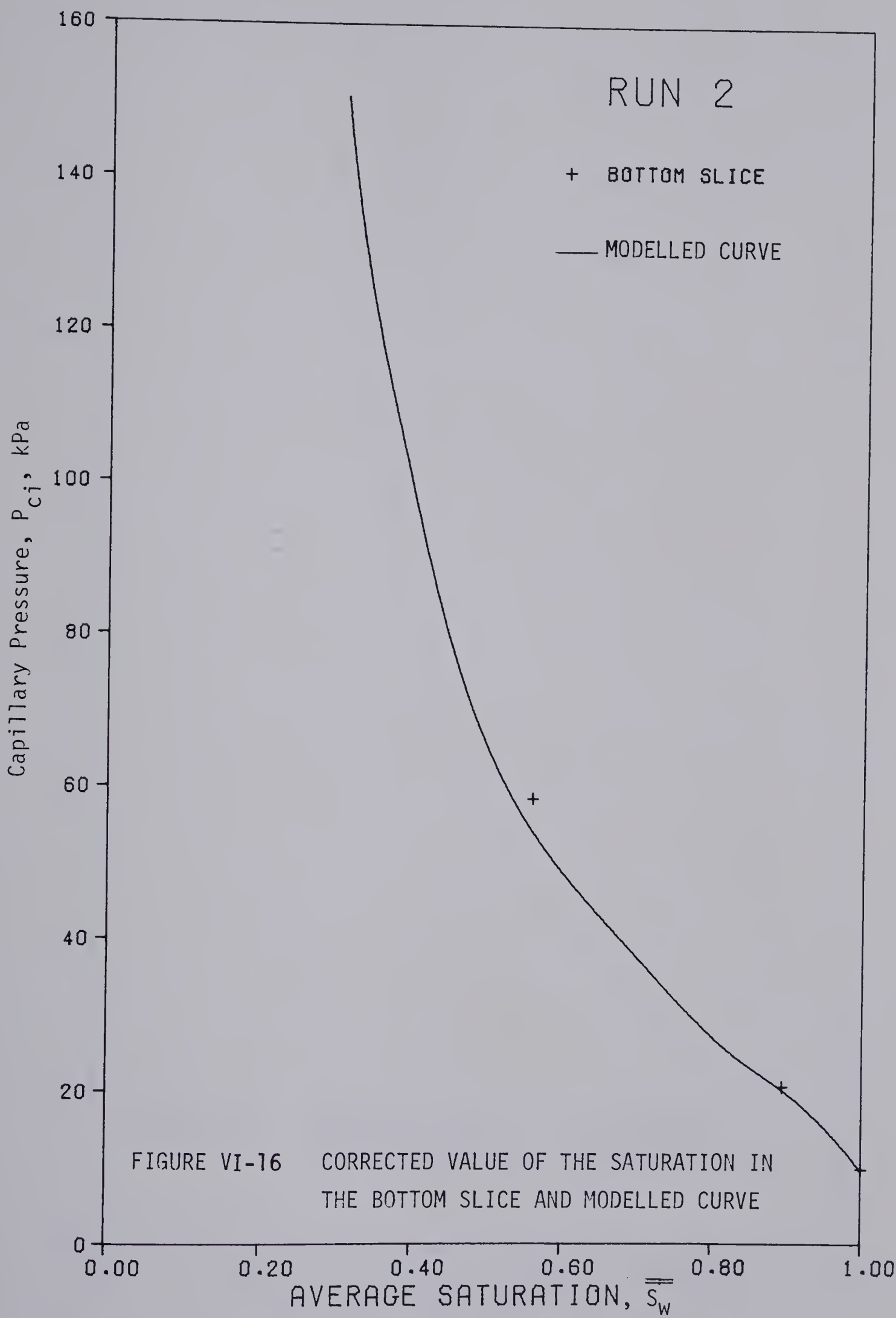
whereas,

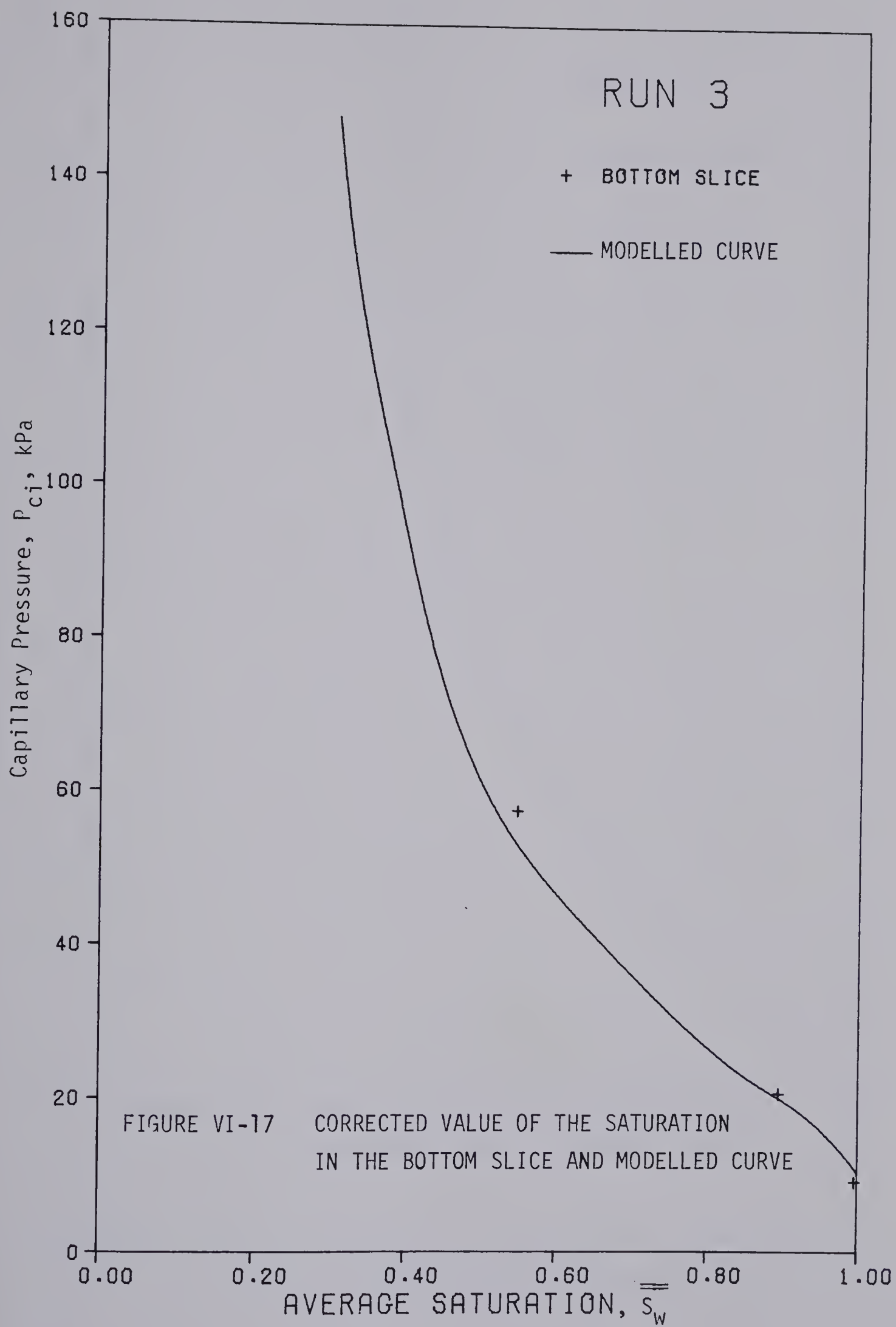
$$\begin{aligned}
 \overline{\overline{S_2^1}} &= S_{wi} + \frac{1 - S_{wi}}{2h} \left[r_e - \sqrt{r_e^2 - \frac{2P_d}{A\Delta\rho\omega_1^2}} \right] \\
 &+ \frac{1 - S_{wi}}{A\Delta\rho\omega_1^2 2h} \left(\frac{1-n}{\sigma} \right)^{\frac{1}{1-n}} \int_{P_d}^{P_1^2} \frac{\frac{1}{1-n} dP_c}{\sqrt{r_e^2 - \frac{2P_c}{A\Delta\rho\omega_1^2}}}
 \end{aligned} \tag{6-9}$$

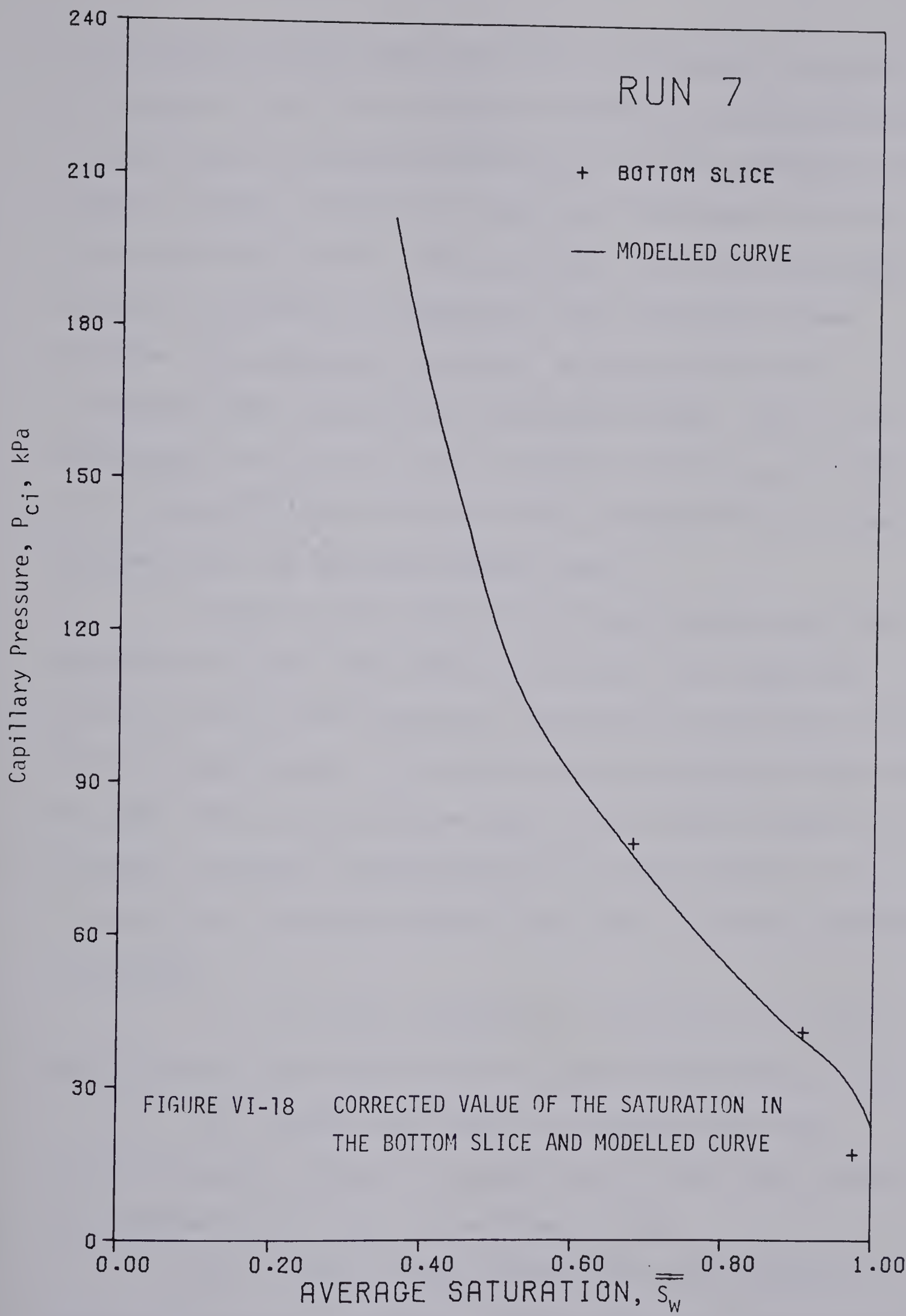
Hence, in spite of the fact that $P_1^2 = P_2^1$, $\overline{\overline{S_1^2}}$ is not strictly equal to $\overline{\overline{S_2^1}}$. Figures VI-16 through VI-18 show that the corrected data pertaining to the bottom slices are not on the modelled curve.

This system is, therefore, peculiar in that it does not allow the obtainment of conventional experimental curves, if different speeds of rotation are used in a single experiment. Moreover, the time required to obtain equilibrium at each speed of rotation was found to be quite long, up to 47 hours for the tightest core.

The cores used in Run 1, Run 5, Run 6, and Run 8 were made of six slices, each about 1.2 cm long. Increasing the number of



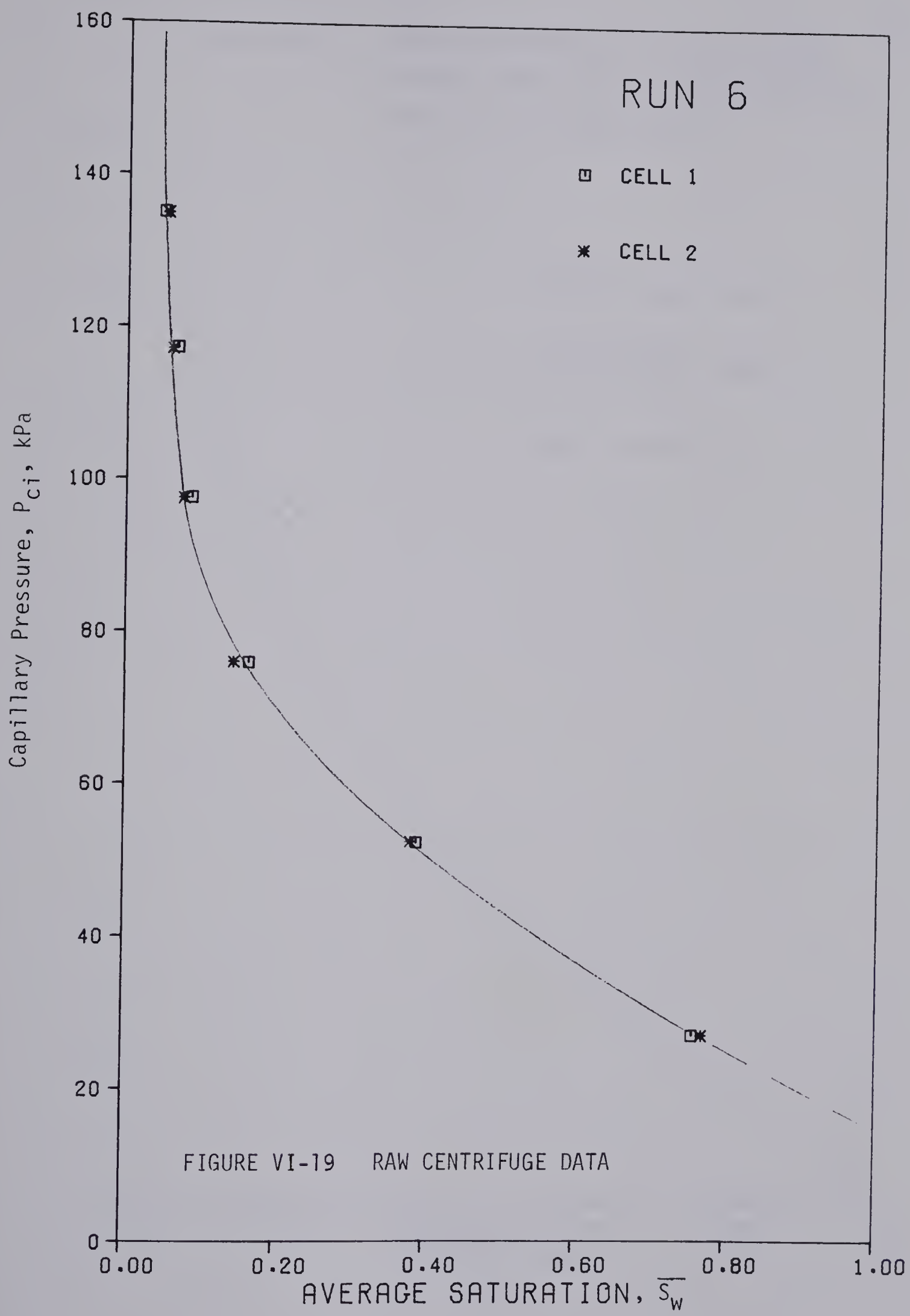


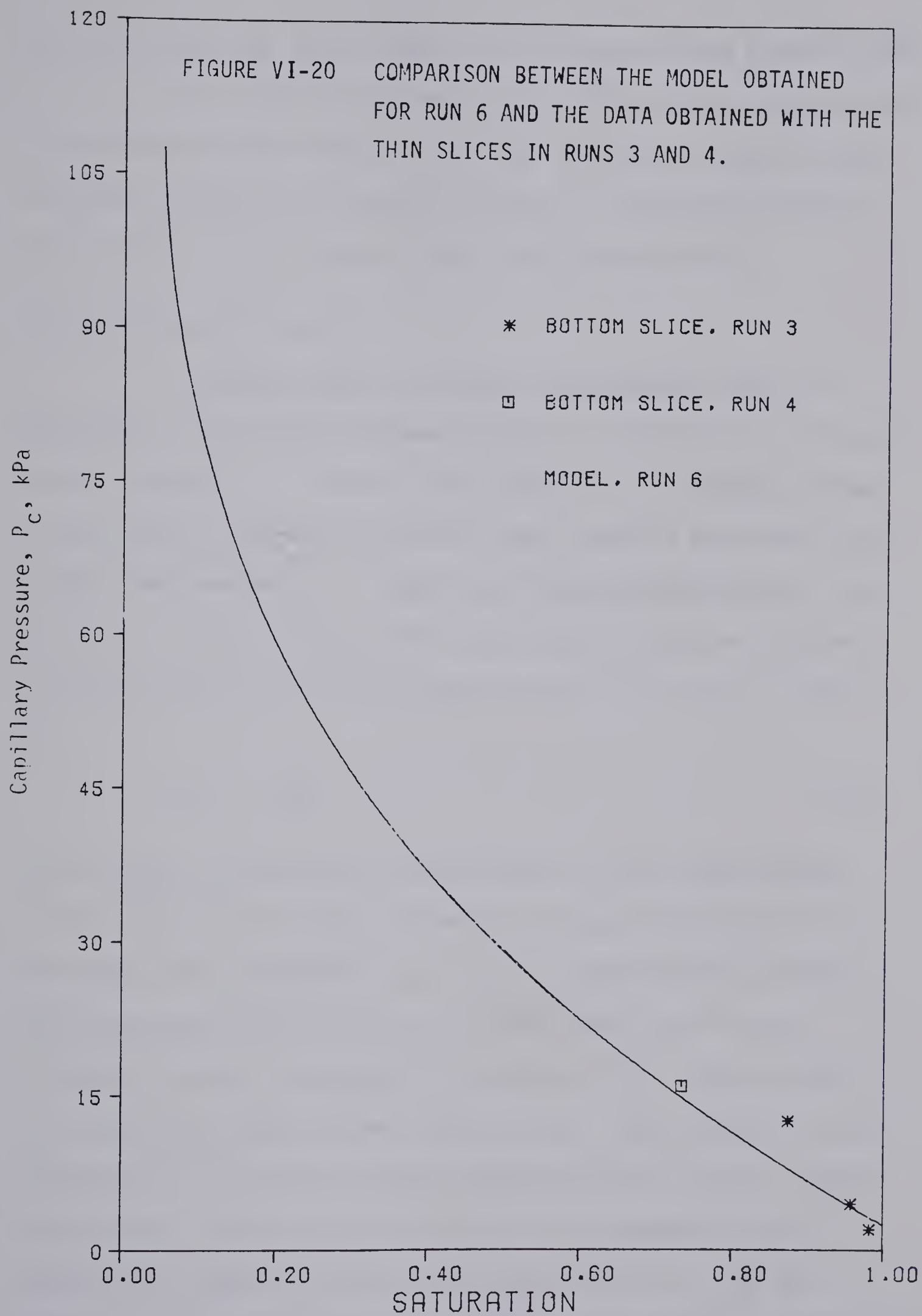


slices has the advantage that more points are obtained at once, and, if the size of the slices and speed of rotation are adequately chosen, an entire capillary pressure-saturation curve can be obtained at one speed of rotation. Because the bottom slice was always partially desaturated after each run, the experimental capillary displacement pressure was obtained by extrapolation; this measurement cannot, therefore, be considered as accurate. On the other hand, the irreducible water saturation was very nearly obtained. Again, two experimental curves can be drawn by plotting either P_{ci} against \bar{S}_w or P_{ci} against $\overline{\bar{S}_w}$ [Figure VI-19 and VI-6]. Neither of these curves represents the true capillary pressure curve.

In order to get a better view of what the true capillary pressure curve should look like, Run 3 and Run 4 were conducted. They are similar to Run 2 and Run 5 respectively, with, however, the following modification: the bottom of each core was cut in two slices; the outer slice was about 0.5 cm long, and the effect of gravity is, therefore, expected to become small due to a small variation of P_c from the inlet to the outlet face of the slice. It is very interesting to note that:

- i) the points corresponding to the thin outer slices do not fall on the experimental capillary pressure curve [Figure VI-3].
- ii) although they display an inflection point near maximum saturation, these data are much closer to the model than the data obtained for the large slices [Figure VI-20].
- iii) the extrapolated capillary displacement pressure is drastically different and smaller than that obtained by extrapolating





the data pertaining to the large slices [Figure VI-3 and Figure VI-20].

iv) the saturation measured in these small slices is still an average saturation and is, therefore, slightly too high. A true capillary pressure curve should, therefore, slightly deviate from these points and be located to their left [Figure VI-20].

VI.3.1.2 Numerical Results

The program used to estimate the parameters makes it possible to let all the parameters float, or, conversely, to fix any chosen parameter. If some of these parameters are strongly related to each other, a variation of one of them induces a variation in the others, and conversely. In such a case the algorithm diverges very quickly. This was the case for n and σ , which determine the area under the curve and are very strongly related; this area is given by

$$\text{area} = \frac{\sigma}{2-n} + P_d \quad (4-7)$$

The term $\frac{\sigma}{2-n}$ is represented in Figure VI-21 by the shaded portion of the area under the curve. Therefore, it was necessary to fix n . The three other parameters, S_{wi} , σ , and P_d , were allowed to float, and convergence was obtained in all cases after five to nine iterations, with a convergence criterion $\epsilon = 10^{-5}$. Another value of n was then chosen, and the program rerun. The standard error of estimate was the criterion used to determine which value of n gave the best fit. In all but one run, Run 4, the standard error of estimate was found to increase continuously with n , or, on the contrary, to decrease continuously with an increasing n . In the first

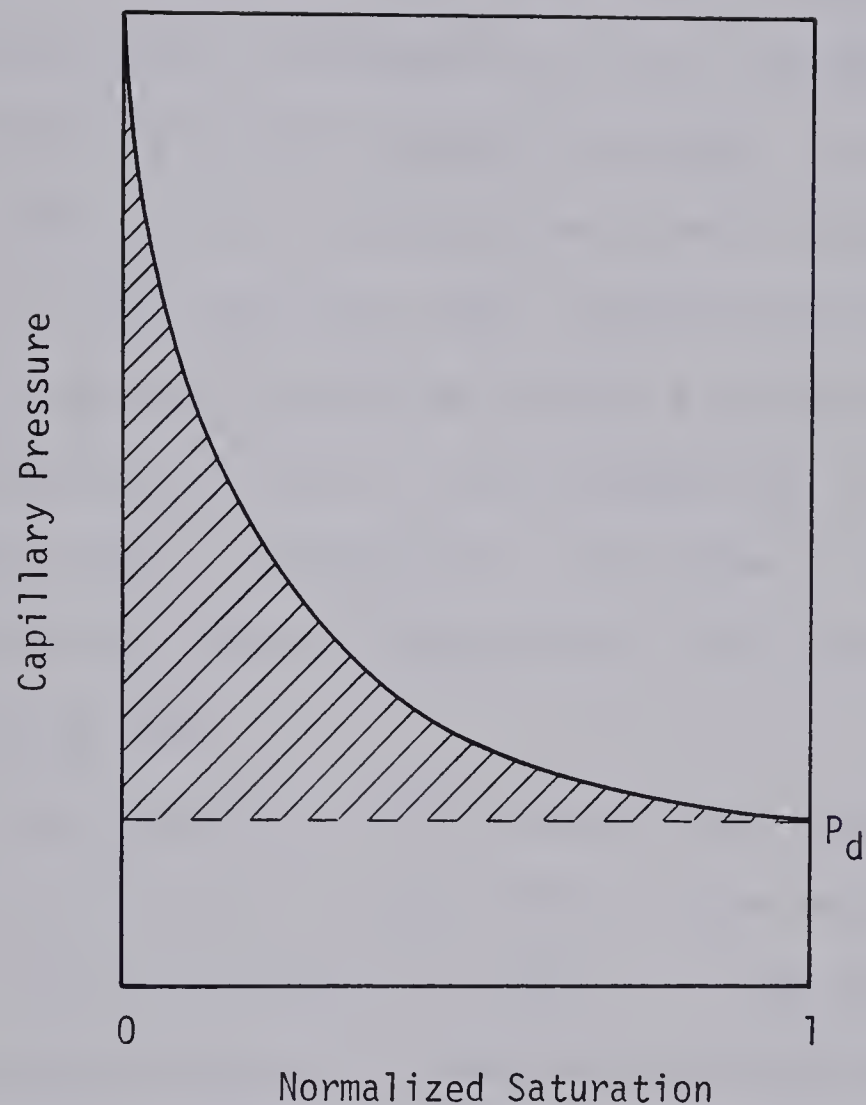


FIGURE VI-21 MEANING OF $\frac{\sigma}{2-n}$

case, n was lowered until a mathematical impossibility would obtain; the last value of n for which the calculations could be carried through, and the corresponding values of S_{wi} , P_d and σ , were chosen as the best estimates of the parameters for the particular run. In such cases, the logarithmic model was found at times to be totally inadequate, because no combination of initial parameters could be found that would allow the program to converge. On the other hand, when the standard error of estimate was found to decrease for increasing n , the logarithmic model converged easily and gave the best fit; it was not possible to increase n continuously to one due to prohibitively high values of the exponent $\frac{1}{1-n}$, involved in the calculations, when n approaches one. The highest acceptable value of n was found to be of the order of 0.97, after which the logarithmic model had to be used.

The standard error of estimate ranged between 0.484×10^{-2} and 1.835×10^{-2} , which is quite similar to the values 0.368×10^{-2} and 1.537×10^{-2} , obtained by Anli (97). The linear confidence limits for the parameters are given in Table VI-3; they are consistently higher for σ than for S_{wi} and P_d , a fact which has been already pointed out by Anli (98).

It seems that the estimates of the parameters are fairly constant for comparable experiments, but that they vary widely with the experimental procedure, that is the size and number of slices and speed(s) of rotation. Hence, they are comparable for Run 2 and Run 3 on the one hand, and comparable for Run 5 and Run 6 on the other hand, but the two sets thus obtained are very different. This is not

surprising, however, because the model is not grounded on physical considerations but is merely a fit; therefore, it is not reasonable to expect the individual parameters to remain constant, even though the conditions of the experiments may change. This is true particularly in the case where the parameters are obtained by extrapolation. Run 4 is an illustration of this fact: the estimated value of P_d for this run is negative, in spite of the fact that the core was water-wet.

Strictly speaking, a model which does not exactly reflect the physics of the phenomenon under study should not be extrapolated beyond the range of available experimental data, because every point has an equal weight in the determination of the parameters; the best estimates of the latter are, therefore, best only for the given set of experimental data. However, if a combination of two or more parameters can be given a physical meaning, it is worthwhile investigating this combination.

It has been previously stated that the area under the capillary pressure-saturation curve corresponds to the reversible external work, and if equilibrium has been reached, one may expect this work to be almost constant and independent of the experimental procedure. The value of the area under each curve is given in Table VI-3. The average for sample P-12-C is 31.29 with a standard deviation of 2.20; for P-6-C, the average is 52.06 with a standard deviation of 0.75. These values are, therefore, meaningful. Of particular interest is Run 4; the value of the area under this curve falls within 2% of the average obtained for sample P-12-C, although

the estimated parameters, for this run, are particularly far from those obtained in the other runs, and even meaningless as far as P_d is concerned.

VI.3.1.3 Capillary Displacement Pressure - End Effect

It is commonly accepted that extrapolating experimental data to $S_w = 1$ yields P_d . Anli (99) reports the observation of a significant discrepancy between the values of estimated and extrapolated capillary displacement pressure for all his runs and suggests that there is a linear correlation between the discrepancy and the permeability of the cores; the discrepancy increases with permeability. The largest discrepancy was obtained for his shortest core and does not fit the correlation; neither does the discrepancy for the tightest core.

Anli (100) points out that the displacement capillary pressure, obtained by extrapolation, is expected to be higher than the true capillary displacement pressure and argues that

"the deviation of the estimated P_d from that observed is not necessarily a quantitative representation of the end effect, but could also be a result of the heterogeneity of the sample".

It would, indeed, be difficult to estimate quantitatively the end effect or the role played by gravity and sample heterogeneity. But one can argue that if the discrepancy between estimated and extrapolated P_d were due to heterogeneity of the samples, there would be no apparent reason for which this discrepancy always goes in the same direction. According to Szabo (89), the measured capillary pressure curve is always under the true capillary pressure

curve; therefore, the discrepancy would always be opposite to that obtained by Anli (99). The reason is that Szabo (89) plots the capillary pressure at the bottom of the core against \bar{S}_w , whereas Anli (101) plots the capillary pressure at the top of the core against \bar{S}_w . The true capillary pressure curve is, of course, expected to be somewhere in between. The deviation is, therefore, more likely due to a combination of gravity effect and end effect, than to the heterogeneity of the samples.

It is worthwhile, at this point, to investigate Eq.(4-9) in connection with the end effect. In order for the water to be expelled from a water-wet porous medium, there must be a capillary pressure inversion inside the core, so that the pressure in the water phase, at the outlet end of the core, is higher than the pressure in the oil phase at the same point (102). Therefore, the assumption commonly accepted, that $P_c = 0$ at the outlet end of the core, is always violated. This results in higher displacement and capillary pressures than what would be obtained without end effect, until the end effect becomes so small that it can be neglected.

The drainage capillary pressure equation is

$$P_c = A\Delta\rho\omega^2 \left(r_e - \frac{h}{2}\right) h \quad (4-9)$$

and the displacement capillary pressure is given by

$$P_d = A\Delta\rho\omega^2 \left(r_e - \frac{h^*}{2}\right) h^*$$

where h^* is the location where $P_c = P_d$ for the angular speed ω .

P_d has a finite, positive value for a water-wet core.

Therefore, when ω goes to infinity, h^* must go to zero, and P_d is finite, not equal to zero. But, by hypothesis, $P_c = 0$ at $h = 0$.

Thus there is a contradiction.

Let $h^0(\omega)$ be the location at which $P_c = 0$. One has:

$$P_c = A\Delta\rho\omega^2 \left(r_e - \frac{h + h^0}{2}\right)(h - h^0) \quad (6-10)$$

Then, at the outlet end of the core,

$$P_c(h = 0) = -A\Delta\rho\omega^2 \left(r_e - \frac{h^0}{2}\right) h^0 \quad (6-11)$$

When ω goes to infinity, and for $P_c(h = 0)$ to be finite, it is necessary that

$$\lim_{\omega \rightarrow \infty} h^0 = h^0(\infty) = 0$$

This was expected a priori, because the end effect becomes very small at high speeds of rotation. Therefore, if an experiment is conducted at a single speed of rotation, as was the case in Runs 1, 4, 5, 6 and 8, h^0 is fixed, whereas it varies in experiments such as Runs 2, 3 and 7. In the first case, if P_{c1} and P_{c2} are the capillary pressures, calculated with Eq.(6-10), at h_1 and h_2 ,

$$P_{c1} - P_{c2} = A\Delta\rho\omega^2 \left(r_e - \frac{h_1 + h_2}{2}\right)(h_1 - h_2) \quad (6-12)$$

The difference in capillary pressures, calculated at two different locations within the core, is independent of h^0 . Therefore, the end effect is only to shift the curve upwards. Conversely, the capillary

pressure at the same location in a core rotated at two different speeds, ω_1 and ω_2 , is dependent upon h_1^0 and h_2^0 , where h_1^0 and h_2^0 are the locations at which $P_c = 0$ for the angular speeds ω_1 and ω_2 respectively:

$$P_{c1} - P_{c2} = A\Delta\rho[(r_e - \frac{h}{2})h(\omega_1^2 - \omega_2^2) - \omega_1^2 h_1^0(r_e - \frac{h_1^0}{2}) + \omega_2^2 h_2^0(r_e - \frac{h_2^0}{2})] \quad (6-13)$$

Because P_c increases with ω , whereas h^0 decreases with ω , the discrepancy due to the end effect is expected to increase towards high saturations and to be the highest at $S = 1$; that is, for the displacement capillary pressure. Therefore, an experimental procedure whereby the angular speed is varied to obtain the capillary pressure curve is more subject to errors due to the end effect, than is a method whereby the curve can be obtained at a single high speed of rotation.

VI.3.2 Imbibition

A rigorous analysis of the system under study is difficult. Due to the difference in pressure gradients in the oil and water phases, the capillary pressure was always higher at the inner end of the core than at the outer end. The semi-permeable membrane, placed between the water reservoir and the inner end of the core, was fully water saturated, which resulted in a saturation discontinuity at the contact plane between the core and the membrane. The core and membrane were kept in capillary contact by means of a disc of Kleenex paper.

If, for a given r_w and r_o , the speed of rotation is chosen so that the capillary pressure at the inner end of the core, calculated with Eq.(4-23), corresponds to S_{wi} , imbibition is not possible, and no change occurs in the system. If the speed of rotation is decreased sufficiently, so that the forces due to interfacial tensions and wettability overcome the force due to the excess pressure in the oil phase as compared to the pressure in the water phase, imbibition should occur.

At the start of the experiment, the capillary pressure inside the core is much larger than the capillary pressure calculated with Eq.(4-23). If imbibition occurs, r_w increases and r_o decreases; therefore, the calculated capillary pressure increases in the course of the experiment, whereas it decreases in the core as a result of imbibition. It is therefore believed that the water should progress towards the outer end of the core, and that the location at which equilibrium obtains should, in the same manner, progress from the inlet to the outlet. Let us, indeed, suppose that at a time T_1 , a state of equilibrium is obtained at the distance ℓ_1 from the inlet end of the core; if the state of equilibrium progresses outwardly, at time $T_1 + \delta T$, the imposed hydrostatic pressure has increased at the location ℓ_1 , as a result of imbibition in the remainder of the core. Consequently, the saturation at ℓ_1 must decrease by a corresponding amount, in order for a new state of equilibrium to obtain. This is possible because, by hypothesis, the remainder of the core is not yet at equilibrium, and the excess water at ℓ_1 can move towards the outer end of the core. On the contrary, if

equilibrium were first obtained at the outer end and progressed towards the inner end of the core, there would be no way for the excess water in the lower part of the core to escape, as the imposed hydrostatic pressure increases as a result of further imbibition in the upper part of the core.

As a result of this analysis, it seems that the saturation at one point inside the core oscillates continuously, until equilibrium is eventually reached in the entire core. This is not desirable, because it is equivalent to an alternation of imbibition and drainage cycles. The amplitude of the oscillations is not measurable, and, as a result, it is not possible to evaluate the consequences of this effect on the experimental results.

Another drawback of the method is that, whereas it was desirable to have a high $\Delta\rho$ in the drainage experiments, it is desirable to have a small $\Delta\rho$ in the imbibition experiments. Indeed, if L is the length of the core, and if P_o and P_{ci} are the capillary pressures at the outer and inner ends respectively of the core, then

$$P_{ci} = P_o + \frac{A\omega^2}{2} L (2r_e - L) \Delta\rho \quad (6-14)$$

In order for imbibition to occur quickly, it is desirable to use as high an ω as possible, and to keep, at the same time, a fairly low P_{ci} ; therefore $\Delta\rho$ should be small. This would be even more critical in the case of unconsolidated porous media, for which the capillary pressures involved are small.

The reasons for the failure of these experiments are not known with certainty. The cores were water-wet. Therefore, the

most probable reason is that the capillary pressure at the inner end of the core was too high. This suggests that it should be extremely small; the minimum possible speed of rotation of the centrifuge was 500 rpm; therefore, a lowering of capillary pressure would be possible only by controlling r_w and r_o . But this control is not sufficient at very low capillary pressures. Indeed, when the term $[(r_e - h)^2(\rho_o - \rho_w) + r_w^2 \rho_w - r_o^2 \rho_o]$ of Eq.(4-23) becomes very small, a small error in the measurement of r_w has an important effect, and the term may easily become negative. Moreover, the centrifugal acceleration distorts somewhat the free oil and water levels. Therefore, the calculated values of P_c would be totally erratic. In his experiments, Szabo (103) was able to use speeds as low as 195 rpm and had, therefore, better control over the value of P_c .

CHAPTER VII

CONCLUSIONS AND RECOMMENDATIONS

An attempt has been undertaken to gain a better understanding of the significance of the experimental capillary pressure - average saturation data obtained with the centrifuge method on multi-slice cores. The size and number of slices were varied in the experiments, and one or several speeds of rotation were used in the course of the experiments. A new mathematical model, to fit the data, was studied and compared with another model already studied in the literature. Attempts have been undertaken to obtain the imbibition branch of the hysteresis loop with the centrifuge. As a result of this investigation, the following conclusions can be drawn; it is pointed out that conclusions 1, 2 and 4 are relevant to the centrifuge method conducted on multi-slice cores, whereas conclusions 3, 5, 6 and 7 are relevant to both the conventional centrifuge method and the quick method:

- 1) the experimental data vary with the parameters of the experiments, such as size of the slices and whether one or several speeds of rotation are used in the course of the experiments.
- 2) at least two experimental curves can be obtained for a given set of data, depending on whether capillary pressure is plotted against the average saturation in each slice or against the average saturation between the outer end of the core and the plane at which P_c is calculated. This suggests that experimental data

alone do not represent the true capillary properties of the medium under study.

3) extrapolated data, such as displacement capillary pressure, are not reliable, especially when the size of the slices is large enough for the gravity effect to be important. This was already shown by Anli.

4) if different speeds of rotation are used in the course of an experiment conducted on a multi-slice core, a conventional capillary pressure - average saturation curve cannot be obtained experimentally.

5) the assumption that $P_c = 0$ at the bottom of the core, although it is probably acceptable in view of the accuracy of the data obtained, bears in itself a contradiction; this contradiction can be removed only by introducing the notion of end effect.

6) although the end effect is probably small, data obtained by varying the speed of rotation are more likely to be distorted than those obtained at a single high speed of rotation.

7) the most probable reason for the failure of the imbibition experiments is that the capillary pressure at the top of the core could not be sufficiently lowered. The centrifuge method, however, does not seem to be a very sound method for obtaining imbibition data, because water must penetrate the core on the side where the saturation is the lowest; that is, on the side where the permeability to water is the lowest.

The following suggestions can be made:

1) drainage data could be improved by using slightly larger cores, made of slices about 0.7 cm long, so that the outer slice would remain almost fully saturated, whereas the inner slice would have irreducible water saturation, when using a single, well chosen, speed of rotation.

2) displacement capillary pressure should be measured by the diaphragm method, because this method is free from end effect.

3) once P_d and S_{wi} are known experimentally, the best values of n and σ could be evaluated by using the proposed model. The curve thus generated is expected to give a fairly good representation of the true capillary properties of the system under study.

4) if it is desired to have a single value of n for the drainage model, a value of 0.90 would be suggested; this is not based on theoretical considerations, but it was found that with such a value of n , it was always easy to find initial values of the parameters which allowed the algorithm to converge. Moreover, the variation of the standard error of estimate with n is very small, and the values of the parameters thus estimated are close to those which define the best estimate.

5) unless a centrifuge capable of very low speeds of rotation is available, it does not seem advisable to use the centrifuge method on unconsolidated cores, or to try to obtain imbibition curves. If imbibition data are obtained with the centrifuge, it would be necessary to compare the results to those

obtained with the diaphragm method on a similar system of fluids and porous medium, in order to check the validity of the centrifuge method.

6) a method could possibly be devised, so as to yield the true capillary pressure curve of a system by using dye and measuring the density of light passing through transparent pictures of the faces of the slices. Because the amount of dye is proportional to the amount of water, there is a relationship between the amount of light transmitted and the saturation.

7) care should be taken in the core preparation. If the cores contain large amounts of water of crystallization, they should not be heated up to high temperatures in order to prevent evaporation and subsequent uptake of water of crystallization during the saturation process.

8) although no problem of false minima was encountered in the course of this study, this has not always been the case. Consequently, great care should be taken in using the Marquardt algorithm. It is desirable to make an approximate evaluation of the parameters before using this algorithm in order to avoid using meaningless values of the parameters.

REFERENCES

1. Leverett, M.C.: "Capillary Behavior in Porous Solids", Trans. AIME, Vol.142, 165 (1941).
2. Buckley, S.E. & Leverett, M.C.: "Mechanism of Fluid Displacement in Sands", Trans. AIME, Vol.146, 107 (1942).
3. Buckley, S.E. & Leverett, M.C., ibid., p.111.
4. Fayers, F.J. & Sheldon, J.W.: "The Effect of Capillary Pressure and Gravity on Two-Phase Fluid Flow in a Porous Medium", Trans. AIME, Vol.216, 147 (1959).
5. Bentsen, R.G.: "Conditions Under Which the Capillary Term May Be Neglected", Jour. of Can. Pet. Tech., Vol.17, No.4, 25 (1978).
6. Szabo, M.T.: "New Methods for Measuring Imbibition Capillary Pressure and Electrical Resistivity Curves by Centrifuge", Soc. Pet. Eng. Jour., Vol.14, 243 (1974).
7. Bentsen, R.G. & Anli, J.: "A New Displacement Capillary Pressure Model", Jour. of Can. Pet. Tech., Vol.15, No.3, 75 (1976).
8. Leverett, M.C., ref.1, p.154.
9. Leverett, M.C., ibid., p.155.
10. Gibbs, J.W.: The Collected Works, Vol.1, Longmans, Green and Co., New York (1928), p.229.
11. Champion, F.C. & Davy, N.: Properties of Matter, Prentice Hall, New York (1937), p.99.
12. Leverett, M.C., ref.1, p.155.
13. Leverett, M.C., ibid., p.156.
14. Hassler, G.L., Brunner, E. & Deahl, T.J.: "The Role of Capillarity in Oil Production", Trans. AIME, Vol.155, 160 (1944).
15. Morrow, N.R. & Harris, C.C.: "Capillary Equilibrium in Porous Materials", Soc. Pet. Eng. Jour., Vol.5, 17 (1965).
16. White, N.F., Duke, H.R., Sunada, D.K. & Corey, A.T.: "Physics of Desaturation in Porous Materials", Jour. of the Irr. and Drain. Div., Proceedings of the Am. Soc. of Civ. Eng., Vol.96, 178 (1970).
17. Morrow, N.R. & Harris, C.C., ref.15, p.20.

18. Hassler, G.L., Brunner, E. & Deahl, T.J., ref.14, p.160.
19. White, N.F., Duke, H.R., Sunada, D.K. & Corey, A.T., ref.16, p.165.
20. Morrow, N.R.: "Physics and Thermodynamics of Capillary", Ind. and Eng. Chem., Vol.62, No.6, 48 (1970).
21. White, N.F., Duke, H.R., Sunada, D.K. & Corey, A.T., ref.16, p.185.
22. Haines, W.B.: "Studies in the Physical Properties of Soil. IV. A Further Contribution to the Theory of Capillary Phenomena in Soil", Jour. Agri. Sci., Vol.17, 264 (1927).
23. Heller, J.P.: "The Drying Through the Top Surface of a Vertical Porous Column", Soil Sci. Soc. Am. Proc., Vol.32, 780 (1968).
24. Morrow, N.R., ref.20, p.45.
25. Singhal, A.K. & Dranchuk, P.M.: "The Use of Modified Threshold Pressure for Determining the Wettability of Packs of Equal Spheres", Powder Technology, Vol.11, 48 (1975).
26. Morrow, N.R., ref.20, p.47.
27. Melrose, J.C.: "Interfacial Phenomena as Related to Oil Recovery Mechanisms", Can. Jour. of Chem. Eng., Vol.18, 644 (1970).
28. Melrose, J.C., ibid., p.643.
29. Melrose, J.C., ibid., p.638.
30. Naar, J. & Henderson, J.H.: "An Imbibition Model - Its Application to Flow Behavior and the Prediction of Oil Recovery", Soc. Pet. Eng. Jour., Vol.1, 61 (1961).
31. Melrose, J.C.: "Wettability as Related to Capillary Action in Porous Media", Soc. Pet. Eng. Jour., Vol.5, 259 (1965).
32. White, N.F., Duke, H.R., Sunada, D.K. & Corey, A.T., ref.16, p.165.
33. Melrose, J.C. & Brandner, C.F.: "Role of Capillary Forces in Determining Microscopic Displacement Efficiency for Oil Recovery by Waterflooding", Jour. of Can. Pet. Tech., Vol.13, No.4, 54 (1974).
34. Leverett, M.C., ref.1, p.159.
35. Leverett, M.C.: "Flow of Oil-water Mixtures Through Unconsolidated Sands", Trans. AIME, Vol.132, 167 (1939).

36. Rose, W. & Bruce, W.A.: "Evaluation of Capillary Character in Petroleum Reservoir Rocks", Trans. AIME, Vol.186, 131 (1949).
37. Brown, H.W.: "Capillary Pressure Investigations", Trans. AIME, Vol.192, 72 (1951).
38. Burdine, N.T.: "Relative Permeability Calculations from Pore Size Distribution Data", Trans. AIME, Vol.198, 71 (1953).
39. Corey, A.T.: "The Interrelation Between Gas and Oil Relative Permeabilities", Producers Monthly, Vol.19, No.1, 38 (1954).
40. Brooks, R.H. & Corey, A.T.: "Hydraulic Properties of Porous Media", Hydrology Papers, Colorado State University, Fort Collins, Colorado, No.3, 3 (March, 1964).
41. Brooks, R.H. & Corey, A.T., ibid., p.4.
42. Sigmund, P.M. & McCaffery, F.G.: "An Improved Unsteady-State Procedure for Determining the Relative - Permeability Characteristics of Heterogeneous Porous Media", Soc. Pet. Eng. Jour., Vol.19, 16 (1979).
43. Craig, F.F.: The Reservoir Engineering Aspects of Waterflooding, Monograph Vol.3, Society of Petroleum Engineers of AIME, 12-28 (1971).
44. Garrison, A.D.: "Selective Wetting of Reservoir Rock and Its Relation to Oil Production", Drill. and Prod. Prac., API, 132 (1935).
45. Schilthuis, R.J.: "Connate Water in Oil and Gas Sands", Trans. AIME, Vol.127, 199 (1938).
46. Andresen, K.H.: "Nature and Importance of Surface Forces in Production of Petroleum" - Discussion -, Drill. and Prod. Prac., API, 447 (1938).
47. Hassler, G.L., Brunner, E. & Deahl, T.J., ref.14, p.163.
48. Kinney, P.T. & Nielsen, R.F.: "The Role of Wettability in Oil Recovery", Producers Monthly, Vol.14, No.3, 29 (1950).
49. Kinney, P.T., Killins, C.R. & Nielsen, R.F.: "Some Applications of Capillary Pressure Measurements on Pennsylvania Sands", Producers Monthly, Vol.16, No.3, 26 (1952).
50. Alba, P.: "Effect of Fractional Wettability on Multiphase Flow Through Porous Media", - Discussion -, Trans. AIME, Vol.216, 432 (1959).

51. Raza, S.H., Treiber, L.E. & Archer, D.L.: "Wettability of Reservoir Rocks and Its Evaluation", Producers Monthly, Vol.32, No.4, 2 (1968).
52. Craig, F.F., ref.43, p.12.
53. Melrose, J.C. & Brandner, C.F., ref.33, p.55.
54. Morrow, N.R. & Mungan, N.: "Mouillabilité et Capillarité en Milieux Poreux", Revue IFP, 629 (Juillet-Aout, 1971).
55. Morrow, N.R.: "The Effects of Surface Roughness on Contact Angle with Special Reference to Petroleum Recovery", Jour. of Can. Pet. Tech., Vol.14, No.4, 42 (1975).
56. Benner, F.C. & Bartell, F.E.: "The Effect of Polar Impurities Upon Capillary and Surface Phenomena in Petroleum Production", Drill. and Prod. Prac., API, 341 (1941).
57. Denekas, M.O., Mattax, C.C. & Davis, G.T.: "Effects of Crude Oil Components on Rock Wettability", Trans. AIME, Vol.216, 330 (1959).
58. Craig, F.F., ref.43, p.14.
59. Wagner, O.R. & Leach, R.O.: "Improving Oil Displacement Efficiency by Wettability Adjustment", Trans. AIME, Vol.216, 69 (1959).
60. Brown, R.J.S. & Fatt, I.: "Measurements of Fractional Wettability of Oilfield Rocks by the Nuclear Magnetic Relaxation Method", Trans. AIME, Vol.207, 262 (1956).
61. Coley, F.H., Marsden, S.S. & Calhoun, J.C.: "A Study of the Effect of Wettability on the Behaviour of Fluids in Synthetic Porous Media", Producers Monthly, Vol.20, No.8, 40 (1956).
62. Amott, E.: "Observations Relating to the Wettability of Porous Rock", Trans. AIME, Vol.216, 156 (1959).
63. Donaldson, E.C., Thomas, R.D. & Lorenz, P.B.: "Wettability Determination and Its Effect on Recovery Efficiency", Soc. Pet. Eng. Jour., Vol.9, 13 (1969).
64. Fatt, I. & Klikoff, W.A.: "Effect of Fractional Wettability on Multiphase Flow Through Porous Media", Trans. AIME, Vol.216, 428 (1959).
65. Morrow, N.R. & Mungan, N., ref.54, p.640.

66. Everett, D.H. & Whitton, W.I.: "A General Approach to Hysteresis", Trans. Faraday Soc., Vol.48, 750 (1952).
67. Everett, D.H. & Whitton, W.I., ibid., p.749.
68. Everett, D.H. & Smith, F.W.: "A General Approach to Hysteresis", Part 2 - "Development of the Domain Theory", Trans. Faraday Soc., Vol.50, 187 (1954).
69. Everett, D.H.: "A General Approach to Hysteresis", Part 3 - "A Formal Treatment of the Independent Domain Model of Hysteresis", Trans. Faraday Soc., Vol.50, 1077 (1954).
70. Poulovassilis, A.: "Hysteresis of Pore Water, an Application of the Concept of Independent Domains", Soil Science, Vol.93, 405 (1962).
71. Pickell, J.J., Swanson, B.F. & Hickman, W.B.: "Application of Air-Mercury and Oil-Air Capillary Pressure Data in the Study of Pore Structure and Fluid Distribution", Soc. Pet. Eng. Jour., Vol.6, 55 (1966).
72. Pickell, J.J., Swanson, B.F. & Hickman, W.B., ibid., p.56.
73. White, N.F., Duke, H.R., Sunada, D.K. & Corey, A.T., ref.16, p.171.
74. Morrow, N.R., ref.20, p.37.
75. Topp, G.C. & Miller, E.E.: "Hysteretic Moisture Characteristics and Hydraulic Conductivities for Glass-Bead Media", Soil Sci. Soc. Am. Proc., Vol.30, 161 (1966).
76. Bruce, W.A. & Welge, H.J.: "Restored State Method for Determination of Oil in Place and Connate Water", Oil and Gas Jour., Vol.46, No.12, 223 (1947).
77. Amyx, J.W., Bass, D.M. & Whiting, R.L.: Petroleum Reservoir Engineering, McGraw-Hill Book Company (1960), p.144.
78. Purcell, W.R.: "Capillary Pressures - Their Measurement Using Mercury and the Calculation of Permeability Therefrom", Trans. AIME, Vol.186, 39 (1949).
79. Brown, H.W., ref.37, p.69.
80. Hassler, G.L.: "Method and Apparatus for Permeability Measurement", U.S. Patent No.2,345,935, April 4, 1944.
81. McCullough, J.J., Albaugh, F.W. & Jones, P.H.: "Determination of the Interstitial-Water Content of Oil and Gas Sand by Laboratory Tests of Core Samples", Drill. and Prod. Prac., API, 180 (1944).

82. Hassler, G.L. & Brunner, E.: "Measurement of Capillary Pressures in Small Core Samples", Trans. AIME, Vol.160, 114 (1945).
83. Hassler, G.L. & Brunner, E., *ibid.*, p.117.
84. Slobod, R.L., Chambers, A. & Prehn, W.L.: "Use of Centrifuge for Determining Connate Water, Residual Oil, and Capillary Pressure Curves of Small Core Samples", Trans. AIME, Vol.192, 127 (1951).
85. Szabo, M.T., *ref.6*, p.247.
86. Bentsen, R.G. & Anli, J.: "Using Parameter Estimation Techniques To Convert Centrifuge Data Into a Capillary-Pressure Curve", Soc. Pet. Eng. Jour., Vol.17, 57 (1977).
87. Szabo, M.T., *ref.6*, p.244.
88. Szabo, M.T., *ibid.*, p.245.
89. Szabo, M.T.: "The Role of Gravity in Capillary Pressure Measurements", Soc. Pet. Eng. Jour., Vol.12, 86 (1972).
90. Douglas, J.J., Blair, P.M. & Wagner, R.J.: "Calculation of Linear Waterflood Behavior Including the Effects of Capillary Pressure", Trans. AIME, Vol.213, 99 (1958).
91. Hagoort, J.: "Displacement Stability of Water Drives in Water-Wet Connate-Water-Bearing Reservoirs", Soc. Pet. Eng. Jour., Vol.14, 72 (1974).
92. Fayers, F.J. & Sheldon, J.W., *ref.4*, p.154.
93. Anli, J.: "A Drainage Capillary Pressure Model", M.Sc. Thesis, University of Alberta, 24 (1973).
94. Caudle, B.H., Slobod, R.L. & Brownscombe, E.R.: "Further Developments in the Laboratory Determination of Relative Permeability", Trans. AIME, Vol.192, 149 (1951).
95. Richardson, J.G., Kerver, J.K., Hafford, J.A. & Osoba, J.S.: "Laboratory Determination of Relative Permeability", Trans. AIME, Vol.195, 188 (1952).
96. Marquardt, D.W.: "An Algorithm for Least-Squares Estimation of Nonlinear Parameters", J. Soc. Indust. Appl. Math., Vol.11, No.2, 431 (1963).
97. Anli, J., *ref.93*, p.65.
98. Anli, J., *ibid.*, p.72.

99. Anli, J., *ibid.*, p.76.
100. Anli, J., *ibid.*, p.79.
101. Anli, J., *ibid.*, pp.57-62.
102. Anli, J., *ibid.*, p.74.
103. Szabo, M.T., *ref.6*, p.248.
104. Bentsen, R.G.: "Scaled Fluid Flow Models with Permeabilities Differing from That of the Prototype", Jour. of Can. Pet. Tech., Vol.15, No.3, 47 (1976).
105. Bentsen, R.G., *ibid.*, p.49.

APPENDIX A

JUSTIFICATION FOR THE MODIFICATION OF
EQ.(5-1) INTO EQ.(5-4)

APPENDIX A

In their study of the effect of capillary pressure and gravity on two-phase fluid flow in a porous medium, Fayers and Sheldon (4) derived the immiscible displacement equation in its Lagrangian form,

$$\frac{\partial X}{\partial T} = \frac{dG}{dS} + \frac{\partial}{\partial S} \left(\frac{C(S)}{\frac{\partial X}{\partial S}} \right) \quad (A-1)$$

Assuming that $X(S, T)$, $C(S)$ and $G(S)$ are well behaved functions, they expanded them about $S=0$, which gives:

$$X = x_0 + S^\alpha \sum_{i=1}^{\infty} x_i(t) S^{i-1} \quad (A-2)$$

$$C = S^\zeta \sum_{i=1}^{\infty} c_i S^{i-1} \quad (A-3)$$

$$G = g_0 + S^\beta \sum_{i=1}^{\infty} g_i S^{i-1} \quad (A-4)$$

The velocity of the foot of the front is thus,

$$\lim_{S \rightarrow 0} \left(\frac{\partial X}{\partial T} \right) \equiv \lim_{S \rightarrow 0} (\zeta - \alpha + 1) \frac{c_1 S^{\zeta - \alpha}}{\alpha x_1} \quad (A-5)$$

and, in order for it to be finite, the condition $\zeta = \alpha$ is required.

Eq.(A-1) was then rewritten as,

$$\frac{\partial X}{\partial T} \left(\frac{\partial X}{\partial S} \right)^2 = \frac{dG}{dS} \left(\frac{\partial X}{\partial S} \right)^2 - C \frac{\partial^2 X}{\partial S^2} + \frac{\partial C}{\partial S} \frac{\partial X}{\partial S} \quad (A-6)$$

Combining Eq.(A-2), Eq.(A-3), Eq.(A-4) and Eq.(A-6) yields:

$$\begin{aligned}
& \left(\frac{dx_0}{dt} + s^\alpha \sum_{i=1}^{\infty} \frac{dx_i}{dt} s^{i-1} \right) \left[\sum_{i=1}^{\infty} (\alpha+i-1) x_i(t) s^{\alpha+i-2} \right]^2 \\
&= \sum_{i=1}^{\infty} (\beta+i-1) g_i s^{\beta+i-2} \left[\sum_{i=1}^{\infty} (\alpha+i-1) x_i(t) s^{\alpha+i-2} \right]^2 \\
&\quad - s^\zeta \sum_{i=1}^{\infty} c_i s^{i-1} \sum_{i=1}^{\infty} (\alpha+i-1)(\alpha+i-2) x_i(t) s^{\alpha+i-3} \\
&\quad + \sum_{i=1}^{\infty} (\zeta+i-1) c_i s^{\beta+i-2} \sum_{i=1}^{\infty} (\alpha+i-1) x_i(t) s^{\alpha+i-2} \tag{A-7}
\end{aligned}$$

With the condition $\alpha=\zeta$, Eq.(A-7) may be rewritten as,

$$\begin{aligned}
& \left(\frac{dx_0}{dt} + s^\alpha \sum_{i=1}^{\infty} \frac{dx_i}{dt} s^{i-1} \right) \left[s^{\alpha-1} \sum_{i=1}^{\infty} (\alpha+i-1) x_i(t) s^{i-1} \right]^2 \\
&= s^{\beta-1} \sum_{i=1}^{\infty} (\beta+i-1) g_i s^{i-1} \left[s^{\alpha-1} \sum_{i=1}^{\infty} (\alpha+i-1) x_i(t) s^{i-1} \right]^2 \\
&\quad - s^\alpha \sum_{i=1}^{\infty} c_i s^{i-1} s^{\alpha-2} \sum_{i=1}^{\infty} (\alpha+i-1)(\alpha+i-2) x_i(t) s^{i-1} \\
&\quad + s^{\alpha-1} \sum_{i=1}^{\infty} (\alpha+i-1) c_i s^{i-1} s^{\alpha-1} \sum_{i=1}^{\infty} (\alpha+i-1) x_i(t) s^{i-1} \tag{A-8}
\end{aligned}$$

Hence, dividing both sides by $S^{2(\alpha-1)}$, and rearranging,

$$\begin{aligned}
 & \sum_{i=1}^{\infty} (\alpha+i-1) x_i(t) S^{i-1} \left\{ \left[\frac{dx_0}{dt} + S^{\alpha} \sum_{i=1}^{\infty} \frac{dx_i}{dt} S^{i-1} - S^{\beta-1} \sum_{i=1}^{\infty} (\beta+i-1) g_i S^{i-1} \right] \right. \\
 & \left. X - \sum_{i=1}^{\infty} (\alpha+i-1) x_i(t) S^{i-1} - \sum_{i=1}^{\infty} (\alpha+i-1) c_i S^{i-1} \right\} \\
 & = - \sum_{i=1}^{\infty} c_i S^{i-1} \sum_{i=1}^{\infty} (\alpha+i-1)(\alpha+i-2) x_i(t) S^{i-1} \tag{A-9}
 \end{aligned}$$

By comparing powers of S on both sides of Eq.(A-9), and supposing that α and β are non-integral, it is easy to see that either

$$\sum_{i=1}^{\infty} \frac{dx_i}{dt} S^{i-1} = \sum_{i=1}^{\infty} (\beta+i-1) g_i S^{i-1} = 0$$

or

$$\alpha = \beta-1$$

The first condition may be rejected because it is equivalent to

$$\frac{dX}{dt} = \frac{dG}{dS} = 0$$

and, therefore, the condition $\alpha = \beta-1$ must hold. Fayers and Sheldon (92), then, showed that, as S goes to zero,

$$\frac{dP}{dS} \underset{S \rightarrow 0}{\equiv} \sigma S^{\beta-\alpha}, \text{ that is, } \frac{dP}{dS} \underset{S \rightarrow 0}{\equiv} \frac{\sigma}{S}.$$

This condition, however, does not originate from the physics of the immiscible displacement, but rather from the chosen mathematical tool, the expansion in series of X , C and G . Other mathematical tools, such as finite differences, may be used to solve the immiscible displacement equation; therefore, it is not necessary to

resort to expansions in series.

By definition (104)

$$C(S) = -\frac{K_{rw}(S) K_{rnw}(S)}{M_r K_{rw}(S) + K_{rnw}(S)} \frac{d\pi_c}{dS} \quad (A-10)$$

If $K_{rw}(S) = \delta(S)S^m$ and $K_{rnw}(S) = \eta(S)(1-S)$, (105),

where $\delta(S) = \frac{a_w + b_w(1-S)}{a_w + 1-S}$

and

$$\eta(S) = \frac{a_{nw} + b_{nw}S}{a_{nw} + S}$$

then, with $\frac{d\pi_c}{dS} = \frac{-1}{S^n}$,

$$\lim_{S \rightarrow 0} C(S) = \frac{a_w + b_w}{a_w + 1} S^{m-n}$$

and the condition, $\lim_{S \rightarrow 0} C(S) = 0$, is still met if $n < m$.

Eq.(5-4) is, therefore, justified.

APPENDIX B

DERIVATION OF EQ.(4-12) AND EQ.(4-11)

APPENDIX B

The drainage capillary pressure is given by Eq.(4-9):

$$P_c = A\Delta\rho\omega^2(r_e - \frac{h}{2})h \quad (B-1)$$

Therefore,

$$h = r_e - \sqrt{r_e^2 - \frac{2P_c}{A\Delta\rho\omega^2}} \quad (B-2)$$

The other solution has no physical meaning. Consequently

$$dh = \frac{dP_c}{A\Delta\rho\omega^2 \sqrt{r_e^2 - \frac{2P_c}{A\Delta\rho\omega^2}}} \quad (B-3)$$

B.1 DERIVATION OF EQ.(4-12)

Let h^* be located in the g^{th} slice. The saturation of the first $g-1$ slices is, then, still the maximum saturation, $S_w=1$. The average saturation of the g^{th} slice is given by:

$$\begin{aligned} \overline{S_{wg}} &= \frac{1}{H_g} \int_{h_{g-1}}^{h_g} S_w dh \\ &= \frac{1}{H_g} \int_{h_{g-1}}^{h^*} dh + \frac{1}{H_g} \int_{h^*}^{h_g} S_w dh \quad (B-4) \end{aligned}$$

$$= \frac{h^* - h_{g-1}}{H_g} + \frac{1}{H_g} \int_{h^*}^{h_g} \left[S_{wi} + (1-S_{wi}) \left(\frac{1-n}{\sigma} \right)^{\frac{1}{1-n}} \left(P_d - P_c + \frac{\sigma}{1-n} \right)^{\frac{1}{1-n}} \right] dh$$

$$= \frac{h^* - h_{g-1}}{H_g} + S_{wi} \frac{h_g - h^*}{H_g} + \frac{1-S_{wi}}{H_g} \left(\frac{1-n}{\sigma} \right)^{\frac{1}{1-n}} \int_{h^*}^{h_g} \left(P_d - P_c + \frac{\sigma}{1-n} \right)^{\frac{1}{1-n}} dh \quad (B-5)$$

Combining Eq.(B-3) and Eq.(B-5) yields,

$$\overline{S_{wg}} = \frac{S_{wi} h_g - h_{g-1}}{H_g} + (1-S_{wi}) \frac{h^*}{H_g} + \frac{1-S_{wi}}{H_g A \Delta \rho \omega^2} \left(\frac{1-n}{\sigma} \right)^{\frac{1}{1-n}} \int_{P_d}^{P_g} \frac{\frac{1}{(P_d - P_c + \frac{\sigma}{1-n})^{\frac{1}{1-n}}}}{\sqrt{r_e^2 - \frac{2P_c}{A \Delta \rho \omega^2}}} dP_c \quad (B-6)$$

and with Eq.(B-2),

$$\overline{S_{wg}} = \frac{S_{wi} h_g - h_{g-1}}{H_g} + \frac{1-S_{wi}}{H_g} \left(r_e - \sqrt{r_e^2 - \frac{2P_d}{A \Delta \rho \omega^2}} \right) + \frac{1-S_{wi}}{H_g A \Delta \rho \omega^2} \left(\frac{1-n}{\sigma} \right)^{\frac{1}{1-n}} \int_{P_d}^{P_g} \frac{\frac{1}{(P_d - P_c + \frac{\sigma}{1-n})^{\frac{1}{1-n}}}}{\sqrt{r_e^2 - \frac{2P_c}{A \Delta \rho \omega^2}}} dP_c \quad (B-7)$$

B.2 DERIVATION OF EQ.(4-11)

The average saturation of any slice j above the g^{th} slice is,

$$\begin{aligned} \overline{S_{wj}} &= \frac{1}{H_j} \int_{h_{j-1}}^{h_j} S_w dh \\ &= \frac{1}{H_j} \int_{h_{j-1}}^{h_j} \left[S_{wi} + (1-S_{wi}) \left(\frac{1-n}{\sigma} \right)^{\frac{1}{1-n}} (P_d - P_c + \frac{\sigma}{1-n})^{\frac{1}{1-n}} \right] dh \\ &= S_{wi} + \frac{1-S_{wi}}{H_j} \left(\frac{1-n}{\sigma} \right)^{\frac{1}{1-n}} \int_{h_{j-1}}^{h_j} (P_d - P_c + \frac{\sigma}{1-n})^{\frac{1}{1-n}} dh \end{aligned}$$

and with Eq.(B-3),

$$\overline{S_{wj}} = S_{wi} + \frac{1-S_{wi}}{H_j A \Delta \rho \omega^2} \left(\frac{1-n}{\sigma} \right)^{\frac{1}{1-n}} \int_{P_{j-1}}^{P_j} \frac{\frac{1}{1-n}}{\sqrt{r_e^2 - \frac{2P_c}{A \Delta \rho \omega^2}}} dP_c \quad (B-8)$$

APPENDIX C

DERIVATION OF EQ.(4-24), EQ.(4-25), EQ.(4-26) AND EQ.(4-27)

APPENDIX C

The imbibition capillary pressure is given by Eq.(4-23)

$$P_c = \frac{A\omega^2}{2} [D^2(\rho_0 - \rho_w) + r_w^2 \rho_w - r_0^2 \rho_0] \quad (C-1)$$

with $D = r_e - h$. Therefore,

$$r_e - h = \frac{1}{\sqrt{\rho_w - \rho_0}} \left(-\frac{2P_c}{A\omega^2} + r_w^2 \rho_w - r_0^2 \rho_0 \right)^{1/2} \quad (C-2)$$

and,

$$dh = \frac{1}{A\omega^2 \sqrt{\Delta\rho}} \left(-\frac{2P_c}{A\omega^2} + r_w^2 \rho_w - r_0^2 \rho_0 \right)^{-\frac{1}{2}} dP_c \quad (C-3)$$

In the following derivations, P_0 is the capillary pressure at the outer end of the core, at the end of the imbibition experiments.

C-1. DERIVATION OF EQ.(4-24) and EQ.(4-25)

Eq.(4-21) can be rewritten as,

$$S_w = S_{wi} + (1 - S_{wi} - S_{or}) \exp \left(-\frac{P_c}{\sigma} \right) \quad (C-4)$$

Combining Eq.(C-4) and Eq.(4-10) yields,

$$\overline{S_{wj}} = S_{wi} + \frac{1 - S_{wi} - S_{or}}{H_j} \int_{h_{j-1}}^{h_j} \exp \left(-\frac{P_c}{\sigma} \right) dh$$

and, with Eq.(C-3),

$$\overline{S_{wj}} = S_{wi} + \frac{1 - S_{wi} - S_{or}}{H_j A\omega^2 \sqrt{\Delta\rho}} \int_{P_{j-1}}^{P_j} \frac{\exp \left(-\frac{P_c}{\sigma} \right)}{\sqrt{-\frac{2P_c}{A\omega^2} + r_w^2 \rho_w - r_0^2 \rho_0}} dP_c \quad (C-5)$$

It follows that,

$$\overline{\overline{S_{wj}}} = S_{wi} + \frac{1-S_{wi}-S_{or}}{h_j A \omega^2 \sqrt{\Delta \rho}} \int_{P_0}^{P_j} \frac{\exp \left(-\frac{P_c}{\sigma} \right)}{\sqrt{-\frac{2P_c}{A \omega^2} + r_w^2 \rho_w - r_0^2 \rho_0}} dP_c \quad (C-6)$$

C.2 DERIVATION OF EQ.(4-26) AND EQ.(4-27)

Eq.(4-22) can be rewritten as

$$S_w = S_{wi} + (1 - S_{wi} - S_{or}) \left(\frac{1-n}{\sigma} \right)^{\frac{1}{1-n}} \left(\frac{\sigma}{1-n} - P_c \right)^{\frac{1}{1-n}} \quad (C-7)$$

Combining Eq.(C-7) and Eq.(4-10) yields,

$$\overline{\overline{S_{wj}}} = S_{wi} + \frac{1-S_{wi}-S_{or}}{h_j} \left(\frac{1-n}{\sigma} \right)^{\frac{1}{1-n}} \int_{h_{j-1}}^{h_j} \left(\frac{\sigma}{1-n} - P_c \right)^{\frac{1}{1-n}} dh$$

and, with Eq.(C-3),

$$\overline{\overline{S_{wj}}} = S_{wi} + \frac{1-S_{wi}-S_{or}}{h_j A \omega^2 \sqrt{\Delta \rho}} \left(\frac{1-n}{\sigma} \right)^{\frac{1}{1-n}} \int_{P_{j-1}}^{P_j} \frac{\left(\frac{\sigma}{1-n} - P_c \right)^{\frac{1}{1-n}}}{\sqrt{-\frac{2P_c}{A \omega^2} + r_w^2 \rho_w - r_0^2 \rho_0}} dP_c \quad (C-8)$$

Therefore,

$$\overline{\overline{S_{wj}}} = S_{wi} + \frac{1-S_{wi}-S_{or}}{h_j A \omega^2 \sqrt{\Delta \rho}} \left(\frac{1-n}{\sigma} \right)^{\frac{1}{1-n}} \int_{P_0}^{P_j} \frac{\left(\frac{\sigma}{1-n} - P_c \right)^{\frac{1}{1-n}}}{\sqrt{-\frac{2P_c}{A \omega^2} + r_w^2 \rho_w - r_0^2 \rho_0}} dP_c \quad (C-9)$$

APPENDIX D

DERIVATION OF EQ.(5-2), EQ.(5-1) AND EQ.(4-23)

APPENDIX D

D.1 DERIVATION OF EQ.(5-2)

Let M_w be the mass of water in the slice at the end of the run.

M_o be the mass of oil in the slice at the end of the run.

M_L be the mass of oil and water contained in the slice at the end of the run.

V_p be the pore volume of the slice.

ρ_w and ρ_o be respectively the densities of water and oil.

Then,

$$V_p = \frac{M_w}{\rho_w} + \frac{M_o}{\rho_o} \quad (D-1)$$

and,

$$M_L = M_o + M_w \quad (D-2)$$

Combining Eq.(D-1) and Eq.(D-2) yields,

$$V_p = \frac{M_L - M_o}{\rho_w} + \frac{M_o}{\rho_o}$$

Consequently,

$$V_p - \frac{M_L}{\rho_w} = \frac{M_o}{\rho_o} \left(1 - \frac{\rho_o}{\rho_w}\right)$$

or,

$$\frac{M_o}{\rho_o} = \frac{V_p - \frac{M_L}{\rho_w}}{1 - \frac{\rho_o}{\rho_w}} \quad (D-3)$$

With Eq.(D-1), one gets

$$\frac{M_w}{\rho_w} = V_p - \frac{V_p - \frac{M_L}{\rho_w}}{1 - \frac{\rho_0}{\rho_w}} \quad (D-4)$$

This equation represents the volume of water contained in the slice at the end of the run; therefore,

$$\overline{S}_w = 1 - \frac{V_p - \frac{M_L}{\rho_w}}{V_p \left(1 - \frac{\rho_0}{\rho_w}\right)} \quad (D-5)$$

If M'_w is the mass of water contained in the 100% water saturated slice, then,

$$V_p = \frac{M'_w}{\rho_w} \quad (D-6)$$

Combining Eq.(D-5) and Eq.(D-6) yields,

$$\overline{S}_w = 1 - \frac{M'_w - M_L}{V_p \Delta \rho} \quad (D-7)$$

where $\Delta \rho = \rho_w - \rho_0$. Eq.(D-7) is equivalent to Eq.(5-2).

D.2 DERIVATION OF EQ.(5-1)

Let P_a be the atmospheric pressure

P_{wi} and P_{oi} be the pressures at the inner end in the water and oil phases respectively.

P_{oe} be the pressure in the oil phase at the outer end of the core.

H_o , h_s , r_o , r_e and r_i are defined in Figure D-1.

By definition,

$$P_{oi} = P_a + \omega^2 \left[(H_o - h_s) \left(r_o + \frac{H_o - h_s}{2} \right) \rho_o \right] \quad (D-8)$$

and,

$$P_{oe} = P_a + \omega^2 \left[H_o \left(r_o + \frac{H_o}{2} \right) \rho_o \right] \quad (D-9)$$

If we assume that P_o , the capillary pressure at the outer end of the core, is zero, then,

$$P_{wi} = P_{oe} - \omega^2 \left[h_s \left(r_e - \frac{h_s}{2} \right) \rho_w \right] \quad (D-10)$$

and, with Eq.(D-9),

$$P_{wi} = P_a + \omega^2 \left[H_o \left(r_o + \frac{H_o}{2} \right) \rho_o - h_s \left(r_e - \frac{h_s}{2} \right) \rho_w \right] \quad (D-11)$$

By definition, the capillary pressure at the inner end of the core is:

$$\begin{aligned} P_{ci} &= P_{oi} - P_{wi} \\ &= \omega^2 \left[h_s \left(r_e - \frac{h_s}{2} \right) \rho_w - h_s \left(r_o + H_o - \frac{h_s}{2} \right) \rho_o \right] \end{aligned}$$

But,

$$r_o + H_o = r_e$$

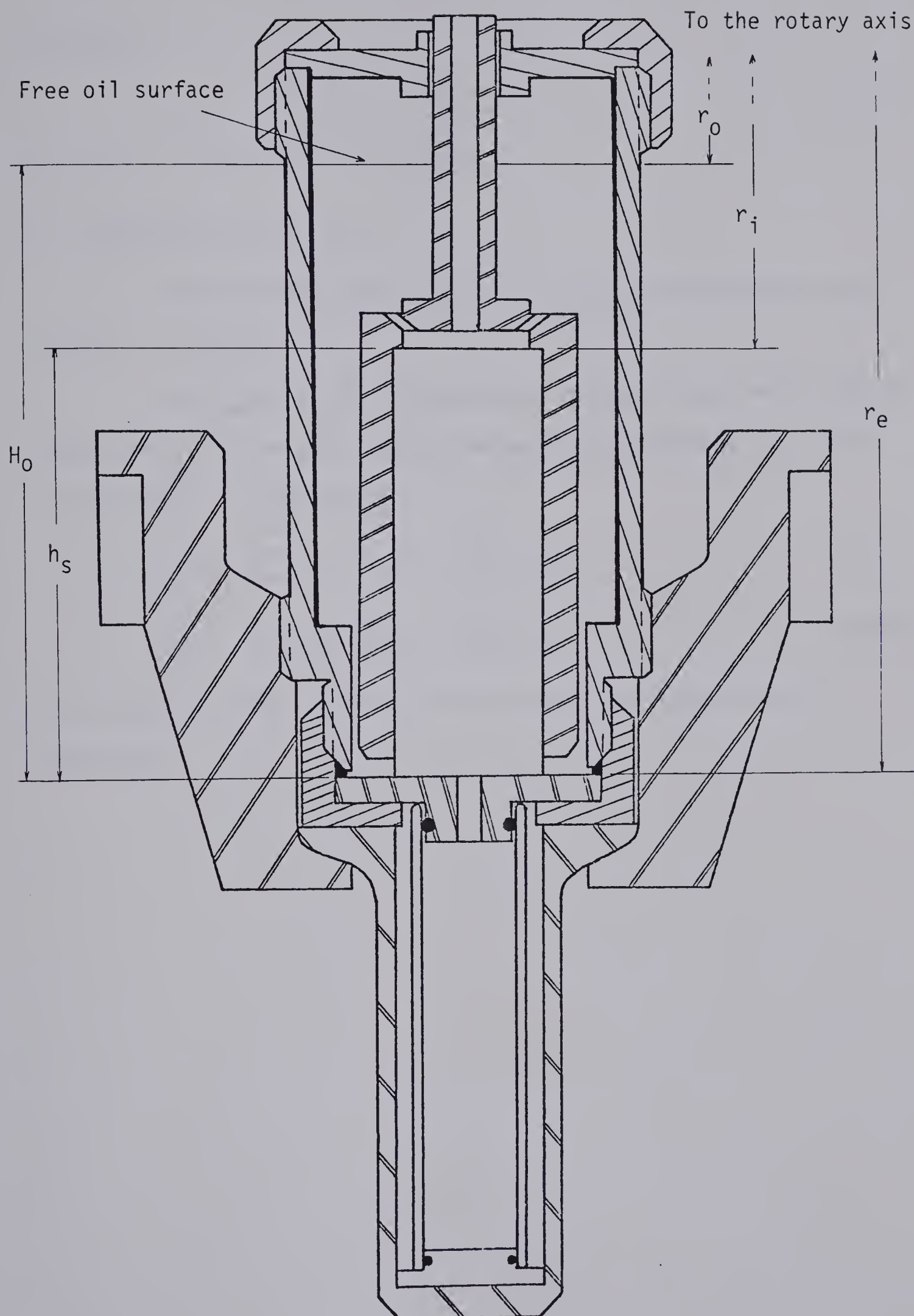


FIGURE D-1 DRAINAGE CAPILLARY PRESSURE CELL

therefore,

$$P_{ci} = \omega^2 \Delta \rho h_s (r_e - \frac{h_s}{2}) \quad (D-12)$$

Eq.(D-12) is equivalent to Eq.(5-1)

D.3 DERIVATION OF EQ.(4-23)

The different terms used in the following equations are defined in Figure D-2.

Let P_{nw} and P_w be the pressures in the oil and water phases respectively, at the point where the capillary pressure, P_c , is to be calculated. By definition,

$$P_{nw} = P_a + \omega^2 [h_o (r_o + \frac{h_o}{2}) \rho_o] \quad (D-13)$$

$$P_w = P_a + \omega^2 [h_w (r_w + \frac{h_w}{2}) \rho_w] \quad (D-14)$$

By design, the water and the oil reservoirs are opened to the atmosphere.

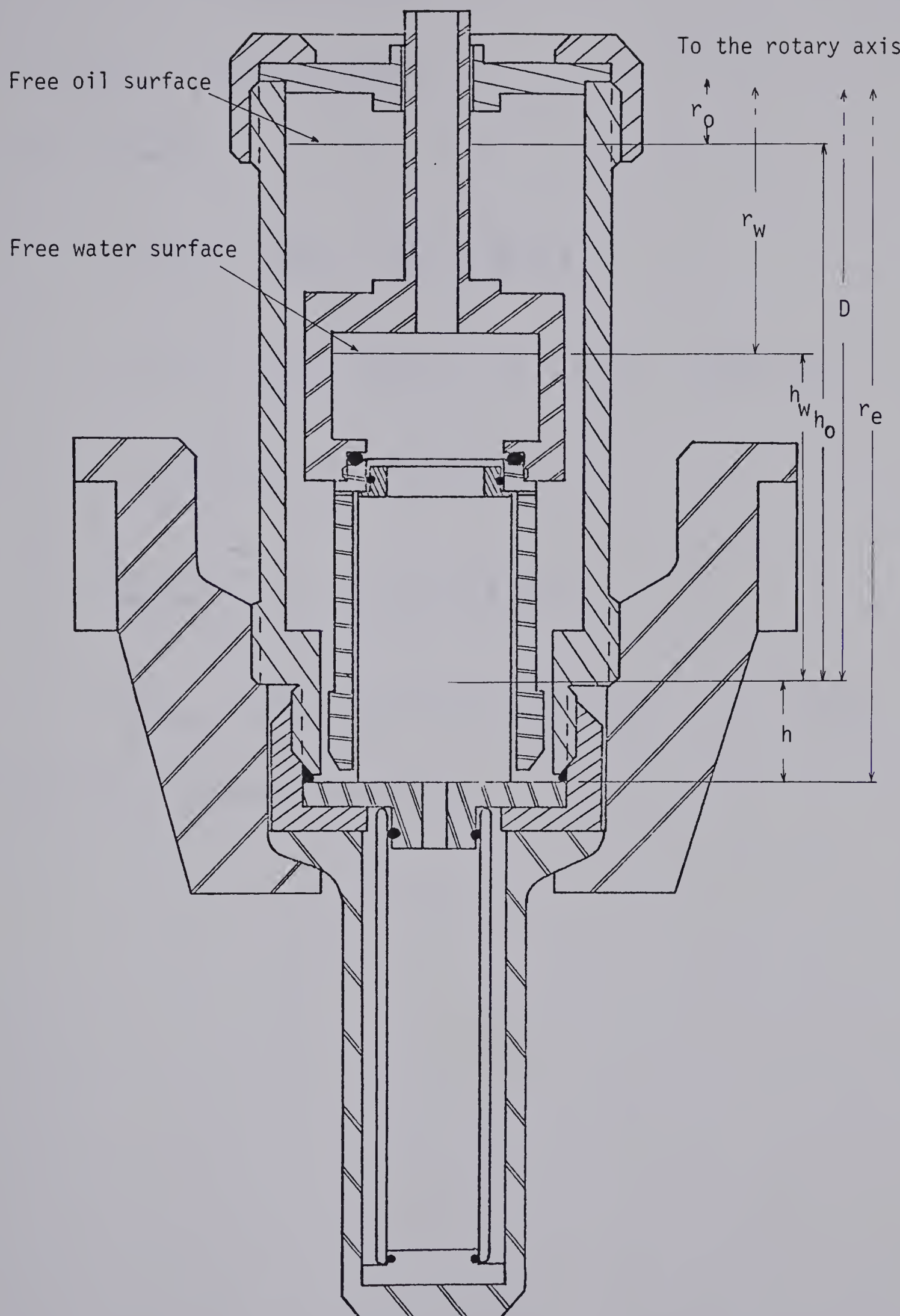


FIGURE D-2 IMBIBITION CAPILLARY PRESSURE CELL

The capillary pressure is, then,

$$\begin{aligned}
 P_C &= P_{nw} - P_w \\
 &= \omega^2 \left[h_o \left(r_o + \frac{h_o}{2} \right) \rho_o - h_w \left(r_w + \frac{h_w}{2} \right) \rho_w \right] \\
 &= \omega^2 \left[(D - r_o) \left(r_o + \frac{D - r_o}{2} \right) \rho_o + (D - r_w) \left(r_w + \frac{D - r_w}{2} \right) \rho_w \right] \\
 &= \omega^2 \left[\left(\frac{D^2 - r_o^2}{2} \right) \rho_o - \left(\frac{D^2 - r_w^2}{2} \right) \rho_w \right] \\
 &= \frac{\omega^2}{2} \left[D^2 (\rho_o - \rho_w) + r_w^2 \rho_w - r_o^2 \rho_o \right] \\
 &= \frac{\omega^2}{2} \left[(r_e - h)^2 (\rho_o - \rho_w) + r_w^2 \rho_w - r_o^2 \rho_o \right] \quad (D-15)
 \end{aligned}$$

Eq.(D-15) is equivalent to Eq.(4-23).

APPENDIX E

PARAMETERS OF THE EXPERIMENTS

TABLE E-1: RUN #1

Sample	: Sandstone	
Number of slices per core:	6	
Speed of rotation	: 2310 rpm for 50 hours	
Length of slices, cm	#1: 1.208	#7: 1.204
	#2: 1.206	#8: 1.200
	#3: 1.213	#9: 1.207
	#4: 1.202	#10: 1.211
	#5: 1.198	#11: 1.213
	#6: 1.206	#12: 1.220

TABLE E-2: RUN #2

Sample	: P-12-C	
Number of slices per core:	3	
Speed of rotation	: 1035 rpm for 15 hours	
	1500 rpm for 20 hours	
	2520 rpm for 7 hours	
Length of slices, cm	#1: 2.403	#4: 2.401
	#2: 2.402	#5: 2.402
	#3: 2.405	#6: 2.407

TABLE E-3: RUN #3

Sample	: P-12-C	
Number of slices per core:	4	
Speed of rotation	: 1000 rpm for 45 hours	
	1500 rpm for 42 hours	
	2500 rpm for 46 hours	
Length of slices, cm	#1: 2.402	#5: 2.403
	#2: 2.403	#6: 2.401
	#3: 1.900	#7: 1.902
	#4: 0.500	#8: 0.498

TABLE E-4: RUN #4

Sample	: P-12-C	
Number of slices per core:	7	
Speed of rotation	: 2820 rpm for 39 hours	
Length of slices, cm	#1: 1.204	#8: 1.201
	#2: 1.209	#9: 1.201
	#3: 1.206	#10: 1.204
	#4: 1.207	#11: 1.205
	#5: 1.200	#12: 1.204
	#6: 0.700	#13: 0.701
	#7: 0.500	#14: 0.498

TABLE E-5: RUN #5

Sample	: P-12-C	
Number of slices per core:	6	
Speed of rotation	: 2480 rpm for 44 hours	
Length of slices, cm	#1:	1.204
	#2:	1.209
	#3:	1.206
	#4:	1.207
	#5:	1.200
	#6:	1.205
	#7:	1.204
	#8:	1.201
	#9:	1.201
	#10:	1.204
	#11:	1.205
	#12:	1.204

TABLE E-6: RUN #6

Sample	: P-12-C	
Number of slices per core:	6	
Speed of rotation	: 2385 rpm for 50 hours	
Length of slices, cm	#1:	1.204
	#2:	1.209
	#3:	1.206
	#4:	1.207
	#5:	1.200
	#6:	1.205
	#7:	1.204
	#8:	1.201
	#9:	1.201
	#10:	1.204
	#11:	1.205
	#12:	1.204

TABLE E-7: RUN #7

Sample	: P-6-C	
Number of slices per core:	3	
Speed of rotation	: 1360 rpm for 20 hours	
	2120 rpm for 47 hours	
	2920 rpm for 22 hours	
Length of slices, cm	#1: 2.397	#4: 2.402
	#2: 2.385	#5: 2.400
	#3: 2.402	#6: 2.403

TABLE E-8: RUN #8

Sample	: P-6-C	
Number of slices per core:	6	
Speed of rotation	: 2910 rpm for 216 hours	
Length of slices, cm	#1: 1.195	#7: 1.193
	#2: 1.194	#8: 1.191
	#3: 1.198	#9: 1.158
	#4: 1.199	#10: 1.194
	#5: 1.193	#11: 1.193
	#6: 1.197	#12: 1.161

APPENDIX F

EXPERIMENTAL AND CALCULATED DATA

TABLE F-1: RUN #1

h, cm	P _c , kPa	Experimental		Calculated
		$\overline{\overline{S}_w}$	$\overline{\overline{S}_w}$	$\overline{\overline{S}_w}$
1.206	25.55	0.6165		0.6050
1.220	25.84	0.5900		0.6016
2.405	49.19	0.4222		0.4123
2.433	49.73	0.3982		0.4094
3.606	69.89	0.3307		0.3232
3.644	71.80	0.3131		0.3214
4.819	91.50	0.2837		0.2747
4.852	92.02	0.2690		0.2737
6.025	109.98	0.2519		0.2450
6.052	110.36	0.2391		0.2445
7.233	126.70	0.2324		0.2250
7.256	127.00	0.2136		0.2247

TABLE F-2: RUN #2

h , cm	ω , rpm	P_c , kPa	Experimental $\overline{\overline{S}}_w$	Calculated $\overline{\overline{S}}_w$
2.401	1035	9.86	0.9823	0.9997
2.403	1035	9.87	0.9828	0.9996
4.803	1035	18.32	0.9198	0.9194
4.805	1035	18.33	0.9319	0.9193
2.401	1500	20.71	0.9036	0.8944
2.403	1500	20.73	0.9003	0.8943
7.210	1035	25.37	0.8027	0.8218
7.210	1035	25.37	0.8141	0.8218
4.803	1500	38.48	0.6871	0.6918
4.805	1500	38.49	0.6849	0.6916
7.210	1500	53.30	0.5611	0.5647
7.210	1500	53.30	0.5717	0.5647
2.401	2520	58.46	0.5698	0.5594
2.403	2520	58.51	0.5688	0.5591
4.803	2520	108.60	0.3769	0.3763
4.805	2520	108.63	0.3662	0.3762
7.210	2520	150.43	0.2951	0.3066
7.210	2520	150.44	0.3198	0.3066

TABLE F-3: RUN #3

h , cm	ω , rpm	P_c , kPa	Experimental $\overline{\overline{S}_w}$	Calculated $\overline{\overline{S}_w}$
2.400	1000	9.20	0.9926	0.9965
2.400	1000	9.20	0.9866	0.9965
4.801	1000	17.09	0.9426	0.9383
4.803	1000	17.10	0.9491	0.9383
2.400	1500	20.71	0.8834	0.8946
2.400	1500	20.71	0.8907	0.8947
7.204	1000	23.67	0.8255	0.8393
4.801	1500	38.46	0.6834	0.6769
4.803	1500	38.47	0.6807	0.6767
7.204	1500	53.26	0.5604	0.5463
2.400	2500	57.52	0.5528	0.5471
2.400	2500	57.52	0.5334	0.5472
4.801	2500	106.84	0.3571	0.3694
4.803	2500	106.87	0.3697	0.3694
7.204	2500	147.95	0.2978	0.3044
7.205	2500	147.97	0.3174	0.3044
0.498	1000	2.02	0.9816	
0.500	1000	2.03	0.9825	
0.498	1500	4.54	0.9461	
0.500	1500	4.56	0.9568	
0.498	2500	12.62	0.8493	
0.500	2500	12.66	0.8736	

TABLE F-4: RUN #4

h, cm	P _c , kPa	Experimental $\overline{\overline{S}}_w$	Calculated $\overline{\overline{S}}_w$
0.498	16.05	0.7376	0.7341
0.500	16.11	0.7319	0.7335
1.200	37.89	0.5580	0.5711
1.200	37.91	0.5769	0.5713
2.400	73.18	0.4040	0.3945
2.404	73.30	0.3973	0.3941
3.606	106.02	0.2954	0.2929
3.609	106.11	0.2834	0.2928
4.813	136.22	0.2328	0.2311
4.814	136.24	0.2249	0.2311
6.015	163.67	0.1882	0.1912
6.021	163.82	0.1967	0.1910
7.216	188.49	0.1598	0.1637
7.225	188.68	0.1688	0.1635

TABLE F-5: RUN #5

h, cm	P_c , kPa	Experimental		Calculated	
		$\overline{\overline{S}_w}$	$\overline{\overline{S}_w}$	$\overline{\overline{S}_w}$	$\overline{\overline{S}_w}$
1.204	29.41	0.7292		0.7418	
1.205	29.43	0.7505		0.7414	
2.404	56.70	0.5404		0.5347	
2.410	56.82	0.5401		0.5339	
3.611	82.09	0.3953		0.4041	
3.614	82.15	0.4040		0.4039	
4.815	105.40	0.3225		0.3219	
4.817	105.44	0.3161		0.3218	
6.016	126.61	0.2736		0.2687	
6.026	126.77	0.2661		0.2683	
7.220	145.84	0.2365		0.2325	
7.230	145.99	0.2309		0.2322	

TABLE F-6: RUN #6

h, cm	P_c , kPa	Experimental	Calculated
		$\overline{\overline{S}_w}$	$\overline{\overline{S}_w}$
1.204	27.21	0.7704	0.7662
1.205	27.21	0.7582	0.7657
2.404	52.44	0.5732	0.5695
2.410	52.55	0.5747	0.5686
3.611	75.93	0.4360	0.4363
3.614	75.98	0.4309	0.4361
4.815	97.47	0.3426	0.3478
4.817	97.52	0.3482	0.3477
6.016	117.10	0.2859	0.2885
6.026	117.25	0.2916	0.2881
7.220	134.88	0.2470	0.2477
7.230	135.02	0.2508	0.2474

TABLE F-7: RUN #7

h, cm	ω , rpm	P_c , kPa	Experimental	Calculated
$\overline{\overline{S}_w}$	$\overline{\overline{S}_w}$			
2.397	1360	17.00	0.9906	0.9755
2.402	1360	17.04	0.9884	0.9760
4.782	1360	31.51	0.9723	0.9677
4.802	1360	31.62	0.9768	0.9670
2.397	2120	41.31	0.8910	0.9078
2.402	2120	41.40	0.8856	0.9073
7.184	1360	43.69	0.9115	0.8780
7.205	1360	43.79	0.9186	0.8772
4.782	2120	76.57	0.6732	0.6773
4.802	2120	76.84	0.6802	0.6758
2.397	2920	78.38	0.6778	0.6800
2.402	2920	78.53	0.6602	0.6792
7.184	2120	106.18	0.5292	0.5358
7.205	2120	106.41	0.5326	0.5349
4.782	2920	145.26	0.4541	0.4483
4.802	2920	145.78	0.4319	0.4472
7.184	2920	201.43	0.3726	0.3570
7.205	2920	201.87	0.3554	0.3565

TABLE F-8: RUN #8

h, cm	P _c , kPa	Experimental		Calculated
		$\overline{\overline{S}_w}$	$\overline{\overline{S}_w}$	$\overline{\overline{S}_w}$
1.161	39.08	0.8572		0.8651
1.197	40.25	0.8686		0.8567
2.354	76.53	0.6368		0.6371
2.389	77.62	0.6207		0.6321
3.548	111.26	0.5135		0.5027
3.589	112.42	0.4918		0.4992
4.706	142.31	0.4410		0.4227
4.787	144.40	0.4100		0.4183
5.897	171.54	0.3821		0.3687
5.981	173.51	0.3548		0.3657
7.090	198.08	0.3354		0.3314
7.176	199.87	0.3172		0.3291

B30249